國立臺灣大學理學院心理學研究所

博士論文

Graduate Institute of Psychology
College of Science
National Taiwan University

Doctoral Dissertation

色彩在對稱知覺各階層的角色

The Role of Color in Symmetry Detection – from Local to Global

吳佳瑾

Chia-Ching Wu

指導教授：陳建中 博士

Advisor: Chien-Chung Chen, Ph.D.

中華民國 100 年 6 月

June, 2011

國立台灣大學理學院心理學研究所

論文口試委員會審定書

吳佳瑾先生所提論文 色彩在對稱知覺各階層的角色

經本委員會審議，符合博士學位標準，特此證明。

論文考試委員會

主席 葛榮杰

委員 葛榮杰 陳建中

黃淑麗 孫慶文

簡惠珍 姜自強

指導教授：陳建中

所主任：翁儷禎

中華民國100年 6月 1 日

致謝

2008 年春，是我博士班生涯的一個重要轉捩點。當時，我從原來高等思考推理的領域轉進了陳建中老師的視知覺實驗室。這三年來，在陳老師的帶領與指導下，我得以一窺視知覺這個領域的奧妙，也深深感受到身為一個優秀研究者所需要的學識、涵養、熱忱與責任。這篇論文的完成，首先要感謝、也最要感謝的，也是我的指導教授陳建中老師。

其次要感謝的是所有的口試委員--黃榮村校長、黃淑麗老師、孫慶文老師、簡惠玲老師、姜自強老師、與葉素玲老師。幾位老師在論文計劃口試和學位論文口試時都給了我相當寶貴的意見，他們思考的深度與廣度、以及對做學問的態度，每每讓我在短短兩個小時的口試中獲益良多。

再來，我也要特別感謝我的三位受試者，願意花這麼多時間參與實驗，因為有他們的全力配合，實驗才得以順利進行。此外，也感謝所有視覺實驗室的成員們一路上的陪伴和幫忙，以及冠嫻助教總是親切且有條不紊地為我們這些研究生處理相關的行政事務，讓我們可以無後顧之憂，專心在學業上。

最後，我要感謝的是在漫長博士班生涯中陪伴我、支持我的家人和朋友。謝謝我的父母無條件的支持，一路走來只有鼓勵和信任，而沒有給我任何壓力。也謝謝所有關心我、陪伴我、支持我的朋友們：有著堅定革命情感的緯倫、純慧、蓓蓓；同在學術路上互相扶持互相砥勵的蔚倫、幸釗、延叡、婷文、慧雅；以及我最最親愛的好友們：士凱、寶哥、阿恕、小外、毓倫、奕晴、小珊、曉萍、曦羽、惠棠、阿鍾…等。也許隨著時空的遷移，我們已分散在不同的城市不同的國家，但那些共同的回憶卻永遠深藏在我心中。


國立臺灣大學
人格品學兼優

中文摘要

對稱是一高階的視覺特徵，其辨識須仰賴人類視覺系統的複雜運算。在自然情境中，對稱圖形或物體通常伴隨著多種顏色，因此視覺系統必須整合顏色和形狀的訊息才能偵測到彩色的對稱圖形。本研究以五個實驗來探討顏色在對稱知覺中所扮演的角色。我們將對稱偵測機制分為兩階段—配對與統合，並分別檢驗此兩階段是否對顏色有選擇性反應。研究結果顯示此兩階段均對顏色有選擇性的反應，此表示視覺系統中有一組對顏色選擇性反應的對稱偵測系統。我們進一步操弄了影像中所包含的顏色數目，來探討視覺系統如何整合這些對稱偵測系統來偵測彩色對稱。研究結果顯示無論觀察者是否知道對稱圖案的對稱軸方向，一影像中顏色數目的增加都可以促進對稱偵測的表現。我們也比較了當兩不同顏色對稱圖形共享相同的對稱軸與否時的對稱偵測表現，以探討是否不同顏色能區隔兩圖形而促進對稱的偵測。研究結果顯示，當兩圖形共享一對稱軸時，其對稱的偵測會比兩圖形的對稱軸方向不同時要佳。我們提出一整合了線性的對稱偵測機制、非線性的反應模式、反應干擾的特性與多個系統的決策歷程的彩色對稱偵測模型來解釋以上的結果。此模型顯示一影像中顏色數目的增加會減少對稱偵測系統中的抑制作用，進一步促進對稱偵稱的表現。此外，當兩對稱圖形共享同一對稱軸時，兩對稱偵測系統間的抑制作用會減少，而導致其對稱偵測表現較兩圖形的對稱軸有不同方向的對稱軸時來得佳。

關鍵詞：對稱偵測、高階色彩視覺、顏色與形狀的整合、心理物理學、雜訊遮蔽。


國立臺灣大學
博愛 · 學術 · 品德 · 教育

The Role of Color in Symmetry Detection

– from Local to Global

Chia-Ching Wu

Abstract

Symmetry is a higher-order form that requires a complicated computation in the visual system. In a nature scene, symmetric objects or stimuli may come with any combination of color. Hence, human visual system needs to integrate both color and form information to detect chromatic symmetry. In this study, we conducted five experiments to investigate the role of color in symmetry detection. We distinguished two stages, that is, matching and pooling stage, of the symmetry encoder and examined the color selectivity of these two stages of symmetry encoder. Our results showed that these two stages are color-selective. This suggests that there are a band of color-selective symmetry channels in our visual system. We further manipulated the number of the colors in the images to investigate how human visual system integrates the response of these symmetry channels to detect chromatic symmetry. Our results showed that the increment of the number of the colors facilitated the symmetry detection performance, regardless the observers had prior knowledge of the symmetry axis orientation or not. Finally, we examined the symmetry detection in two images sharing the same axis or not, to see whether the segmentation of two images with different colors helps symmetry detection. The results however showed better symmetry detection performance when two symmetric patterns shared the same axis

than those did not. All these results can be accounted for by a computational model that incorporated linear symmetry encoding mechanisms, nonlinear transducer response, noise manipulation and a multiple channel based decision making process. The model fitting results suggests that the increment of the number of the color reduces the inhibition of the symmetry channels, and in turn facilitates the symmetry detection performance when the images contain more than one color. In addition, the inhibition between channels responding to the two symmetric patterns sharing the same axis is smaller than that between channels responding to two patterns in different axes, in turn facilitates the symmetry detection performance when the two images shared the same symmetry axis.

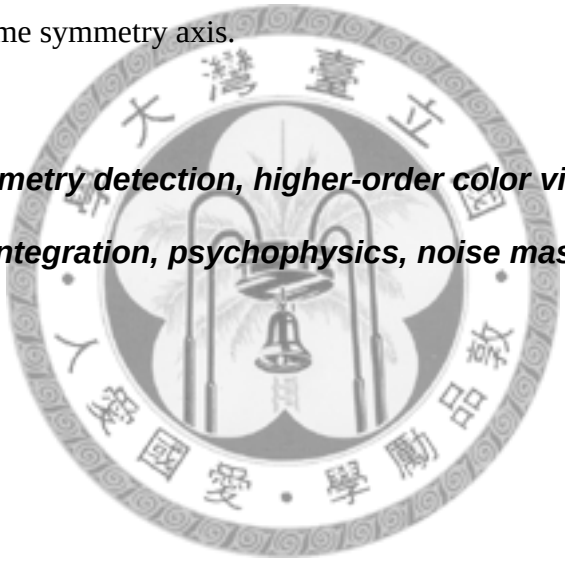

Keywords: symmetry detection, higher-order color vision, color and form integration, psychophysics, noise masking.

Contents

List of Tables


國立臺灣大學
博愛 · 學問 · 品德

List of Figures

Chapter 1 Introduction

Mirror symmetry (henceforth, symmetry) is one of the principal organizational factors in the perceptual grouping of discrete objects (Koffa, 1935; Köhler, 1929; Wertheimer, 1938) that can facilitate figure ground segmentation, object recognition and shape representation (e.g., Blum, 1973; Burbeck & Pizer, 1995; Driver, Baylis, & Rafal, 1992; Kovacs, Feher, & Julesz, 1998; Leeuwenberg & Buffart, 1984; Marr, 1982). Since human visual system can detect symmetry as quickly as in less than 100 ms, symmetry detection is regarded as an intrinsic, fundamental process of the human visual system (e.g., Barlow & Reeves, 1979; Carmody, Nodine, & Locher, 1977; Hogben, Julesz, & Ross, 1976; Julesz, 1971; Locher & Nodine, 1989; Wagemans, Van Gool, & d'Ydewalle, 1991; Wagemans, Van Gool, Swinnen, & Van Horebeek, 1993). Several simple spatial features in the image are important to symmetry perception, such as contrast, spatial frequency, edge, and the orientation of symmetry axis. However, few researches investigated the role of color in symmetry detection (Huang & Pashler, 2002; Morales & Pashler, 1999; Troscianko, 1987). Actually, since color vision and spatial vision are considered as two different disciplines in vision research, there are few studies on space-color interactions in the higher-order visual process in general.

Symmetry is a higher-order image feature that requires a complicated information processing and computation in the visual system (Chen & Tyler, 2010; Tyler & Hardage, 1996). If a symmetric image contains more than one color, human visual system has to integrate both spatial and chromatic information to form chromatic symmetry perception. Hence, investigating the role of the color in

symmetry perception helps us to understand both the mechanisms for higher-order color vision and the mechanisms for complex forms. In this thesis, we used a noise masking paradigm and a computational model to achieve these goals:

(1) To examine how the symmetry channel integrates color information.

(2) To characterize the properties of the color-selective symmetry channel.

(3) To investigate how multiple color-selective symmetry channels interact with each other.

1.1. Higher-Order Color Processing

The extraction of color information in the visual system starts with the spectrum selective response of three different types of retinal photoreceptors, i.e., long- (L), middle- (M), short- (S) wavelength selective cones on the retina (e.g., Bowmaker & Dartnall, 1980; Jacobs & Neitz, 1993; Schnapf, Kraft, & Baylor, 1987; Smith & Pokorny, 1975; van Kries, 1905; Vos & Walraven, 1971). Each cone type absorbs different spectrums of light. Their spectrum selective responses are then sent to the striate visual cortex (V1) through the retinogeniculate pathways. The spectral sensitivities of the retinogeniculate cells are largely consistent with three independent color opponent channels measured with psychophysic methods (for a review, see Knoblauch & Shevell, 2004). The V1 neurons receive inputs from the retinogeniculate pathways and have their fibers project to the extrastriate cortex (V2, V3, and V4) and the inferotemporal (IT) cortex through the ventral pathway (for a review, see Gegenfurther & Kiper, 2004). More than 50% cells in these areas selectively respond to color (Dow & Gouras, 1973; Gegenfurtner, Kiper, & Fenstemaker, 1996; Gegenfurtner, Kiper, & Levitt, 1997; Gouras, 1974; Johnson, Hawken, & Shapley, 2001; Komatsu & Ideura, 1993; Komatsu, Ideura, Kaji, &

Yamane, 1992; Schein & Desimone, 1990; Thorell, De Valois, & Albrecht, 1984; Yates, 1974; Zeki, 1973).

The ventral pathway also processes information about the identity of a visual object, such as the form or shape. Thus, it is possible that the processing of color and that of form are contingent in the visual system. It has been shown that almost all cells in V1 are orientation selective while about 50% cells in V1 are color-selective (Dow & Gouras, 1973; Gouras, 1974; Johnson et al., 2001; Thorell et al., 1984; Yates, 1974). While there are non-color selective neurons respond only to lines or edges in an image regardless their color, many V1 cells can simultaneously encode both the chromatic and spatial characteristics, such as orientation, of a stimulus (Johnson et al., 2001; Leventhal, Thompson, Liu, Zhou, & Ault, 1995). A number of studies identified different organizations of receptive filed of them, such as the double-opponent cells in which the spatial-opponency and the color-opponency coincide exactly, to investigate the color processing in such a spatial information selective mechanism (Livingstone & Hubel, 1984; Michael, 1978a, 1978b, 1978c, 1979; Ts'o & Gilbert, 1988). The psychophysical studies also showed the visual system encodes both chromatic and spatial information with a property similar to that of V1 neurons (Chen, Foley, & Brainard, 2000; Switkes, Bradley, & De Valois, 1988; Webster, De Valois, & Switkes, 1990).

Further downstream, the encoding of color tuning in the higher order visual cortex is not clear. It is shown that neurons in V2 and V4 have distinct color selectivity. However, they may tune to any color on the isoluminance plane rather than just the four cardinal directions (Levitt, Kiper, & Movshon, 1994). To probe the higher order color vision mechanisms, one approach is to study the color processing in complex forms. For instance, some studies used Glass pattern, which contains

randomly distributed dot pairs whose orientations are determined by certain geometric transforms (Glass, 1969; Glass & Perez, 1973), to investigate the color mechanism in the global form processing (Cardinal & Kiper, 2003; Mandeli & Kiper, 2005; Rentzeperis & Kiper, 2010; Wilson & Switkes, 2005). The Glass Pattern detection mechanism contains two stages: a local stage and a global stage. The local stage is considered an early visual processing. It uses linear filters to extract information about pair orientation information. The global stage is a higher-order visual processing. It pools the local orientation information across pairs to exact the global structure (Cardinal & Kiper, 2003; Chen, 2009; Mandeli & Kiper, 2005; Smith, Bair, & Movshon, 2002; Wilson & Switkes, 2005; Wilson, Switkes, & Valois, 2004; Wilson & Wilkinson, 1998). While the previous research agreed that the local stage is color-selective (Mandeli & Kiper, 2005; Wilson & Switkes, 2005), the color selectivity of the global stage is controversial. Wilson and Swikes (2005) suggested that the global stage is mediated by a non color-selective mechanism while Cardinal and Kiper (2003) suggested that Glass patterns are detected by a multitude of mechanisms that sum their inputs linearly. How the global form mechanism integrates the local information to yield a global form percept is unclear. In this thesis, we investigated the role of the color in symmetry detection in order to understand the higher-order color and pattern vision. The benefit of using symmetric patterns is that the symmetry computation, unlike in Glass patterns where the local grouping plays an important role, always requires long-range interactions and thus provides a better picture of long-range color processing.

1.2. Mechanism of Symmetry Detection

Symmetry is a higher-order image feature. A visual stimulus is symmetric if some part of this stimulus is a reflection of another part about an axis, called symmetry axis. To determine whether an image is symmetric, the observer has to compare whether two points of the image are identical, and, if yes, whether the middle points of these matches forms an axis. Such operation requires a higher-order visual mechanism to take the information from early stage into computation.

Currently, in the literature, two types of theories have been proposed to explain how the visual system achieves this task. The first, the relational structure theory, suggests that the visual system may simply analyze the spatial relationship among individual image elements and determine an image to be symmetric if the relative position of a sufficient proportion of image elements supports it. That is, symmetry detection would be based solely on the signal-to-noise ratio or "weight of evidence" in the image (Csathó, van der Vloed, & van der Helm, 2004; van der Helm & Leeuwenberg, 1996, 1999). The second, the spatial filtering theory, assumes that a band of linear filters, whose sensitivity profiles contain multiple excitatory and inhibitory regions, extract symmetry information from an image. (Dakin & Hess, 1997; Dakin & Watt, 1994; Gurnsey, Herbert, & Kenemy, 1998; Osorio, 1996; Rainville & Kingdom, 1999, 2000, 2002; Scognamillo, Rhodes, Morrone, & Burr, 2003; Tjan & Liu, 2005). These filters may be oriented (Dakin & Watt, 1994; Rainville & Kingdom, 2000) or have different phase sensitivity (Rainville & Kingdom, 1999, 2000, 2002; Scognamillo et al., 2003). These filters operate on the input images. If an input image is symmetric, the filtered image would contain features at or across the symmetry axis that can be picked up by a second-order filter that has an orientation similar to that of the symmetry axis (Gurnsey et al., 1998;

Scognamillo et al., 2003) or by a simple mathematical operator operating orthogonal to the symmetry axis (Dakin & Hess, 1997; Dakin & Watt, 1994; Rainville & Kingdom, 1999, 2000, 2002).

Both theories propose a two-stage processing for symmetrical perception. For the relational structure theory, the symmetry detection mechanism has to decide which image elements have the spatial properties that are consistent with a symmetric pair (signal) and which are not (noise). Then a higher-order mechanism collects these local pairs to compute the overall signal-to-noise ratio. The spatial filtering theory also needs a higher-order filter to monitor the output of lower order linear filters, which extracts symmetry information from an image. For these two theories to work, however, one has to make an assumption about the location and orientation of the symmetry axis, on which all the operations on the image depend. However, mirror symmetry can occur at any orientation in a nature scene. While these two theories perform well to explain the data from experiments with a known symmetry axis orientation, their generalization is limited as they do not address the situation where the symmetry axis orientation is unknown to the observers. To solve this problem, Chen and Tyler (2010) manipulated the cueing of the axis orientation and the axis salience and measured the target detection threshold at various noise density levels under these conditions. Their results showed facilitation effect of both cueing of axis orientation and high axis salience. However, the amount of cueing effect and the nonlinear axis salience effect cannot be explained by the above two theories. Hence, they incorporated the property of two-stage encoding process, adding a nonlinear process that was neither addressed by the relational structure nor by the filter approach, to explain the effect of uncertainty about axis orientation in the framework of the Signal Detection Theory (Green & Swets, 1966).

Their model contains two stages: a perception stage and a decision stage (Figure 1.1). In the perception stage, there are a band of orientation-selective symmetry encoders that are sensitive to symmetry in an image. Each encoder is sensitive to the mirror symmetry about one axis. The contribution of each encoder is limited by both the internal noise inherited in the system (Na in Figure 1.1) and the external noise provided by the noise patterns (Ne in Figure 1.1). The nonlinear response of the perception stage is sent to the decision stage. The detection performance relies on the maximum response of all monitored channels. The observers detect symmetry when the difference of responses between two intervals reaches unity. If the observers have prior knowledge of the axis orientation, the decision stage only needs to monitor a relevant channel, whose symmetry selectivity matches that of the symmetric image. However, if there is uncertainty of the axis orientation, the decision stage needs to monitor more channels than the relevant one. This uncertainty impairs the performance of symmetry detection when there is no prior knowledge of the axis orientation.

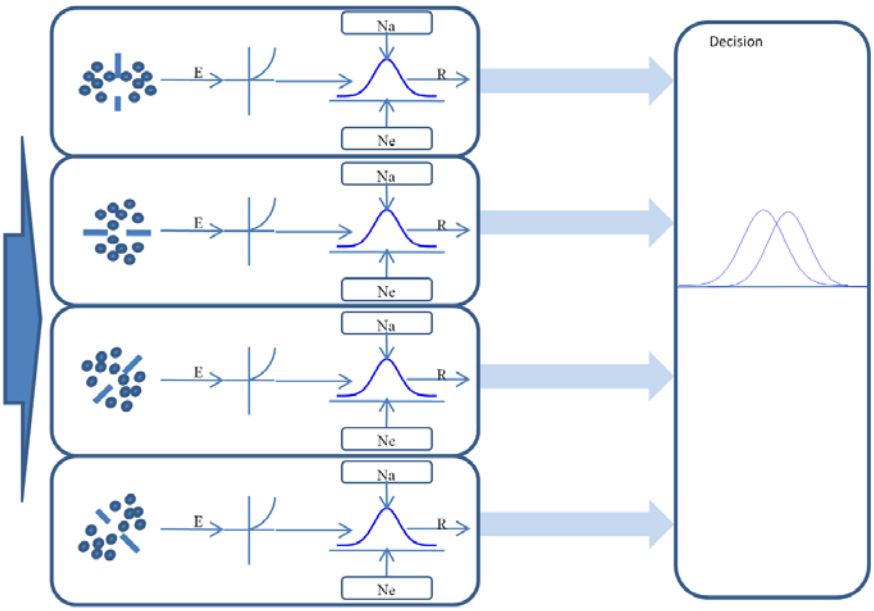

Figure 1.1. Diagram of the model. See text for details.

This model has an extra nonlinear process than the spatial filtering theory and relational structure theory as these two theories are incapable of explaining Chen and Tyler (2010) data. This model is therefore more powerful than other two approaches. This model provides us a good theoretical basis for exploring the possible mechanisms underlying color processing in symmetry perception. In this thesis, we extend Chen-Tyler model (2010), taking the chromatic information into consideration, to investigate the mechanism of chromatic symmetry detection.

1.3. Chromatic Symmetry Detection

The symmetric objects or images in the natural scene often contain more than one color. To form a chromatic symmetry percept, human visual system has to integrate both spatial and chromatic information. Previous research showed that the observers can discriminate the yellow symmetrical pattern from random pattern on isoluminant green background (Troscianko, 1987). It suggested that color can support symmetry. The symmetry detection mechanism must be capable of processing color information. However, how visual system integrates both spatial and color information is unclear. In this thesis, we expand Chen-Tyler model (2010) to cover both spatial and color information in symmetry detection.

Figure 1.2 illustrates our model for chromatic symmetry detection. There are a band of symmetry channels sensitive to the symmetry of the image in this model. Each channel has its symmetry encoder, which is sensitive to the mirror symmetry of a certain color about one axis. The main difference between this model and Chen-Tyler model (2010) is that there are many symmetry encoders each with a different color selectivity. Notice that each symmetry channel tunes to only one color. This is only plotted here only to convey the idea of multiple channels.

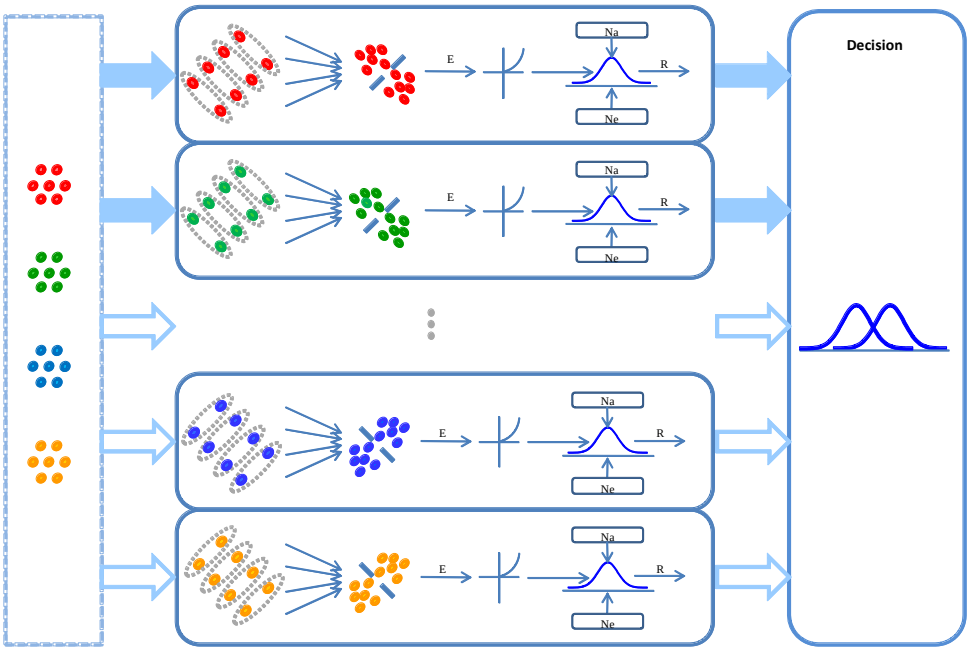

Figure 1.2. Diagram of the chromatic symmetry detection model. See text for details.

To recognize chromatic symmetry, the symmetry encoders need to encode chromatic symmetry information first, that is, to decide which color pairs are the signal while other are not. Computationally, each symmetry encoder can be divided into two steps. In the first step, matching, the symmetry encoder has to extract corresponding color features in an image; and then, pooling, the symmetry encoder has to analyze those color pairs to determine whether their equal-distance points form a symmetry axis. In this stage, the pairs of the same color with the equal-distance points about a symmetry axis are regarded as the signal of that orientation axis while other dots are noise. The registered signal excites the symmetry channel selective to that axis and the color of the signal. The visual system needs to integrate the information from these color-selective symmetry channels to form a chromatic percept.

1.4. Overview of this Thesis

This chromatic symmetry detection model provides us a framework to investigate the color processing in the symmetry detection. We examined the properties of the matching and pooling stages in this thesis, and then investigated how visual system integrates these channels to detect chromatic symmetry. We used a two-alternative forced choice (2AFC) noise masking paradigm to characterize the response properties of the symmetry channels to probe this issue. In Chapter 2, we will introduce the noise masking paradigm used in this thesis. Chapter 3 introduces the details of our chromatic symmetry detection model when it is applied to a 2AFC noise masking paradigm. In Chapter 5 to 9, we will report five experiments, each of which investigated the role of color in different levels of symmetry processing. The general methods used in all the experiments will be introduced in Chapter 4.

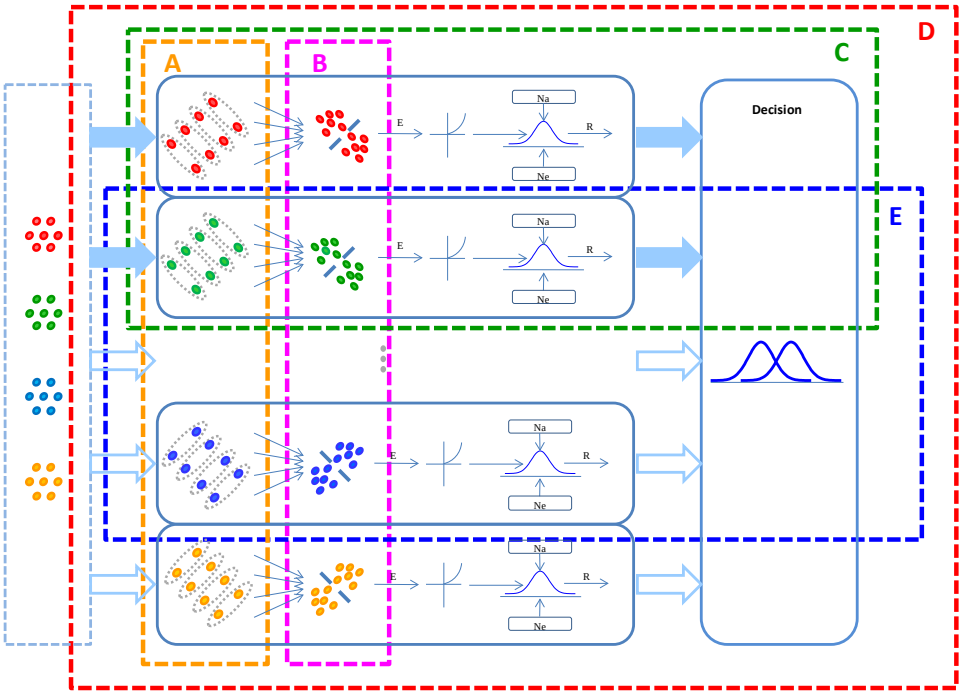

Figure 1.3. The components of chromatic symmetry detection model Chapter 5 to 9 involves. See text for details.

Figure 1.3 illustrates the different components of the model to be investigated by different chapters. Chapter 5 and 6 concern the color selectivity of symmetry encoders (box A and B in *Figure 1.3*). In the Chapter 5, we manipulated the colors of the signal pairs in the symmetric patterns as the same or different and compared their detection thresholds, to investigate the color-selective property of the matching stage of the symmetry encoders (box A in *Figure 1.3*). Chapter 6 concerns the color selectivity of the pooling stage of the symmetry encoders. We measured the target detection thresholds at noises of various colors to examine the existence of the independent symmetry encoders (box B in *Figure 1.3*). In Chapter 7 to 9, we measured the target detection thresholds at various noise densities to get the target threshold vs. noise density (TvD) functions in different conditions, to reveal the characteristics of different channels and their interaction. Chapter 7 concerns the integration of color-selective symmetry channels selective to the same orientation (box C in *Figure 1.3*). We manipulated the number of the colors in the images containing a vertical symmetric pattern to probe this issue. Chapter 8 concerns how visual system integrates the symmetry channels selective to different colors and orientations to detect symmetry when there is uncertainty of axis orientation (box D in *Figure 1.3*). We manipulated the number of the colors in the images containing either a left- or right-diagonal symmetric pattern and compared their TvD functions to achieve this goal. In Chapter 9, we compared the characteristics of the integration between two symmetry channels selective to the same axis (box C in *Figure 1.3*) with two symmetry channels each with different orientation selectivity (box E in *Figure 1.3*). We superimposed two symmetric patterns that share the same symmetry axis or have different orientation selectivity on each other and measured their TvD functions to achieve this goal. This can help us to understand through what mechanism our visual

system forms one coherent symmetry percept rather than two. Chapter 10 is a general discussion about the above studies. We will discuss the implication, the contribution and the limitation of our studies in this chapter.

Chapter 2　2AFC Noise Masking Paradigm

We used a 2AFC noise masking paradigm to measure the target density threshold in all the experiments throughout this project. In a trial of the 2AFC noise masking paradigm, the observer was presented with two intervals, one of which contained a symmetric target (the exception is the experiment in Chapter 9, in which there were two targets superimposed on each other, see method section of Chapter 9 for details) while another one contained a random-dot noise control. Both target and noise control were superimposed on the different amounts of random noise mask. The observer's task was to judge which interval contained a target.

The noise masking paradigm allows us to measure the detection threshold of different symmetry types at various noise levels and thus provide information that reveals the internal response properties of human observers (for a review, see Lu & Dosher, 2008). According to Signal Detection Theory (Green & Swets, 1966), the observer's decisions are based on the probability distributions of internal response to the noise and to the signal plus the noise. (*Figure 2.1a*). In a 2AFC task, these two distributions are provided by the responses to the two test intervals in a trial. That is, in each trial, the observer compares the magnitudes of the two internal responses and decides which one of the two intervals generates a greater internal response and thus contains the target. Mathematically, this comparison can be achieved by observing whether the response difference to the two intervals to be greater than zero. Thus, our main concern can be placed on the distribution of the difference between the internal responses to the two intervals (*Figure 2.1b*).

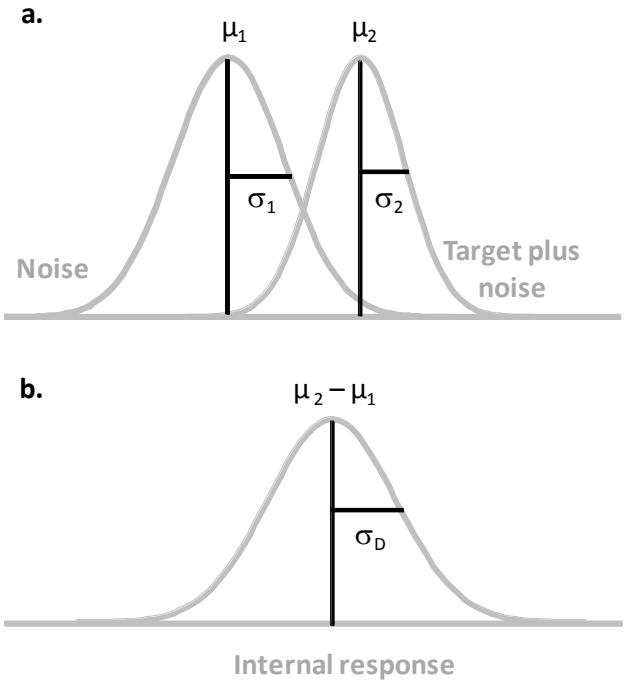

Figure 2.1. The internal representation in a two-alternative forced-choice (2AFC) noise masking task. (a) The stimuli in the interval that contains the target and noise and that contains the noise generate different internal response distributions. An observer compares the magnitudes of two response distributions to make a decision about which interval contains a target. (b) The internal response of comparison is the distribution of the differences between the internal responses to the two intervals.

The variability of the internal response distributions comes from two sources, the external noise manipulated by the experimenter and the intrinsic noise of the system. If the external noise is relatively low, the variability of the distribution is dominated by the internal noise. Thus, the performance is not affected by the change in the external noise. A relatively constant amount of signal is required for the observer to detect the target (the dashed horizontal line in *Figure 2.2*). However, when the external noise is much greater than the internal noise, the variability of the response distribution is determined by the external noise. Increasing the amount of signal is

thus necessary for the observer to detect the symmetry target as external noise increases (the dashed oblique line in *Figure 2.2*). At the transition point of these two regimes, the amounts of the internal and the external noises are equal (N_{eq} in *Figure 2.2*).

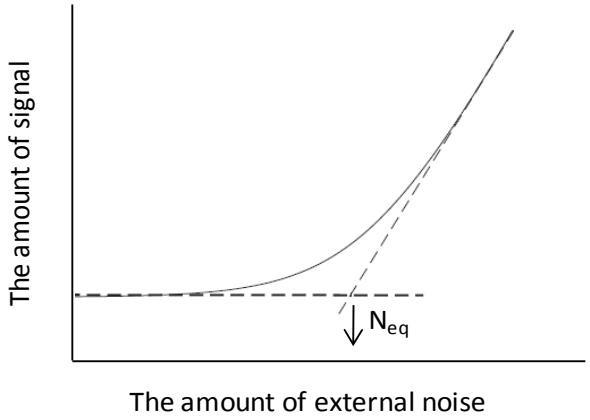

Figure 2.2. An illustration of the amount of signal required to detect target at different amounts of external noise. When the amount of external noise is relatively small, the increase of the external noise does not influence the amount of signal required. When the amount of external noise is much larger than that of internal noise, the amount of signal required increases with the increment of the external noise. The transition point (N_{eq}) of these two regimes reveals the magnitude of the internal noise of the system.

Hence, by manipulating the amounts of the external noise, we can measure the target detection threshold at different amounts of noise, and in turn the target threshold vs. noise density (TvD) function. The transition point on the TvD function reveals the magnitude of the internal noise of the system. The slope of the TvD function reflects the nonlinear property of the response mechanism. This allows us to estimate the internal response properties of human observers more accurately, to

investigate the response properties of symmetry channels. To investigate how human visual system integrates the responses of color-selective symmetry channels in symmetry detection, we manipulated the number of the colors in the stimuli in the 2AFC noise mask task and got their TvD functions. The properties of the TvD functions allow us to investigate the interaction of the channels in different conditions. The next chapter introduces our chromatic symmetry detection model and how we used it to account for the properties of the TvD functions in the 2AFC noise masking paradigm.

Chapter 3 Chromatic Symmetry Detection Model

In this chapter, we introduce our chromatic symmetry detection model and describe how we apply it to the 2AFC noise masking task used in the experiments. Note that in each trial of the task, the stimuli consisted of either a symmetric target or a non-symmetric random-dot control superimposed on a random-dot mask. All stimuli in a trial contained the same number of the colors with equal probability, in which the number of the color (*n*) was from 1 to 4.

As *Figure 1.2* shown, the chromatic symmetry detection model contains two stages: a perception stage and a decision stage. The perception stage concerns the noise-limited sensitivity of a visual mechanism to the stimuli limited by both internal and external noise, while the decision stage concerns the effect of uncertainty on the decision criterion.

The first step of the perception stage is a band of color-orientation selective symmetry encoders that are sensitive to symmetry in an image. Each encoder is sensitive to the mirror symmetry about one axis with a certain color. As mentioned in Chapter 1, each encoder contains two steps, matching and pooling. The matching stage extracts the corresponding color features in an image while the pooling stage analyzes those color pairs to determine whether their equal-distance points form a symmetry axis. In other words, these symmetry encoders are long-range pairs of local multiplicative color detectors that register a signal whenever there is their target color at two locations in the field equidistant from a symmetry axis. The outputs of all such pairs of detectors relative to a given symmetry axis are linearly summed to form the symmetry signal relative to that location. Only when a number of them line up with

respect to a particular symmetry axis, the symmetry encoders regard the chromatic pattern as symmetry.

In the 2AFC noise masking task, the image in the interval that contains target plus mask can be considered to consist of two components: the symmetric target and the noise mask, while the image in the interval that contains noise control plus mask can be considered to consist of just one component with a density that is the sum of the control and the mask.

For a sparse n-color random-dot pattern, the excitation of the j-th color-selective symmetry encoder to the i-th image component, E_{ji}, is

$$E_{j,i} = Se_{j,i} \cdot \frac{1}{n} D_i \qquad (1)$$

where $Se_{j,i}$ is the sensitivity of the j-th symmetry encoder to i-th image component, while $1/n*D_i$, is the dot density of the pattern of the j-th encoder' target color in i-th image component. The total excitation of j-th encoder, E_j, is the sum of excitations produced by all image components,

$$E_j = \sum_i E_{j,i} \; . \qquad (2)$$

The response of the perception stage is the excitation of the j-th symmetry encoder, E_j, raised by a power p, and then divided by a divisive inhibition term I_j plus an additive constant z,

$$R_j = \frac{E_j^p}{I_j + z} \tag{3}$$

where I_j is the summation of a non-linear combination of the inhibition from all image components to mechanism j. This divisive inhibition term I_j can be represented as

$$I_j = \sum_i \left[\left(Si_{j,i.tc} \cdot \frac{1}{n} D_i \right)^q + \left(Si_{j,i.nc} \cdot \frac{n-1}{n} D_i \right)^q \right] \tag{4}$$

where $Si_{j,i.tc}$ and $Si_{j,i.nc}$ are a positive value serving as the inhibition term from the image components consisting of the target color and of the non-target color respectively.

The contribution of each channel to the visual performance is limited by both internal noise of that channel and the external noise provided by the noise patterns. The variability of the internal noise, σ_a^2, is a constant for all symmetry channels. The variability of external noise, σ_e^2, is proportional to the square of the density of random noise mask, that is, $\sigma_e^2 = v * D_b^2$ in which v is a scalar constant and the index b denotes the noise mask. Pooled together, in each channel the standard deviation of the response distribution is

$$\sigma_r = \left(v \cdot D_b^2 + \sigma_a^2 \right)^{1/2}. \tag{5}$$

The output of the perception stage is then sent to the decision stage. The decision stage monitors more channels than those that are relevant to the visual tasks (Pelli, 1985). The performance of the system is limited not only by the noise in the relevant

channels but also by that in the irrelevant channels. In our experiment, the task of the observer was to detect the symmetry component in an image. Hence, a relevant channel is the one whose color-orientation selectivity matches that of the image. The observer detects a symmetric pattern if the maximum response of all monitored channels to an image is greater than the response of a random-dot pattern by an amount that exceeds the level of noise in the system (Green & Swets, 1966).

When there are *m* channels, in which n channels are relevant while *m*-*n* channels are irrelevant, to be monitored, the maximum response of these channels can be described by a distribution whose mean approximates a fourth-power summation over these m channels (Graham, Robson, & Nachmias, 1978; Quick, 1974; Pelli, 1985), though the Gaussian distribution theory of Tyler and Chen (2000) shows that the fourth power exponent is valid only for the restricted conditions of a particular attention model and a linear signal transducer. Hence, for the target plus mask images where there are n channels responding the symmetry image component, the mean of the response R' can be expressed as

$$R'_{b+t} = \left(\sum_{j=1}^{n} R_{j,(b+t)}^{4} + \sum_{j=n+1}^{m} R_{j,(b+c)}^{4} \right)^{1/4}, \quad (6)$$

where the subscript b and t denote the noise control pattern and the symmetry component in the images respectively. Instead, the mean of the response R' for the noise control plus noise mask images is

$$R'_{b+c} = \left(\sum_{j=1}^{m} R_{j,(b+c)}^{4} \right)^{1/4}, \quad (7)$$

in which the subscript b+c indicates that the image contains both the noise mask and a control pattern with the same number of dots as the corresponding symmetry target. The decision variable, d', is the difference of the response to the image with the symmetry component and the response to the random-dot control image divided by the standard deviation of the max distribution, σ_p. That is,

$$d' = \left(R'_{b+t} - R'_{b+c}\right) / \sigma_p \tag{8}$$

The threshold is defined when d' reaches unity. Note that the standard deviation of the max distribution of multiple independently and identically distributed samples is k times the standard deviation of the original distribution, in which the variable k can be estimated by the method Chen and Tyler (1999) proposed. Thus, $\sigma_p = \sigma_r$ for 1-color condition while $\sigma_p = k*\sigma_r$ for n-color conditions.

The above is the description of our chromatic symmetry detection model that applies to a 2AFC noise masking task. In Chapter 5 and 6, we examined the color-selective property of the symmetry encoders in the model. In Chapter 7 to 9, we manipulated the number of the colors in the images and measured the symmetry detection threshold to get the TvD functions, to investigate the integration of these symmetry channels in different conditions. The details of the model implementation are described in each chapter.

Chapter 4 General Method

In this thesis, our aim is to understand how visual system integrates both color and spatial information to form symmetry perception. To understand how symmetry mechanism processes the color information of the images coming from different color channels, we selected the colors in the stimuli on the MB-DKL color space, in which the chromatic content of color is defined by three cardinal axes based on the response properties of three post-receptoral mechanisms (Derrington, Krauskopf, & Lennie, 1984; Krauskopf, Williams, & Heeley, 1982; MacLeod & Boynton, 1979). This chapter introduces the way we constructed the color space to define the color content of the stimuli and the general method among all the experiments.

4.1. Equipment

All experiments in this study used the same equipment. The visual stimuli were presented on a 24-inch calibrated LCD monitor controlled by a Macintosh computer via a Radeon 7200 graphic board which provided 10-bit digital-to-analog converter depth. The LCD monitor was calibrated with a PhotoResearch PR655 radiometer for both luminance and chromaticity. The viewing distance was set in a way that each pixel extended 2^{o} visual angles. The refresh rate of the monitor was 60Hz.

4.2. Specification of the Chromatic Content of the Stimuli

In all of the experiments, the display had a mean luminance of 76.81 cd/m^2 and mean chromaticity at (0.33, 0.33) in CIE 1931-xy coordinates. All the colors of the display were along a straight line in cone excitation space. The color can be

represented by a cone contrast vector (Brainard, 1996) at each point in space. Since the stimuli were composed of 8-th power Gaussian spots, we described their contrast by giving the three cone contrast at the center of the spots. The L-cone contrast, C_L, was defined as $\Delta L/L_0$ where L_0 was the L-cone excitation produced by the background and $\Delta L = L - L_0$ was the L-cone excitation deviation at the central point of the spots. If there was a decrement in cone excitation at the central point, the cone contrast was negative. The M-cone and S-cone contrasts, C_M and C_S, were defined similarly and each color was given by the column vector $\boldsymbol{C} = [C_L, C_M, C_S]^T$. Cone excitations and contrasts were calculated using the Stockman-Sharpe estimates of the cone spectral sensitivities (Stockman & Sharpe, 2000). For calculations, each sensitivity was normalized to a maximum of one and spectra were expressed in units of watts/($sr - m^2 - nm$). The LMS cone excitation vector of background was $[6.056\ 5.235\ 2.701]^T$.

We specified all the colors in term of their contrast and chromoluminance direction. Chromoluminace direction was given by the normalized vector, $\boldsymbol{C} / \| \boldsymbol{C} \|$, where the notation $\| \boldsymbol{C} \|$ denoted the length of the vector $\boldsymbol{C}$. The contrast of each color was defined as $c = (C_L^2 + C_M^2 + C_S^2)^{0.5}/(3)^{0.5}$. This measure was proportional to the square-root of cone contrast energy and varies between 0 and 1. Contrast was expressed in dB re 1 which equaled $20 \log_{10} c$. The contrast of each color in all the experiments was set at its three fold threshold for each observer, based on a subjective sensitivity experiment (see Appendix for details).

Except for some colors in the experiment of Chapter 6, all the colors of the stimuli were in the cardinal directions of the color space (Derrington et al., 1984; Krauskoph et al., 1982; MacLeod & Baynton, 1979). As shown in *Figure 4.1*, the black and white were in the luminance direction (-90° – +90°), of which the L, M, S cone contrasts is [0.577, 0.577, 0.577]. The red, green, blue, and yellow were in the

Red/Green (0°–180°) and Blue/Yellow (90°–270°) isoluminant directions whose cone contrasts were [0.416, -0.909, 0] and [0, 0, 1] respectively. The nominal isoluminant directions were orthogonal to the CIE2007 luminous efficiency function V_λ (CIE, 2007), which corresponded to the normalized column vector $[0.853, 0.522, 0]^T$ in the cone contrast space.

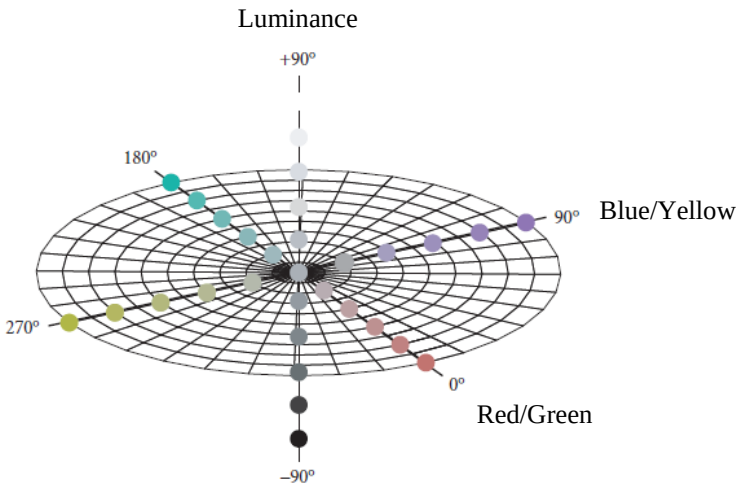

Figure 4.1. Cone contrast color space. The grid corresponds to the isoluminant plane, which includes the Red/Green (0° – 180°) and Blue/Yellow (90° – 270°) cardinal mechanisms axes. The vertical axis is the achromatic axis (-90° – +90°).

For the convenience of discussion, we used descriptive color names rather than cone contrasts for the modulation directions to describe the colors in our stimuli. Table 4.1 lists the descriptive color names of the colors we used, their coordinates in the DKL color space and in the cone contrast space.

Table 4.1

The coordinates of the color space and chromoluminance cone contrast space of the color.

Name	Coordinates in DKL space	Coordinates in the cone contrast space (C_L, C_M, C_S)
White (W)	(0°, 90°)	[0.577, 0.577, 0.577]
Black (K)	(0°, -90°)	[-0.577, -0.577, -0.577]
Red (R)	(0°, 0°)	[0.416, -0.909, 0.000]
Blue (B)	(90°, 0°)	[0.000, 0.000, 1.000]
Green (G)	(180°, 0°)	[-0.416, 0.909, 0.000]
Yellow (Y)	(270°, 0°)	[0.000, 0.000, -1.000]

4.3. Stimuli

All stimuli were chromoluminance images composed of the dots distributed in an invisible grid, excluding some checks at the center region and near axis (see method section in each chapter). The width of each check was 7 pixels, corresponding to 0.21^o visual angle. The display had a 9.9^o visual angle extent in the experiments of Chapter 5 to 7 while a 12.1^o visual angle extent in the experiments of Chapter 8 and 9. Each dot was defined by a 8-th power Gaussian function, or $\boldsymbol{K}(x, y) = \boldsymbol{BG} + \boldsymbol{BG}.* \boldsymbol{C} \exp(x^8/2\sigma^8 + y^8/2\sigma^8)$ where x and y were the distances in degrees from the fixation point, $\sigma = 0.11^o$ was the space constant; $\boldsymbol{BG}$ was a 3 by 1 vector that specified the cone excitation coordinates of the background; **C** was the 3 by 1 cone contrast that specified the color modulation respectively, and the symbol .* denoted element by element multiplication of two vectors.

The stimuli on each trial consisted of three components: the symmetric target, the non-symmetric random-dot control, and the random-dot mask. Both the control

and the mask were composed of random dots. In a symmetric target, half of the displays was a reflection of the other half about an axis whose orientation was either vertical or one of the two diagonals. That is, a pixel at position (x,y) of the symmetric image I has the property I(x', y') = I(-x', y') where x' = x*cosθ + y*sinθ and y' = y*cosθ - x*sinθ. The symbol θ denoted the orientations of the symmetry axis with θ = 0° for the vertical and 45° and 135° for the two diagonal symmetry axes. The density of target, control and mask were described in the method section of each chapter.


國立臺灣大學
人格教育・學生愛國

Chapter 5 Color-Selective Matching Stage

In our chromatic symmetry detection model, we assume that the first step of symmetry detection, the matching stage, is color-selective. In this stage, each color-selective symmetry encoder compares the corresponding features in an image. It extracts the corresponding features of its target color and sends the pairs to the next stage for further operation (box A in *Figure 1.3*). In other words, only the feature of the same color can be paired. In this chapter, we examined the above assumption.

Specifically, we examined three possible ways that color information may affect the symmetry encoding at this stage. First, the symmetry encoder may only pair image features of the same color (*Figure 5.1*a). Such encoder would have a color tuning property similar to that of V4 cells reported by Lennie (1999) who reported that every V4 cell has its own color selectivity. Second, in addition to the same color pairs, the symmetry encoder may be able to pair opponent colors, such as red and green together (*Figure 5.1*b). This notion is consistent with the notion proposed by De Valois and de Valois (1993) that the visual cortex contains pairs of neurons whose color selectivity is from rectified responses of the same color opponent channel. Third, it is also possible that the symmetry encoder just receives inputs from a wide range of earlier mechanisms and thus has no color selectivity itself. That is, the symmetry encoder may pair the corresponding image features regardless their colors (*Figure 5.1*c).

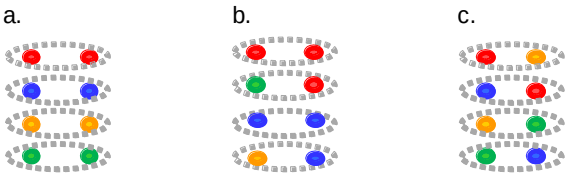

Figure 5.1. Three possible ways the symmetry encoder acts in the matching stage. (a) The symmetry encoder only pairs the image features of the same color. (b) The symmetry encoder can pair the image features of the opponent colors. (c) The symmetry encoder is not color-selective. It pairs the corresponding image features regardless their colors.

In the luminance domain, several studies measured the symmetry detection performance when the corresponding image features were opposite luminance polarity, called anti-symmetry (*Figure 5.2b*) (Brooks & van der Zwan, 2002; Mancini, Sally & Gurnsey, 2005; Saarinen & Levi, 2000; Tyler & Hardage, 1996; Wenderoth, 1996; Zhang & Gerbino, 1992). There is no consistency in the results from the studies with achromatic patterns. Some showed difficulty in detecting anti-symmetry (Brooks & van der Zwan, 2002; Mancini et al. 2005; Wenderoth, 1996; Zhang & Gerbino, 1992) while others did not (Mancini et al. 2005; Saarinen & Levi, 2000; Tyler & Hardage, 1996). Mancini et al. (2005) used stimuli composed of large image elements in different luminance (*Figure 5.2*). They manipulated the proportion of the matched image elements and measured the coherence threshold of symmetry detection (e.g., the proportion of the matches required for an image to be discriminated from a random pattern). They showed no difference in the coherence threshold between detecting symmetric and anti-symmetric patterns. Similar result was also reported in other studies with achromatic stimuli composed of large image elements (Saarinen &

Levi, 2000; Tyler & Hardage, 1996). On the other hand, some studies reported that it was more difficult in detecting anti-symmetry than detecting symmetry in images composed of small image elements, in either coherence threshold measurement (Mancini et al. 2005) or correct rate and response time (Brooks & van der Zwan, 2002; Wenderoth, 1996; Zhang & Gerbino, 1992).

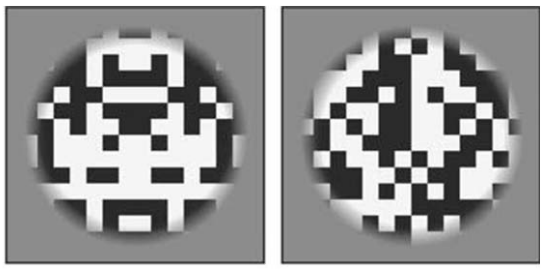

Figure 5.2. The stimulus composed of achromatic large image elements. Panel a and b were symmetry and anti-symmetry respectively. (From Mancini et al., 2005)

It seems that the symmetry detection performance is not the same for the images composed of small and large image elements. The studies using images composed of large image elements showed that detecting anti-symmetry was as easy as detecting symmetry (Mancini et al. 2005; Saarinen & Levi, 2000; Tyler & Hardage, 1996). It suggested that the matching process is not necessarily restricted to the image elements with the same luminance. However, the studies using images composed of small image elements showed that the detection performance for a symmetric pattern was better than an anti-symmetric one (Brooks & van der Zwan, 2002; Mancini et al. 2005; Wenderoth, 1996; and Zhang & Gerbino, 1992). It suggested that matching process is restricted to image elements with identical luminance.

There are only a handful of studies concerning the color selectivity of the matching stage of symmetry detection. Pashler and his colleges investigated the role of color in symmetry detection (Huang & Pashler, 2002; Morales & Pashler, 1999). They presented their observers patterns composed of colored squares. The arrangement of squares were either completely symmetric about the vertical axis or contained one or two pairs that were mismatched in color. Their observers needed to indicate whether the pattern was color-symmetrical (Morales & Pashler, 1999). *Figure 5.3a* shows an example of their stimuli. Similar procedure was applied when the patterns were anti-symmetric (i.e., the corresponding regions across the symmetry axis have opposite color, *Figure 5.3b*) (Huang & Pashler, 2002). Their data showed that it was more difficult for their observers to detect anti-symmetry than symmetry. The response time (2569 ms) was much longer and the error rate (0.19) was larger for the anti-symmetry condition than the symmetry condition (RT = 1187 ms, error rate = 0.05).

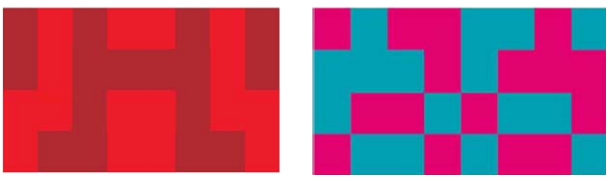

Figure 5.3. The stimuli Pashler and his colleges used. Panel a is a 2-color symmetric display. Panel b is an anti-symmetric display. Both are the examples of symmetry. (From Morales & Pashler, 1999 and Huang & Pashler, 2002.)

The studies using achromatic images showed that symmetry detection performance was not the same for the images composed of small and large image elements. However, even the images were composed of large image elements, the

symmetry detection performance was still different when the images were composed of achromatic elements and chromatic elements. Detecting achromatic anti-symmetry was as easy as detecting achromatic symmetry (Mancini et al. 2005; Saarinen & Levi, 2000; Tyler & Hardage, 1996) while detecting chromatic anti-symmetry was more difficult than detecting chromatic symmetry (Morales & Pashler, 1999; Huang & Pashler, 2002). It seems that the symmetry detection for chromatic and achromatic images differs. However, the stimuli used by Pashler and his colleges may have some pitfalls so that it is difficult to compare their result with the achromatic one. First, their stimuli were not isoluminant and were not designed to isolate individual color channels from the others. It is not clear which channel is responsible for their results. All three post-receptoral channels might involve in the analysis of their stimuli. Second, their image elements were not adjusted to the equal sensitivity level for the human visual system. Some colors might be more salient than others. Hence, the difficulty in anti-symmetry might be due to the relative salience of a particular color or color pair. Their results thus give us little insight into the matching stage of the chromatic symmetry processing.

In addition, the discrepancy in the literature may be understood in our framework. In the luminance domain, the major discrepancy occurs between the studies with large-and small image elements. For the same display area, the larger the elements are, the fewer the number of the elements is, and *vice versa*. That is, the difference in element size also means a difference in density. Hence, if we present their results as a TvD function, the coherence thresholds for the symmetric images composed of small and large elements would be represented as two points at different noise densities. Hence, the coherence thresholds for symmetry and anti-symmetry are the same for the images composed of large elements also means that they are the same at low noise

densities while the difference in the symmetric and anti-symmetric images composed of small elements also means that they are different at high noise densities. In other words, the discrepancy in the literature means that the TvD functions for symmetric and anti-symmetric patterns have different slopes. Thus, it is possible to account for the diversity of the data in the literature with the same model but with different parameter values.

In sum, current results from the literature do not have a conclusive answer to the property of the matching stage of symmetry processing. In this chapter, we examined the color selectivity of the matching stage of symmetry processing. For a comparison, we also examined the color selectivity in luminance dimension. We deliberately manipulated our stimuli for this purpose. First, we selected the color along the cardinal axis in the color space, in which the chromatic content of color is expressed in a space defined by three cardinal axes based on the response properties of three post-receptoral mechanisms (Derrington, et al., 1984; Krauskopf, et al., 1982; MacLeod & Boynton, 1979), to tag the three post-receporal color mechanisms in symmetry detection. Second, we set the contrast of each color to match the contrast threshold of each observer to that color, and thus controlled the salience of each color. Third, we measured the target detection thresholds at different amounts of external noise. This allowed us to examine whether the number of elements in the images can account for the difference between the images composed of small and large elements mentioned above. We used the stimuli composed of sparse small dots. This allowed us a wide range of noise for manipulation.

We compared the detection performance for two kinds of anti-symmetric patterns, one had two dots in a symmetric pair to be in opponent colors (i.e., opponent anti-symmetry condition) while the other had the two dots in colors of different

cardinal directions (i.e., non-opponent anti-symmetry condition), with that for the symmetric patterns. If the symmetry encoder can only match the image features of the same color, the threshold for both opponent and non-opponent anti-symmetry conditions would be greater than that in the symmetry condition and thus would produce an upward shift of the TvD function relative to that for the corresponding symmetry conditions. However, if the symmetry encoder can match dots of opponent colors, the TvD functions for the opponent anti-symmetry condition and the symmetry condition would be the same, while the TvD functions for the non-opponent anti-symmetry condition would raised from the symmetry condition. If the symmetry encoder has no color selectivity, all the TvD functions should be the same. By observing the TvD functions for different conditions, we can infer the color selectivity of the matching stage of the symmetry processing.

5.1. Method

Participant. Three observers participated in this experiment: CCW, CPY, and HYC. HYC was naïve to the purpose of this experiment.

Stimuli. There were eight conditions in this experiment including four isoluminance and four luminance conditions. The four isoluminance conditions were RG, RB, Anti-RG and Anti-RB and the four luminance conditions were WK, WR, Anti-KW, and Anti-WR, where R, G, B, W, and K refer to red, green, blue, white and black respectively (see Table 4.1 in Chapter 4 for definition of the color). The RG, RB, WK, and WR were symmetry conditions, in which the color in each symmetric dot-pair was the same. The Anti-RG and Anti-KW were opponent anti-symmetry conditions while the Anti-RB and Anti-WR were non-opponent anti-symmetry conditions. In these four anti-symmetry conditions, the colors of each symmetric pair

were opposite. For example, the images in the RG condition were composed of the red-red pairs and green-green pairs, while those in the Anti-RG condition comprised of the red-green and the green-red pairs.

In each trial, the stimuli consisted of a vertical symmetric-dot target (symmetry or anti-symmetry, depends on the condition) or a non-symmetrical random-dot noise control superimposed on a random-dot mask. *Figure 5.4* shows the example of the stimuli. The panel a and b in *Figure 5.4* are the example of the stimuli in the symmetry and anti-symmetry conditions respectively. The purpose of the random-dot control was to balance the local statistics in the image. The colors of dots in the noise mask were the same as the symmetric target and the noise control while were randomly assigned. The densities of the noise mask were 0.2, 1, and 10%. To prevent the observers from using only the local information near axis to make a judgment, the region within 1.4° visual angle width contained no dot.

Procedure. A temporal 2AFC paradigm was used to measure the density threshold of the symmetric target detection. In each trial, the symmetrical dots display was randomly presented in one of the two intervals while the control random dots display was presented in another interval. The duration was 233 ms and the inter-stimulus interval (ISI) was 600 ms. An audio tone indicated the beginning of each interval. The observers' task was to judge which stimulus interval contained a symmetric pattern. They were informed that the orientation of axis was vertical. An audio feedback for the response was provided. The PSI threshold-seeking algorithm (Kontsevich & Tyler, 1999) was used to measure the threshold at 75% correct level. There were 40 trials for each threshold measurement. Each datum point reported was an average of four to eight repeated measurements. The symmetry conditions and the anti-symmetry conditions were run separately. The order of the four symmetry

conditions was randomized. So were the four anti-symmetry conditions.

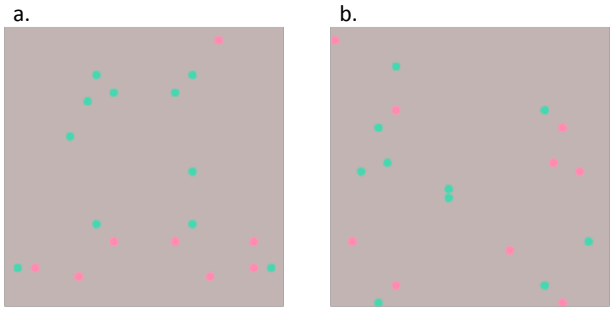

Figure 5.4. The example of the stimulus in this experiment. Panel a is the stimuli in the symmetry conditions, in which a symmetric target was superimposed on the noise mask. Panel b is the stimuli in the anti-symmetry conditions, in which an anti-symmetric target was superimposed on the noise mask.

5.2. Results

Figure 5.5 shows the TvD functions for four isoluminance conditions. The left column is the TvD functions for the opponent anti-symmetry condition (i.e., Anti-RG, red symbols) and its corresponding symmetry condition (i.e., RG, blue symbols). The right column represents the TvD functions for the non-opponent anti-symmetry condition (i.e., Anti-RB, pink symbols) and its corresponding symmetry condition (i.e., RB, green symbols). Each column represents the data of each observer. For these four isoluminance conditions, the target density threshold increased with the noise density. The slope of the functions for all conditions and observers was from 0.88 to 1.15 in log-log coordinates. Averaged across observers, the slopes of the TvD function for the opponent anti-symmetry (M = 1.04, SE = 0.07) and the non-opponent anti-symmetry condition (M = 1.07, SE = 0.03) were not different from their

corresponding symmetry conditions (M = 1.10 and 1.07, SE = 0.008 and 0.02 respectively, all $t(2) < 0.66$, all $p > .58$). Hence, the TvD functions for anti-symmetry and symmetry conditions were parallel.

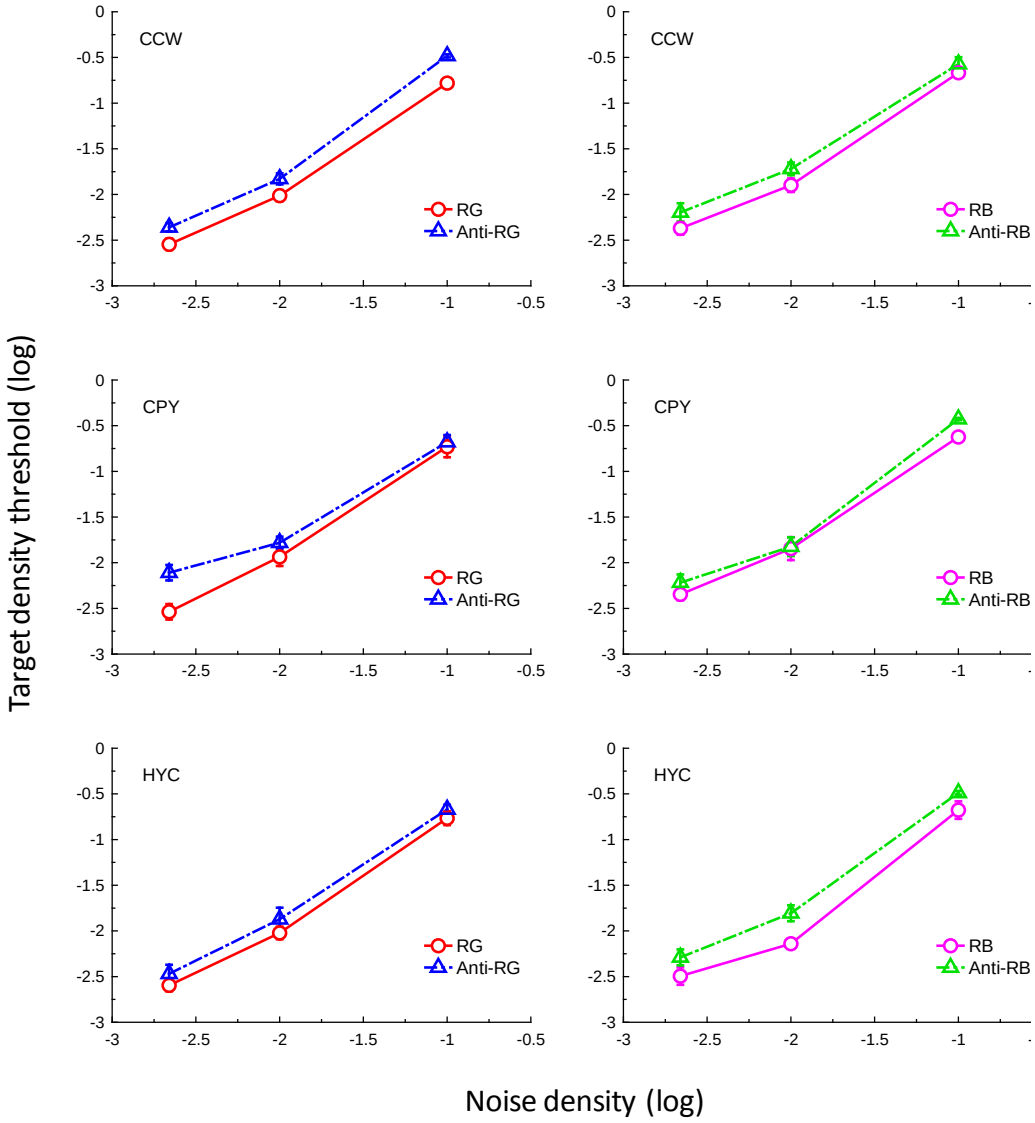

Figure 5.5. The target threshold vs. mask density (TvD) functions for four isoluminance conditions. Each panel represents the data from one observer. The left column represents the TvD functions for the RG (red symbols) and the Anti-RG (blue symbols) conditions. The right column represents the TvD functions for the RB (pink symbols) and the Anti-RB (green symbols) conditions.

Figure 5.6 shows the TvD functions for four luminance conditions. The left column is the TvD functions for the opponent anti-symmetry condition (i.e., Anti-WK, red symbols) and its corresponding symmetry condition (i.e., WK, blue symbols). The right column represents the TvD functions for the non-opponent anti-symmetry condition (i.e., Anti-WR, pink symbols) and its corresponding symmetry condition (i.e., WR, green symbols). Each column represents the data of each observer. The slope of the functions for all conditions and observers was from 0.87 to 1.24 in log-log coordinates. Similarly, the TvD functions for the anti-symmetry and the symmetry conditions were parallel. Averaged across observers, the slopes of the TvD functions for the opponent anti-symmetry (M = 1.06, SE = 0.06) and the non-opponent anti-symmetry condition (M = 1.00, SE = 0.06) were not different from their corresponding symmetry conditions (M = 1.09 and 1.03, SE = 0.06 and 0.03 respectively, all $t(2) < 1.64$, all $p > .24$).

Averaged across observers, our results also showed that the target density thresholds for four anti-symmetry conditions were higher than their corresponding symmetry conditions (all $t(2) > 5.99$, $p < .014$). The pink, green, red and blue symbols in *Figure 5.7* represent the increment of the density thresholds produced by Anti-WK, Anti-WR, Anti-RG, and Anti-RB conditions compared with their corresponding symmetry conditions respectively, averaged across observers. For all anti-symmetry conditions, the magnitude of the threshold elevation was from 0.15 to 0.33 log unit (or a 1.4 to 2.1 fold change). The threshold increments in the luminance conditions were higher than in the isoluminance conditions, regardless of opponent ($t(2) = 2.83$, $p = .05$) or non-opponent pairs ($t(2) = 10.76$, $p = .004$). Moreover, there was no difference in the density threshold elevation between the opponent and the non-opponent anti-symmetry conditions, in both isoluminance ($t(2) = 0.58$, $p = .62$) and luminance

conditions ($t(2) = 1.39$, $p = .30$). These results suggest that the symmetry encoder has difficulty in matching dots with different colors, regardless whether they are opponent colors or not. The difficulty is larger when there is a luminance component involved.

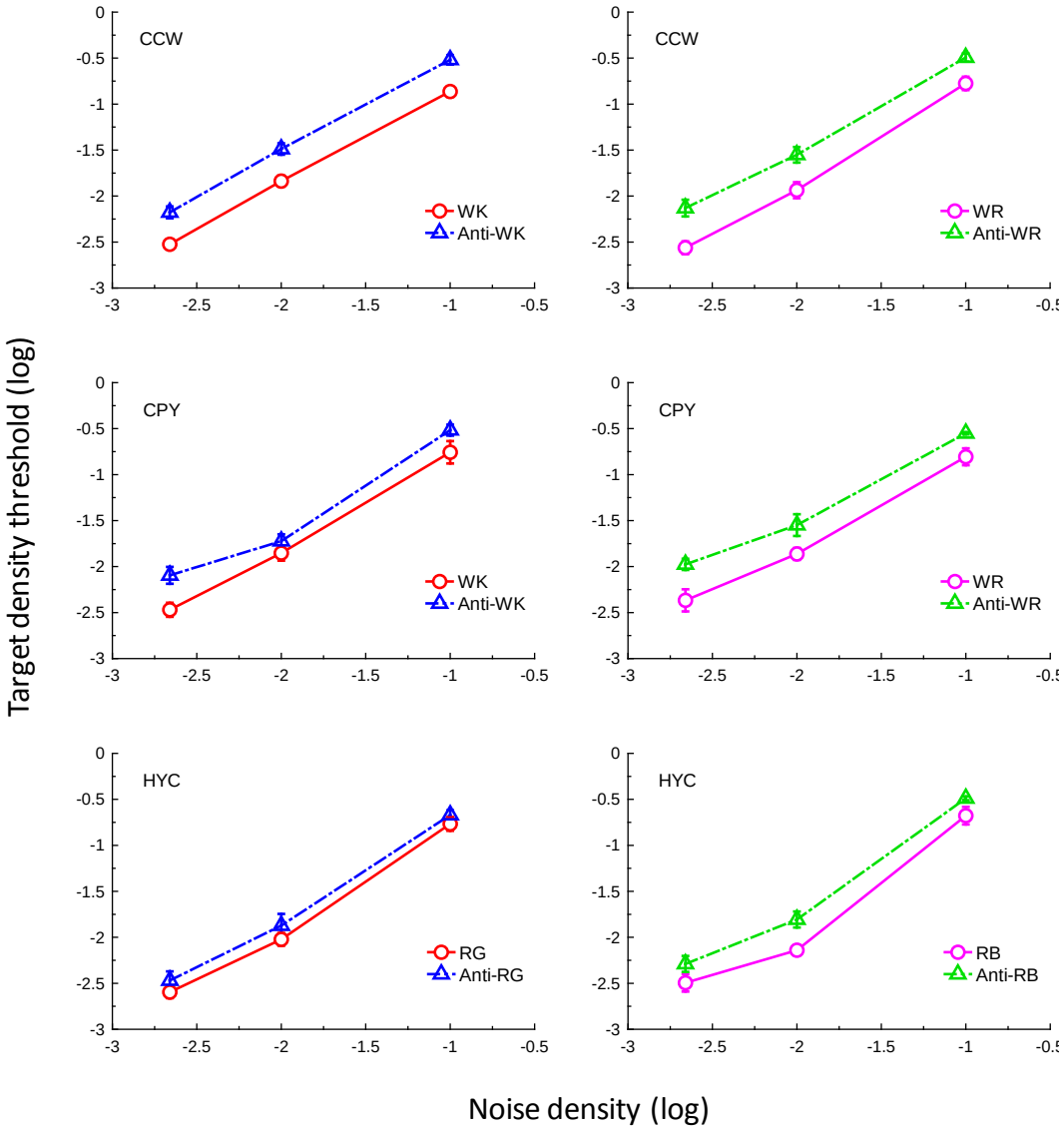

Figure 5.6. The target threshold vs. mask density (TvD) functions for four luminance conditions. Each panel represents the data from one observer. The left column represents the TvD functions for the WK (red symbols) and the Anti-WK (blue symbols) conditions. The right column represents the TvD functions for the WR (pink symbols) and the Anti-WR (green symbols) conditions.

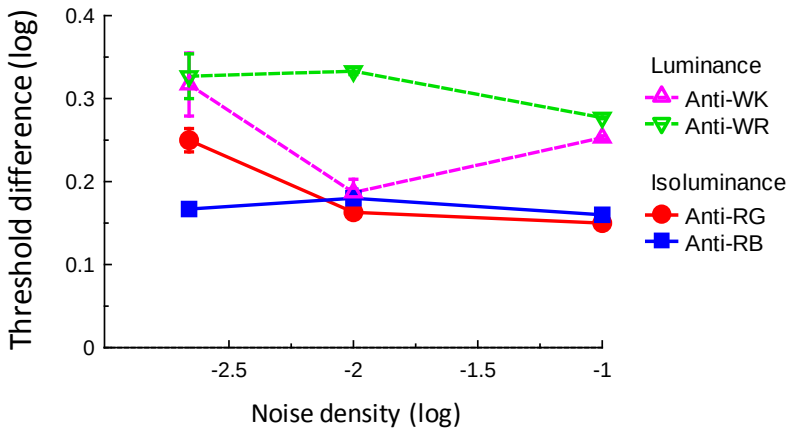

Figure 5.7. The average threshold elevation at different noise densities in four anti-symmetry conditions compared with their corresponding symmetry conditions. The open symbols represent the threshold elevation in luminance conditions (pink up-triangles and green down-triangles for the Anti-WK and the Anti-WR respectively). The filled symbols represent the threshold elevation in isoluminance conditions (red circles and blue squares for the Anti-RG and the Anti-RB respectively).

5.3. Discussion

Our result showed that the matching stage of symmetry encoder is color-selective. The symmetry encoder can easily match the dots of the same color but not those of different colors even these different colors are from the same color opponent channel. Furthermore, it is more difficult for the symmetry encoder to match two dots with luminance difference than those with chromaticity difference.

Such color selectivity suggests that the symmetry encoders have a property similar to that of V4 cells, which has its own color selectivity (Lennie, 1999) but not V1 cells, whose color selectivity is from rectified responses of the same color opponent channels (De Valois & de Valois, 1993). This property suggests that the

symmetry perception is mediated by a neural mechanism beyond V1. This is consistent with neuroimaging evidence, which showed the symmetric visual stimuli produced an increment of fMRI activity in higher-tier human visual cortex, such as V3A, V4, V7, and the lateral occipital complex (LOC) (Sasaki, Vanduffel, knutsen, Tyler, & Tootell; 2005; Tyler, Baseler, Kontsevich, Likova, Wade, & Wandell, 2005).

Our data also showed a selectivity in luminance. This is consistent with the previous studies using the images composed of small elements (Brooks & van der Zwan, 2002; Mancini et al. 2005; Wenderoth, 1996; Zhang & Gerbino, 1992). In addition, our data showed an overall upward shift of the TvD functions for the anti-symmetry conditions, compared with those for their corresponding symmetry conditions. This suggests that the inconsistence between the achromatic images composed of the large and small elements discussed above is not due to the image density. Otherwise, the slopes of the TvD functions for the anti-symmetry and symmetry conditions should differ. We suspect that this inconsistence might be due to some other reasons. For example, the comparison of local information is easier in the images composed of large elements than those composed of small elements, etc.

After equating sensitivity for the isoluminance and luminance stimuli, our data showed that matching two colors with different chromaticity was easier than matching those with different luminance. This might reflect different mechanisms of chromaticity and luminance information processing in the earlier stage. Processing of the luminance-increase is in the ON channel and that of the luminance-decrease information is in the OFF channel (Schiller, 1992). These two processes remain independent in the retina and LGN, with some evidence suggesting that the channels may be functionally segregated as far as the visual cortex (Harris & Parker, 1995). The difficulty in matching two colors with different luminance suggests that

information processed between different channels is difficult to be combined during symmetry processing, as Van der Zwan, Badcock and Parkin (1999) and Dakin and Herbert (1998) suggested. However, as discussed above, the property of the matching stage of symmetry encoders is similar to that of V4 cells that may tune to any color (Lennie, 1999). Hence, the difficulty in matching two chromaticity suggests that information processed between different color channels is difficult to be combined during symmetry processing. However, this difficulty may be smaller than that of luminance channels. This difference suggests that the different properties of earlier color processing are still preserved in the early stage of symmetry processing. Whether this difference preserves in the later stages of symmetry detection process is a question. In the next chapter, we keep concerning this issue when investigate the color-selectivity of the pooling stage following the matching.

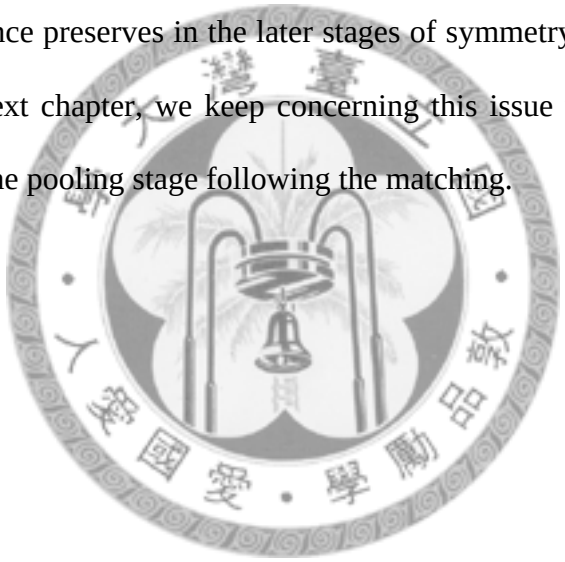

Chapter 6 Color-Selective Pooling Stage

In Chapter 5, we showed that the matching stage is color-selective, as our chromatic symmetry detection model shown. The symmetry encoder is easier to pair the features of the same color (e.g., red-red) than those of different colors (e.g., red-green). In this chapter, we further examined the color selectivity of the next stage, pooling.

Similar to the matching stage, we considered three possible ways the symmetry encoder pools the matched pairs to determine the axis of a symmetric pattern. The first one, the symmetry encoder only counts the pairs of the same color for the computation of the symmetry axis (*Figure 6.1a*). The pairs whose midpoints form an axis are regarded as signal while others are noise. In this case, the color selectivity is preserved at the pooling stage. The second one, the symmetry encoder counts the pairs as signal as long as their colors are from the same color opponent channels (*Figure 6.1b*). For instance, a symmetry encoder may regard both the red-red and the green-green pairs as signal but not the red-red and the blue-blue pairs. The third one, the symmetry encoder is not color-selective. All the pairs are taken into account regardless of their chromaticity (*Figure 6.1c*). These three pooling mechanisms represent different color selectivity of symmetry channels. The first two suggest that there are more than one color selective channels in symmetry processing while the third one suggests that there is only one color-blind symmetry channel.

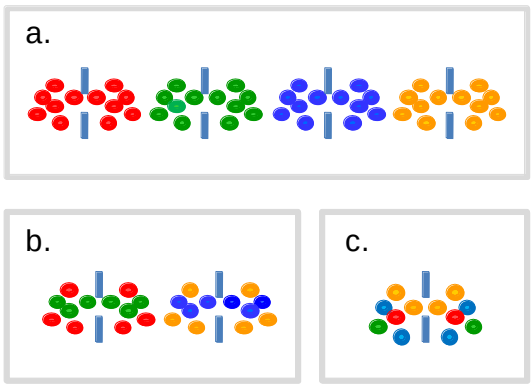

Figure 6.1. Three possible ways the symmetry encoder acts in the pooling stage. (a) The symmetry encoder only counts the pairs of the same color for the computation of the symmetry axis. (b) The symmetry encoder counts the pairs as signal as long as their colors are from the same color opponent channels. (c) The symmetry encoder is not color-selective. All the pairs are taken into account to determine the symmetry axis regardless of their colors.

To the best of our knowledge, there is no published research systematically examines the color selectivity of the pooling stage in symmetry processing. In this chapter, we investigated the color selectivity of the pooling stage of the symmetry encoder, that is, which color pairs can be pooled to determine the symmetry axis. Here we used noise masking paradigm to probe this issue. We measured the target density threshold with the presence of noise masks of various colors. If the response of the underlying mechanism is influenced by the noise mask, the mask would interfere with the target mechanism and thus produce a masking effect, measured as threshold increment, on target detection. Otherwise, the presence of the mask would have no effect on target detection (Giulianini & Eskew, 1998; Gegenfurtner & Kiper, 1992; Hansen & Gegenfurther, 2006). Hence, if the symmetry encoder pools only the pairs of the same color, only the mask of the same color would produce a masking

effect. If the symmetry encoder can pool the pairs of the opponent colors, a symmetry target of a color would be masked by masks both of its own color and its opponent color. If the pooling stage is not color-selective, all the noise masks would show masking effect.

This chapter examines the color selectivity of the pooling stage of symmetry processing. Since Chapter 5 showed the difference in pairing image features with different chromaticity and luminance, we also examined the color-selective properties of the pooling stage in both chromaticity and luminance dimensions. We measured the target detection threshold of the red, blue and white target superimposed on the noise mask of different colors to achieve this goal.

6.1. Method

Participant. Three observers attended this experiment: CCW, CPY and HYC. HYC was naïve to the purpose of the experiment.

Stimuli. In each trial, the stimuli consisted of a vertical symmetric-dot target or a random-dot noise control superimposed on a random-dot noise mask. The color of the target and the noise control was red and blue in the isoluminance conditions while was white in the luminance conditions (see Table 4.1 in Chapter 4 for the definition of the color). The colors of the noise mask were 0°, 22.5°, 45°, 67.5°, 90°, and 180° deviated from the target along the isoluminant plane in the isoluminance conditions and along the plane spanned by the red-green cardinal axis and the luminance axis in the luminance condition. The density of the noise mask was fixed at 0.01. To prevent observers from using only the information near axis to make a judgment, no dot was in the region within 1.4° visual angle width. *Figure 6.2* shows the examples of our stimuli.

Figure 6.2. The example of the stimuli: (a) the red target superimposed on the noise mask of its own color (0° deviation) and (b) the red target superimposed on the noise mask of green color (180° deviation). The mask density was 1%.

Procedure. The 2AFC procedure was the same as the experiment represented in Chapter 5. The observers' task was to judge which stimulus interval contained the target. They were informed that the orientation of axis was vertical. The two chromaticity conditions and one luminance condition were run separately. The order of noise color in both conditions was randomized.

6.2. Results

Our results showed a clear color-selective property of the pooling stage. The highest target density threshold was measured when the noise mask and the target were of the same color in both isoluminance and luminance conditions. *Figure 6.3* shows the target density threshold in the isoluminance conditions. The red and blue circles represent the density threshold for the red and blue target respectively in the presence of the various noise masks. The pink and cyan open triangles represent the

red and blue target density threshold respectively when there is no mask. Each panel represents the data from one observer.

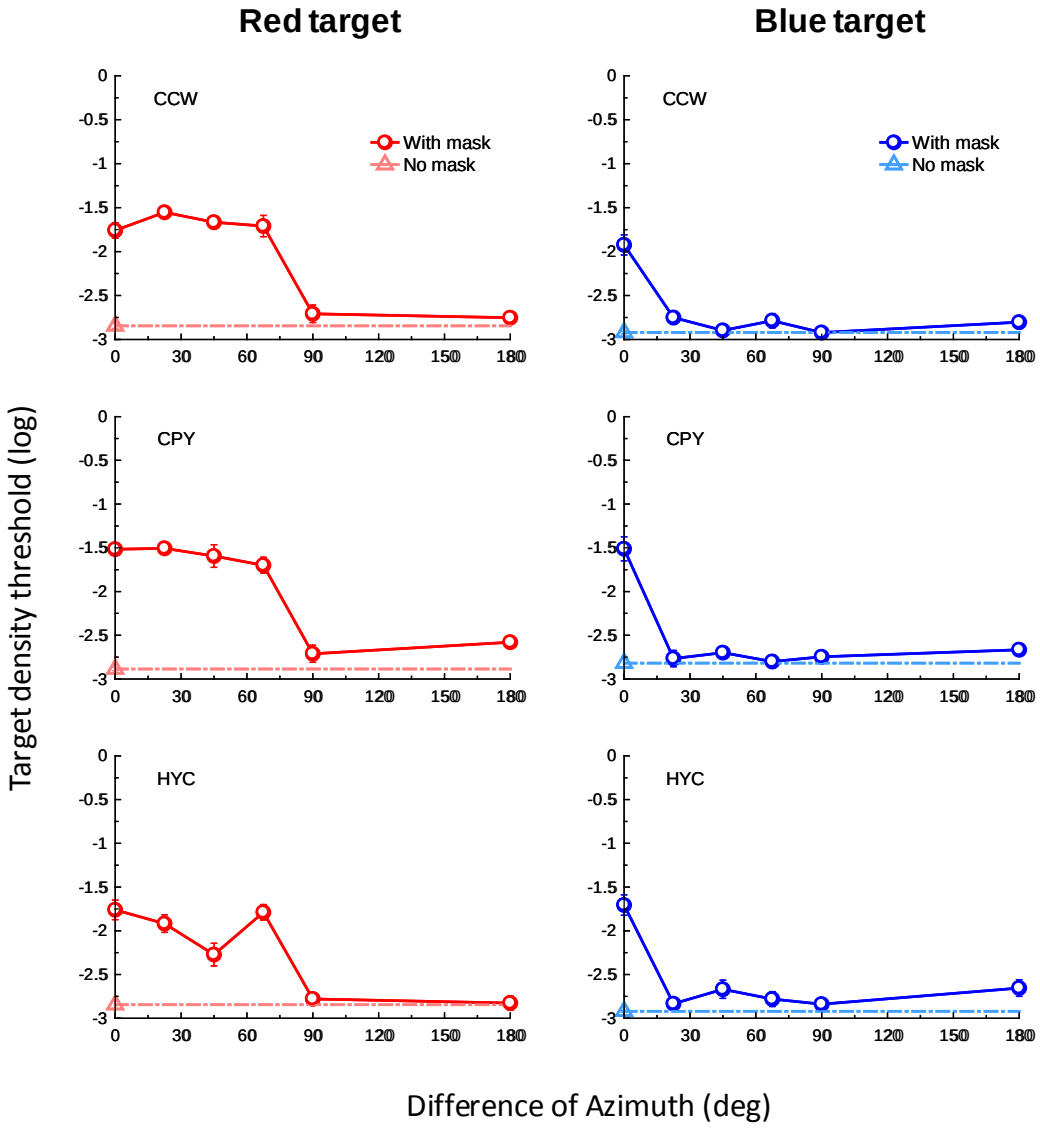

Figure 6.3. The results of isoluminance conditions. Each panel represents data from one observer. The red and blue symbols denote the target density thresholds for red and blue target superimposed on the noise mask of various colors respectively. The pink and cyan symbols denote the red and blue target density threshold when there was no mask, serving as a baseline.

For all observers, the mask of the same color (0° deviation from the target in the isoluminance plane) increased the target detection threshold 1 to 1.37 log unit, which was 10 to 23 fold change. The masking effect decreased as the difference between the target and the mask color increased. The mask of orthogonal color (90° deviation from the target in the isoluminance plane) and opponent color (180° deviation) showed little, if any, masking effect. They increased the target detection threshold about 0 to 0.3 log unit, equivalent to 1 to 2 fold change. This effect was small when compared with the effect of the same color. Hence, our results favored the first hypothesis. That is, the symmetry mechanism pools the pairs of the same color to determine the axis. The visual system has a band of independent color-selective symmetry channels at each orientation axis.

Our data also showed that the color tuning of each color-selective symmetry encoder was not the same. The color tuning of the red symmetry encoder was broader than that of the blue one. The red symmetry encoder responded to a range of colors with different sensitivities (22.5° to 67.5° deviation) while the blue symmetry encoder only responded to a narrower range of colors. The mask of the colors deviated more than 22.5°from the target color produced no masking effect to the target detection. This might be due to the difference in sensitivity between the red-green and the blue-yellow channels

The results of the luminance conditions were similar to those of the isoluminance conditions. *Figure 6.4* shows the data for the luminance conditions. The black and gray symbols represent the target density thresholds in the presence and absence of noise mask respectively. Each panel represents the data from one observer.

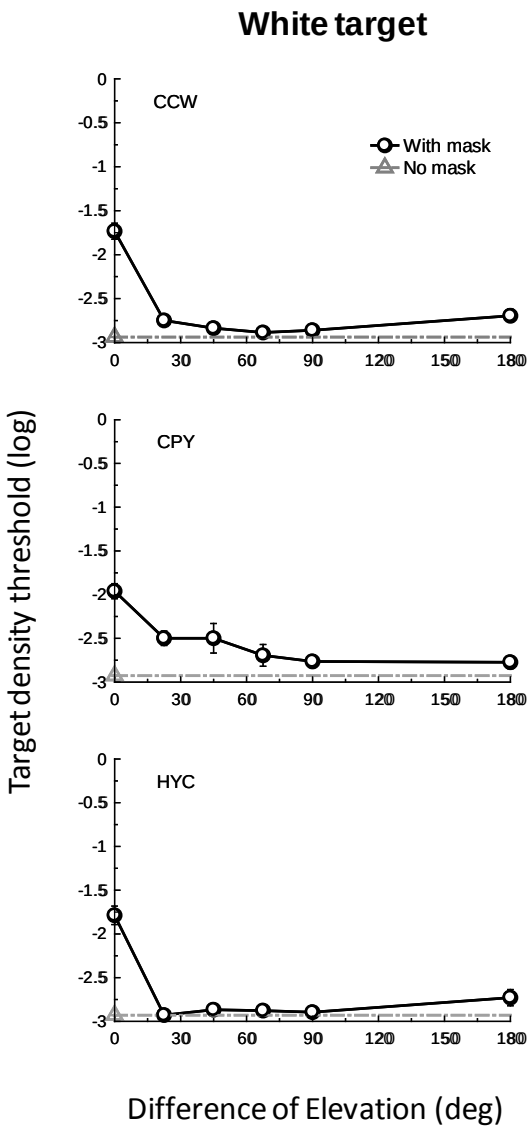

Figure 6.4. The results of luminance conditions. Each panel represents data from one observer. The black symbols denote the target density thresholds for white target superimposed on the noise mask of various colors. The gray symbol denotes the target density threshold when where was no mask, serving as a baseline.

Similar to the isoluminance conditions, the masking effect was largest when the color of the mask was the same as the target. For all observers, the mask of the same

luminance increased the target detection threshold 0.97 to 1.2 log unit (equivalent to 9 to 16 fold change). The masking effect decreased as the difference between the target and the mask luminance increased. The mask of isoluminance color (90° deviation from the target on the plane spanned by the red-green cardinal axis and the luminance axis) and opposite luminance polarity (180° deviation) showed little, if any, masking effect. They increased the target detection threshold about 0.03 to 0.24 log unit (1.08 to 1.75 fold change), much smaller than that produced by the mask of the same luminance. Our results also showed that the white symmetry encoder only responded to a narrower range of colors, narrower than that of the red one. The mask of larger than 45° deviation from the target color produced no masking effect to the target detection.

6.3. Discussion

In this experiment, we used the noise masking paradigm to investigate the color-selective property of the pooling stage of symmetry processing. Our results showed that the noise mask of the same color with the target produced the largest masking effect on the target detection. The masking effect decreased as the difference in the color between the target and the mask increased. This suggests that the color-selective property is preserved in the pooling stage. The symmetry encoder counts only the pairs of the same color for the computation of the symmetry axis. Hence, the presence of dots in a different color would not interfere with symmetry detection. Hence, there are a band of color-selective symmetry encoders at each orientation.

Notice that, our result shows that the symmetry processing is color selective at the encoding stage. It is by no means implying that the symmetry channel is color selective. It is possible that a later mechanism integrates information across different

color selective encoders. However, if this is the case, the integration should occur after a nonlinear operation has been applied to the color specific symmetry channels. Otherwise, such mechanism cannot distinguish information from different colors and thus inherently color blind. Our result does not support such color blind mechanism.

Some might argue that the masking effect we observed may be unrelated to the color-selective pooling stage but due to the color selective matching stage. The noise mask of the same color as the target can be paired with the dots in the target while that of the different colors cannot. Hence, the dots in the noise mask interfered with the symmetric target detection by matching rather than pooling. However, if this is the case, we should expect that the noise mask that has a different color from the target should also show a masking effect, because the symmetry encoders would take all the pairs in the noise mask into consideration to determine the axis of a symmetric pattern. Our results however did not support this claim. Except for the luminance condition of the observer CPY ($t(1) = 37.75$, $p = .008$), the mask of the orthogonal color and opponent color showed no masking effect (all $t(1) < 5.24$, $p > .06$).

Another argument is that the masking effect is unrelated to the color-selective pooling stage but due to selective attention. For example, the observers may just pay their attention to the target color and ignore whatever other colors in the display. Hence, the dots of the other colors are not encoded in the matching stage and are left out in the pooling stage. Hence, the pooling stage is not necessarily color-selective as we claim but color-blind. To exclude this possibility, we carried out a control experiment. We excluded the effect of selective attention to reexamine the color-selectivity of the pooling stage. In this control experiment, we presented two symmetric patterns of different axes superimposed on each other in one interval and a random dot pattern in another interval. The colors of the two symmetric patterns were

the same (i.e., both red or both green, Image A in *Figure 6.5*a) or different (i.e., one red and one green, Image B in *Figure 6.5*b). The random dot pattern contained the same number of red and/or green dots as the interval containing the targets. The observer's task was to detect which interval contained any symmetric pattern. In this experiment, the observers needed to pay attention to all colors in the display to get max information.

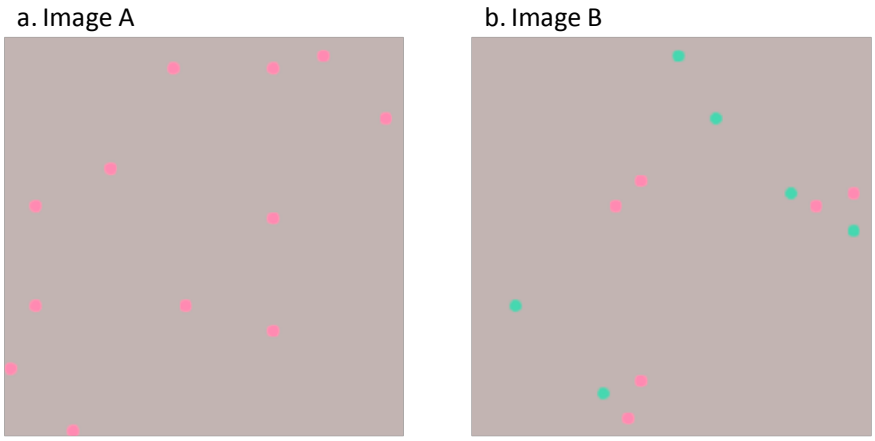

Figure 6.5. The target stimuli of control experiment. Each target image was composed of two symmetric patterns of same or different colors. (a) Image A was a red right-diagonal symmetric pattern superimposed on a red left-diagonal symmetric pattern. (b) Image B was a red left-diagonal symmetric pattern superimposed on a green right-diagonal symmetric pattern.

In this case, the color-selective and color-blind pooling stage hypotheses make different predictions about the symmetry detection performance in these two images. The color-blind hypothesis predicts the same performance in the two images while color-selective one does not. If the pooling stage of symmetry encoder is color-blind, there are only two orientation-selective symmetry encoders, one sensitive to the left-

diagonal and another one, the right-diagonal. For these two symmetry encoders, half of the dots in Image A are signal and another half are noise. So is Image B. Hence, the color-blind hypothesis predicts no difference in symmetry detection performance between these two images. However, if the pooling stage of symmetry encoder is color-selective, there are four symmetry encoders involved in this task: red left-diagonal, red right-diagonal, green left-diagonal, and green right-diagonal ones. The presence of Image A would produce an excitation in the red left-diagonal and red right-diagonal symmetry encoders. In Image A, half of red dots are symmetric about the left diagonal axis while the other half, the right diagonal axis. Thus, for the red left-diagonal symmetry encoder, the red dots that are symmetric about the left diagonal axis are considered as signal while those dots that are symmetric about the right diagonal have no structure to the left diagonal axis and thus are considered as noise. Hence, for the red left-diagonal symmetry encoder, half of the dots in the Image A are signal while another half dots are noise. The same consideration also applies to the red right-diagonal symmetry encoder. On the other hand, the presence of Image B would produce an excitation in the red left-diagonal and green right-diagonal symmetry encoders. For the red left-diagonal symmetry encoder, the red dots that are symmetric about the left diagonal axis are considered as signal. The green dots that are symmetric about the right diagonal have no structure to the left diagonal axis. However, since the symmetry encoder is color-selective, these green dots would not be considered as noise by the red left-diagonal symmetry encoder. Hence, for the red left-diagonal symmetry encoder, half of the dots in the Image B are signal while the other half is ignored. The same argument also applies to the green right-diagonal symmetry encoder. On the other hand, for the green left-diagonal symmetry encoder, there is no signal dots in the image in which the green dots that are symmetric about

the right diagonal axis but are structureless for the left diagonal axis. Hence, for this encoder, half of the dots in the pattern are noise while none is signal. Similar argument can be applied to the red right-diagonal symmetry encoder. Hence, the signal to noise ratios for these two images differ in these color-selective symmetry encoders and in turn the symmetry detection performance. Our results showed such difference in detection performance. The averaged data from three observers showed that the target density threshold for the Image A (M = -1.36, SE = 0.12) is much higher than that for the Image B (M = -2.42, SE = 0.22), $t(4) = 4.25$, $p = .007$. This supports the color-selective hypothesis. There should be a band of color-selective symmetry encoders in our visual system. This implies the existence of a band of color-selective symmetry channels.

The next step is to characterize how our visual system integrates these color-orientation selective symmetry channels to perceive chromatic symmetry. Recall that our visual system needs to integrate the responses of orientation-selective symmetry channels to detect symmetry when there is only one color in the images (Chen & Tyler, 2010). The more orientation-selective symmetry channels the visual system monitors, the worse the symmetry detection performance. If the images contain more than one color, our visual system needs to integrate a band of color-orientation selective symmetry channels to perceive chromatic symmetry. Does the integration of the responses of color-selective symmetry channels differ from that of orientation-selective ones? If yes, what is the difference? If no, whether the increment of the number of the colors in an image increases the uncertainty of symmetry detection, leading to worse performance, just like the uncertainty effect of the orientation axis? Or color facilitates the symmetry detection by other mechanisms? In Chapter 7 to 9, we investigate this issue by the noise masking paradigm mentioned above.

Chapter 7 Integration of the Color-Selective Symmetry Channels

In Chapter 5 and 6, we studied the color-selective property of the symmetry encoder. The result suggests that the symmetry channels are color selective. Hence, to perceive a symmetric object with more than one color in a nature scene, the visual system needs to integrate the responses of these color-selective symmetry channels. This chapter concerns how the human visual system integrates the response of color-selective symmetry channels selective to the same orientation to form a chromatic symmetry percept.

Chen and Tyler (2010) proposed a theory on how the visual system integrates the information from several orientation-selective symmetry channels. The more orientation-selective symmetry channels one has to monitor, the larger uncertainty is in the system. The increment of uncertainty degrades symmetry detection performance. In the context of this study, if an image contains more colors, it would produce a response in more channels in the visual system. Since an observer can detect a target when the response in any of the channels reaches a critical value or threshold, it would be easier for an observer to detect a 2-color and a 4-color pattern than a 1-color pattern if the component of each color in the 2-color and 4-color pattern has the same number of dots as the 1-color pattern. However, for the images of the same density, the number of dots in each component of the 2-color pattern was only half of that in the 1-color pattern while the number of dots in each component of the 4-color pattern was only 1/4 of that in the 1-color pattern. According to the probability summation theory (Quick, 1974), the threshold for the 2-color pattern

should be 1.68 (i.e., $1/(0.5^4 + 0.5^4)^{0.25}$) times that of the 1-color pattern and the threshold for the 4-color pattern, 2.83 (i.e., $1/(0.25^4 + 0.25^4 + 0.25^4 + 0.25^4)^{0.25}$). Hence, the more colors an image contains, the more difficult it is for a human observer to detect the symmetric pattern in the image.

Previous studies showed little consent on this issue. Using chromatic stimuli, Morales and Pashler (1999) and Huang and Pashler (2002) showed that the increment of the number of the colors degraded the symmetry detection performance. They showed their observers images that either were completely symmetric in color about the vertical midline, or contained one pair of squares that were mismatched in color. There were either two or four possible colors in each display. The observers' task was to indicate whether the pattern was symmetric in color. They showed that the response time for detecting 4-color display (1961 ms) was longer than that for detecting 2-color display (1187 ms). However, others showed no difference in both response time and correct rate between 1- and 2-color achromatic symmetric patterns composed of sparse small dots (Brooks & van der Zwan, 2002; Wenderoth, 1996; Zhang & Gerbino, 1992). The increment of the number of the colors did not impair the performance of symmetry detection. The results from the achromatic stimuli were inconsistent with that from the chromatic stimuli. However, as discussed in Chapter 5, the stimuli used by Pashler and his colleges were not isoluminant and were not designed to isolate individual color channels. All three post-receptoral channels might involve in the analysis of their stimuli. In addition, they deliberately chose the colors such that every pair of colors in the 4-color displays was more easily discriminated than the pair in the 2-color displays. For example, the colors in their 2-color displays were crimson and scarlet while whose in the 4-color displays were green, yellow, blue, and red. However, this manipulation might lead to larger luminance difference

between the pairs in the 2-color displays than in the 4-color displays and larger chromatic difference between the pairs in the 4-color displays than in the 2-color displays. Hence, the better detecting performance in the 2-color displays may be due to the larger luminance contribution or the less chromaticity contribution in the 2-color displays than in the 4-color displays. In other words, their results cannot distinguish whether the better performance of detecting symmetry in the 2-color displays than in the 4-color displays was due to the less chromatic symmetry channels involved or large contribution of luminance symmetry channels than chromatic symmetry channels. It is difficult to compare the symmetry detection performance between chromaticity and luminance dimensions from the previous research.

In this chapter, we selected the colors in the cardinal directions of the color space to isolate different symmetry channels and manipulated the number of the colors in vertical symmetric images, from one to four, to investigate how visual system integrates the information from these color-selective symmetry channels to detect chromatic symmetry. We used the noise masking paradigm to measure the target density thresholds at various noise densities and to characterize the response properties of the symmetry channels. We also used both isoluminance and luminance stimuli to investigate whether the chromatic and luminance symmetry mechanisms differ. If the chromatic and luminance symmetry mechanisms differ, we should observe different performance for these two types of stimuli.

7.1. Method

Participant. Three participants attended this experiment: CCW, CPY, and HYC. HYC was naïve to the purpose of this experiment.

Stimuli and Procedure. There were nine conditions in this experiment including five isoluminance and four luminance conditions. The five isoluminance conditions were R, B, RG, RB, and RGBY and the four luminance conditions were W, WK, WR, and WKRG, where R, G, B, Y, W, and K refer to red, green, blue, yellow, white and black respectively (see Table 4.1 in Chapter 4 for the definition of the color). The R, B, and W were 1-color condition. The stimuli contained only one color. In another six conditions, the stimuli contained two (2-color condition, i.e., RG, RB, WK, and WR) or four colors (4-color condition, i.e., RGBY and WKRG) with equal density. The target in each condition was a vertical symmetric-dot pattern containing 1, 2, or 4 colors. The mask was a random-dot noise pattern containing the same color as the target. The stimuli consisted of a target or a random-dot noise control, whose color is the same as the target, superimposed on a mask (*Figure 7.1*). The purpose of the random-dot control was to balance the local statistics in the image. The density of noise masks was from 0 to 1%. The region within 1.4° visual angle from the vertical axis contained no dot to prevent the observers from using only the local information near axis to make a judgment. The 2AFC procedure was the same as that in the previous chapters. The order of five isoluminance and four luminance conditions was randomized.

Figure 7.1. The example of the stimuli. Panel a, b, and c represent the target of 1, 2, and 4 colors superimposed on the noise mask of the same colors as the target respectively.

7.2. Results

Figure 7.2 shows the TvD functions for the five isoluminance conditions respectively. Each panel represents the TvD functions from one observer. The red, blue, green, purple, and pink symbols represent the data points of the R, B, RG, RB, and RGBY conditions respectively. The smooth curves are fits of the model discussed below. For all conditions, the target density threshold increased with noise density. At median to high noise densities, the slope of the increment function reached an average of about 1.15 in log-log coordinates for all conditions and observers. There was no difference in the slope among the 1-, 2-, and 4-color conditions, averaged across three observers (There was no difference in the slope between two 1-color conditions. Hence, we pooled them together for analysis. So were the two 2-color conditions). However, at low noise densities, the slope of the TvD functions varied with the number of the colors (Also, we pooled the two 1-color conditions together and the two 2-color conditions together to analyze for the same reason). Averaged across observers, the slopes of the TvD functions for the 2- and 4-color conditions (0.83 and 0.75 respectively) were smaller than that for the 1-color conditions (1.06, all $t(2) > 3.15$, $p < .05$, see *Figure 7.3*).

Figure 7.4 shows the facilitation effect of the number of the colors in the isoluminance conditions. The green, purple, and orange symbols in *Figure 7.4* denote the threshold difference between the three multi-color conditions (RG, RB, and RGBY) and the average of the two 1-color conditions (The thresholds showed no difference between these two conditions for each observer. Hence, we pooled these two conditions together for analysis.) averaged across three observers respectively. As the figure shown, the threshold reduction in the multi-color conditions increased with the increment of the noise densities at low noise densities. At median to high noise

densities, the threshold reduction was relatively constant. The magnitude of the threshold reduction across three multi-color conditions was from 0.06 to 0.31 log unit (or 1.15 to 2 fold change) at median to high noise densities.

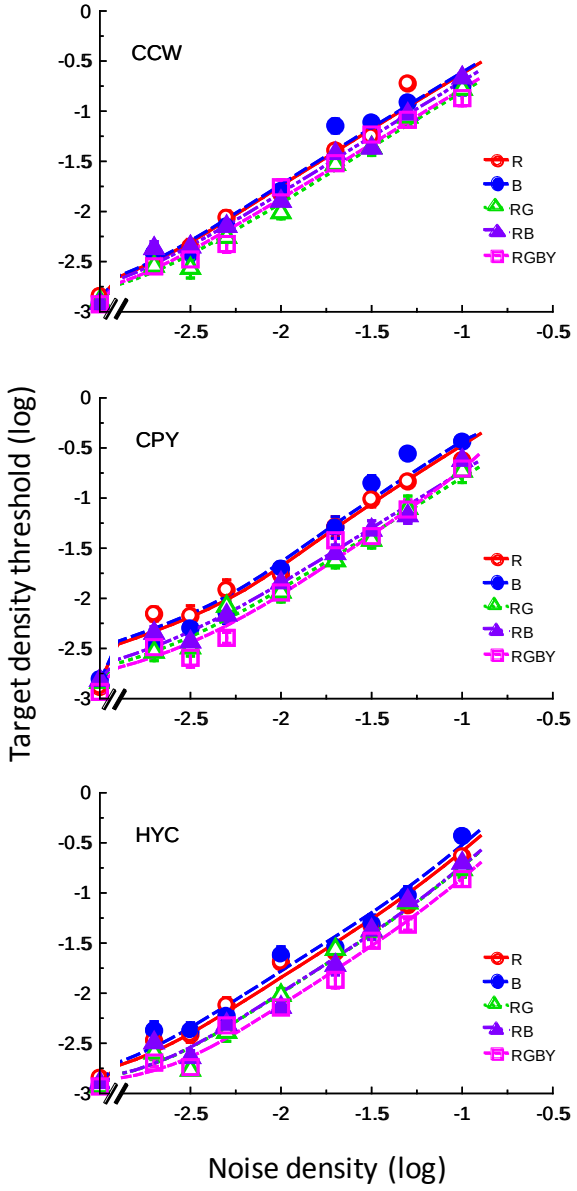

Figure 7.2. Target threshold vs. mask density (TvD) functions for the isoluminance conditions. Each panel represents the data from one observer. The red, blue, green, purple, and pink symbols represent the data points of the R, B, RG, RB, and RGBY conditions respectively. The smooth curves are fits of the model (see text for details).

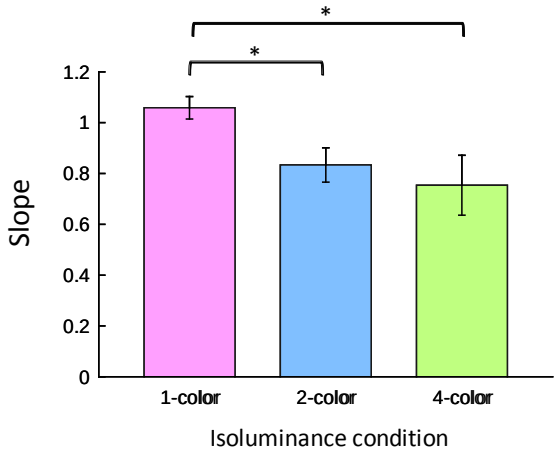

Figure 7.3. The average slopes of the target threshold vs. mask density (TvD) functions for the 1- (red bar), 2- (blue bar) and 4-color isoluminance conditions (green bar) at low noise densities respectively. The error bar represents the stand error. There is significant difference in the slope of the TvD function between the 1- and 2-color conditions and between the 1- and 4-color conditions.

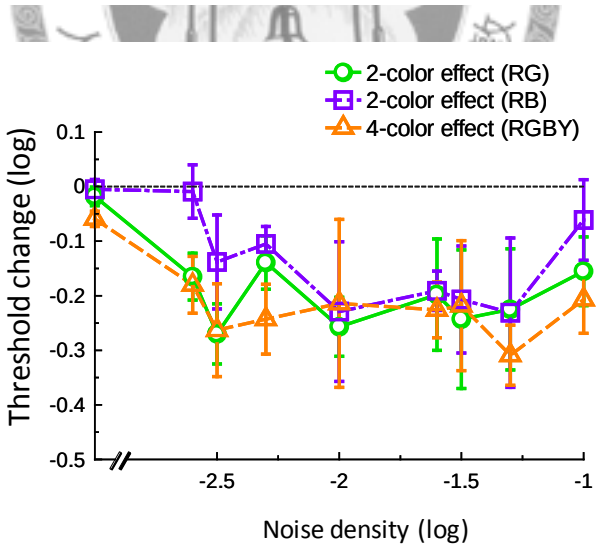

Figure 7.4. The average threshold change produced by the two 2-color (RG and RB, green and blue symbols) and the one 4-color (RGBY, orange symbols) isoluminance conditions at different noise densities. The error bar was the standard error.

Figure 7.5 shows the TvD functions for the four luminance conditions. Each panel represents the TvD functions from one observer. The red, green, purple and pink symbols in *Figure 7.5* denote the data points of W, WK, WR, and WKRG conditions respectively. The smooth curves are fits of the model discussed below. Again, the target density threshold increased with noise density for all conditions. The slope of the TvD functions for the 1-, 2-, and 4-color luminance conditions showed similar pattern as the isoluminance conditions. There was no difference in the slope of the increment function at median to high noise densities among these conditions. At low to median noise densities, the slope of the TvD functions varied with the number of the colors. As shown in *Figure 7.6*, the slopes of the TvD functions for the 2- and 4-color luminance conditions (0.78 and 0.59 respectively) were smaller than that for the 1-color luminance condition (0.98, all $t(2) > 5.62$, $p < .016$), averaged across observers. In addition, averaged across observers, the slope of the TvD function for the 4-color luminance condition was smaller (0.59) than that for the 4-color isoluminance condition, (0.75), $t(2) = 5.33$, $p < .017$.

Also, the increment of the number of the luminance colors in the images facilitated symmetry detection, especially at median to high noise densities. The gray, pink and brown symbols in *Figure 7.7* denote the threshold difference between the three multi-color conditions (WK, WR, and WKRG) and the average of the two 1-color conditions averaged across three observers respectively. As the figure shown, the magnitude of the threshold reduction at median to high noise densities was from 0.12 to 0.40 log unit, equivalent to 1.3 to 2.5 fold change. The magnitude of the threshold reduction in the 4-color luminance condition was larger than that in the two 2-color conditions (all $t(11) > 3.02$, $p < .06$). This 4-color facilitation effect was even larger than that in the isoluminance condition ($t(11) = 1.88$, $p = .04$).

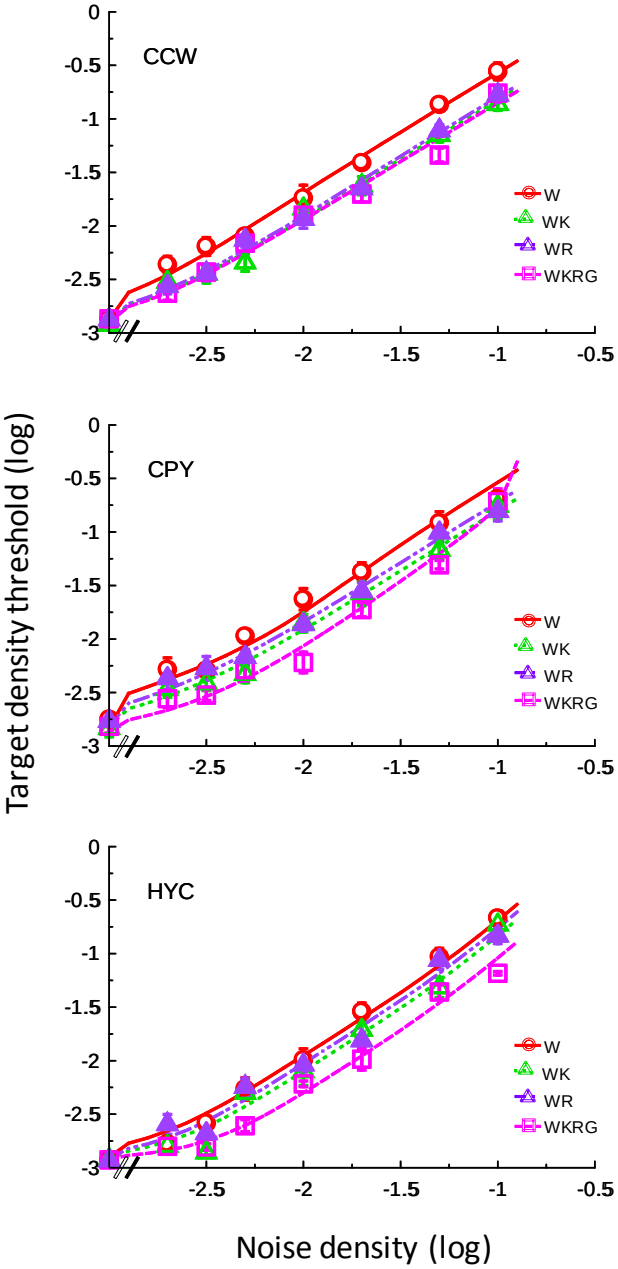

Figure 7.5. Target threshold vs. mask density (TvD) functions for the luminance conditions. Each panel represents the data from one observer. The red, green, purple, and pink symbols represent the data points of the W, WK, WR, and WKRG conditions respectively. The smooth curves are fits of the model (see text for details).

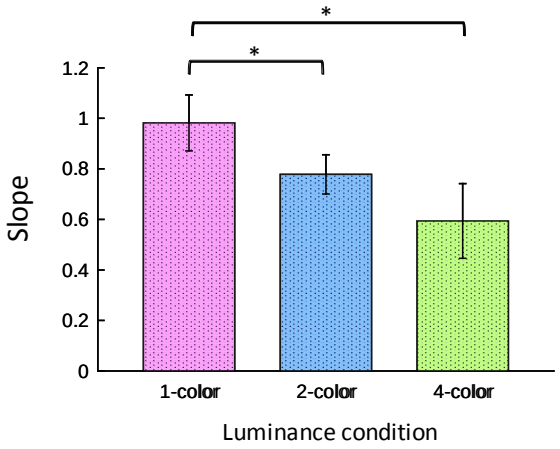

Figure 7.6. The average slopes of the target threshold vs. mask density (TvD) functions for the 1- (red bar), 2- (blue bar) and 4-color luminance conditions (green bar) at low to median densities. The error bar was the stand error. There was significant difference in the slope of the TvD functions between the 1- and 2-color conditions and between the 1- and 4-color conditions.

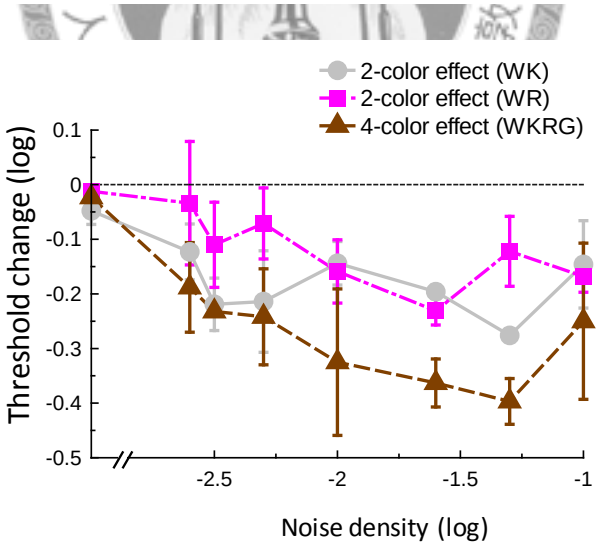

Figure 7.7. The average threshold change produced by the two 2-color (WK and WR, gray and pink symbols) and the one 4-color (WKRG, brown symbols) condition at different noise densities. The error bar was the standard error.

7.3. Discussion

Our results showed that the increment of the number of the colors in the images facilitated the symmetry detection in the images. This result was against the prediction of the probability summation theory (Quick, 1974), which suggests that threshold increases with the increment in the number of the channels monitored. Hence, our result cannot be explained by the probability summation theory theory alone. Here we applied the chromatic symmetry detection model introduced in Chapter 3 to account for this facilitation effect.

Model implementation. In practice, we set the density of the symmetric component in a random-dot noise pattern as the square of the whole density of the pattern. Hence, the Eq. (2) of the model (see Chapter 3) in the interval that contains target plus mask can be presented as

$$E'_{j,b+t} = Se_t \cdot \frac{1}{n} \cdot \left(D_t + D_b^2\right) \tag{9}$$

while in the interval that contains noise control plus mask is

$$E'_{j,b+c} = Se_t \cdot \frac{1}{n} \cdot \left(D_t + D_b\right)^2 . \tag{10}$$

where D_t and D_b are the target and noise density, respectively, Se_t is the sensitivity of the symmetry channel to the symmetric pattern, and *n* is the number of the colors in the image. Hence, the value of *n* in the 1-, 2-, and 4-color conditions is set to be 1, 2, and 4 respectively.

In addition, we used a typical value of 2 for the power for the divisive inhibition input q in Eq. (4) (Foley, 1994; Foley & Chen, 1999; Hegger, 1992). Hence, the response of the individual channel in Eq. (3) in the two intervals thus can be expressed by

$$R_{j,b+t} = \frac{E'^{\,p}_{j,b+t}}{\left(Si_{t.tc}\cdot\frac{1}{n}\cdot D_t\right)^2+\left(Si_{t.nc}\cdot\frac{n-1}{n}\cdot D_t\right)^2+\left(Si_{b.tc}\cdot\frac{1}{n}\cdot D_b\right)^2+\left(Si_{b.nc}\cdot\frac{n-1}{n}\cdot D_b\right)^2+z'} \tag{11}$$

and

$$R_{j,b+c} = \frac{E'^{\,p}_{j,b+c}}{\left(Si_{b.tc}\cdot\frac{1}{n}\cdot D_b\right)^2+\left(Si_{b.nc}\cdot\frac{n-1}{n}\cdot D_b\right)^2+z'} \tag{12}$$

respectively, where $Si_{t.tc}$, $Si_{t.nc}$, $Si_{b.tc}$, $Si_{b.tc}$, z' and p are the parameters in the model.

In this experiment, the task of the observer is to detect vertical symmetry in the chromatic image in each trial. The relevant channel is the one whose color-orientation selectivity matches any vertical chromatic symmetric pattern in the image. Since the observers have full knowledge of the axis orientation of the symmetric pattern in the image so that there is no uncertainty about axis orientation, all color-selective vertical symmetry channels involved are relevant to this visual task. Hence, the number of the monitored channels is equal to that of relevant channel, that is, $m = n$ in Eq. (6), where n is the number of the colors in the image. Hence, the mean of the response R' of the Eq. (6) and (7) can be expressed as

$$R'_{b+t} = \left(\sum_{j=1}^{n} R_{j,b+t}^{4}\right)^{1/4} \tag{13}$$

and

$$R'_{b+c} = \left(\sum_{j=1}^{n} R_{j,b+c}^{4}\right)^{1/4} \tag{14}$$

respectively.

In practice, we replaced the $v*D_b^2$ in Eq. (5) with $(v*D_b)^2$. Hence, Eq(5) can be expressed as

$$\sigma_r = \left((v \cdot D_b)^2 + \sigma_a^2\right)^{1/2}. \tag{15}$$

Recall that the noise pattern contained the same number of dots as the target-plus-mask pattern. Also, the standard deviation of the max distribution of two and four independently and identically distributed samples is 0.82 and 0.71 times the standard deviation of the original distribution respectively (Chen & Tyler, 1999). The decision variable in Eq. (8) thus becomes

$$d' = \frac{\left(R'_{b+t} - R'_{b+c}\right)}{\gamma \cdot \sigma_r} \tag{16}$$

where γ = 1, 0.82, and 0.71 for the 1-, 2- and 4-color conditions respectively.

Eq. (9) to (16) define the whole computation and all the parameters in the model. In practice, we fixed Se_t to be 1000 and the effect of the internal noise, σ_a^2, to be 1 in

all conditions to reduce the mathematical redundancy in the model. Se_t was set the same in all conditions since we set the contrast of each color at its three-fold symmetry detection threshold. σ_a^2 was fixed to be 1 in all conditions for no difference in the TvD functions among three 1-color conditions. We empirically found that fixing all other parameters except $Si_{b.tc}$ and z' provided a good fit to the data.

Model Fits. The model fits are shown as smooth curves in *Figure 7.2* and *Figure 7.5*. The model explains 98% - 99% of the all variability in the thresholds across observers (51 free parameters). The root mean square error (RMSE) is between 0.07 to 0.09 log unit across observers, on par with the average standard error of measurement. Table 7.1 shows the fitted model parameters.

As Table 7.1 shown, the inhibition from the symmetric patterns is relatively small compared with that from the noise. The greatest contribution for the divisive inhibition of a color-selective symmetry channel is from the noise of its target color ($Si_{b,tc}$). Each symbol in *Figure 7.8* represents the value of $Si_{b.tc}$ in each condition. The light-red and dark-gray dotted lines represent the average of $Si_{b.tc}$ in the 1-, 2-, and 4-color isoluminance and luminance conditions respectively. As illustrated in *Figure 7.8,* this inhibition term decreases with the increment of the number of the colors in the images. As the external noise level increases, the denominator of the response function (Eq. (11) and (12)) is gradually dominated by the inhibition from the external noise. Hence, the reduction of this noise-dependent inhibition term produces the pronounced threshold reduction at median to high noise levels than at low noise levels when the images contain more than one color, as observed in *Figure 7.4* and *Figure 7.7*. In addition, this inhibition term from the noise of the isoluminance color is much greater than that of luminance color in the 4-color conditions. This accounts for the better performance in detecting symmetric pattern at median to high noise densities in

the 4-color images in the luminance conditions than in the isoluminance conditions.

Table 7.1.

Fitted model parameters.

			CCW	CPY	HYC
Se_t*			1000	1000	1000
$Si_{t.tc}$			6.81	99.62	5.93
$Si_{t.nc}$			20	308	0.2
$Si_{b.tc}$					
Isoluminance conditions					
	1-color	R	1422	4475	1246
		B	1461	5165	1420
	2-color	RG	1170	1653	1154
		RB	1488	1978	1165
	4-color	RGBY	858	692	1134
Luminance conditions					
	1-color	W	1586	3796	1004
	2-color	WK	1124	1626	952
		WR	1202	2053	1095
	4-color	KWRG	0.01	0.01	785
$Si_{b.nc}$			488	206	7.6
z	1-color		1.92	3.11	1.96
	2-color		0.63	0.66	0.80
	4-color		0.25	0.02	0.35
v			0.001	217	17
p			1.8	2.62	1.85
Other fixed parameters used in the model fits					
σ_a^2*			1	1	1
q*			2	2	2
n*	1-color		1	1	1
	2-color		2	2	2
	4-color		4	4	4
γ*	1-color		1	1	1
	2-color		0.83	0.83	0.83
	4-color		0.71	0.71	0.71

*fixed value, not a free parameter

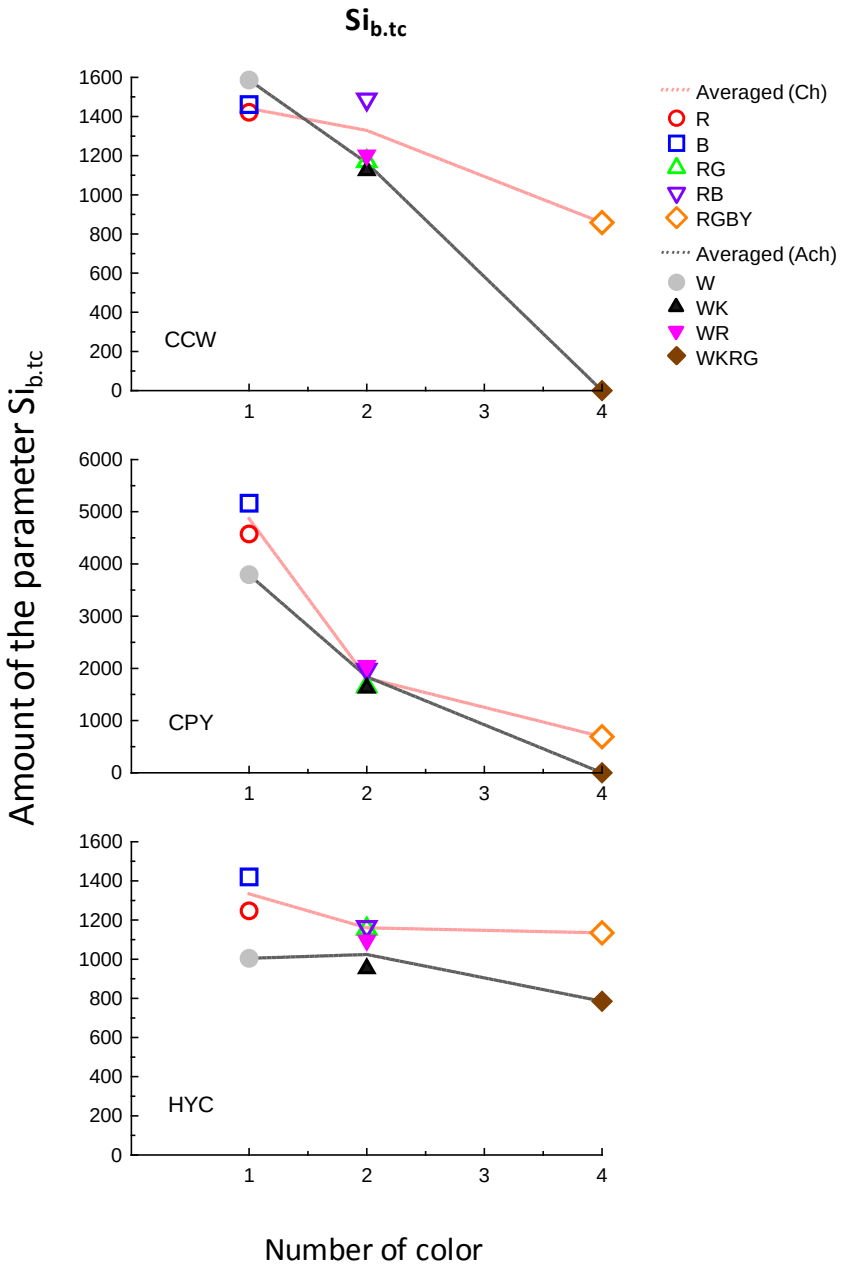

Figure 7.8. The amount of the parameter $Si_{b.tc}$ in five isoluminance and four luminance conditions. The red, blue, green, purple, and orange symbols represent the value of $Si_{b.tc}$ in the R, B, RG, RB, and RGBY condition respectively. The gray, black, pink, and brown symbols represent the value of $Si_{b.tc}$ in the W, WK, WR, and WKRG condition respectively. The light-red and dark-gray dotted lines represent the average of $Si_{b.tc}$ in the 1-, 2-, and 4-color isoluminance and luminance conditions respectively.

Our results also showed that the additive constant z' decreases with the number of the colors in the images (*Figure 7.9*), regardless of the isoluminance or the luminance condition. The reduction is about 20 - 40% and 1 - 18% in the 2- and 4-color conditions respectively. At low noise levels, the inhibition term from the external noise is negligible when compared with the additive constant z'. The denominator of the response function (Eq. (11) and (12)) is mainly dominated by the constant z'. Hence, the decrease of constant z' reduced the threshold at low noise levels in the 2- and 4-color conditions. This additive constant is suggested to change with adaption (Foley & Chen, 1997). It is possible that the more signals for each symmetry channel in the 1-color conditions than that in the multi-color conditions lead to more adaptation levels of the symmetry channel.

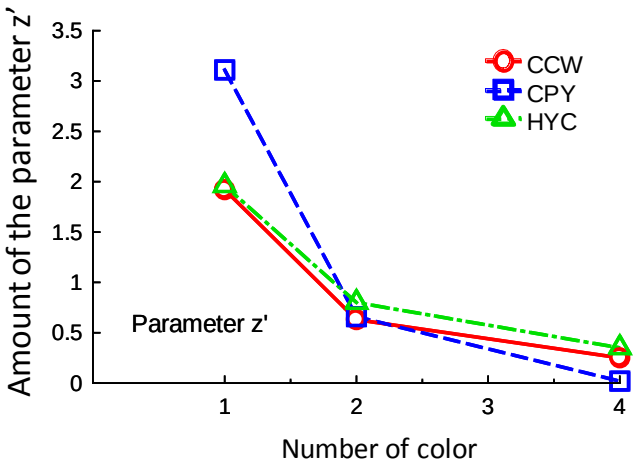

Figure 7.9. The amount of the parameter z' in the 1-, 2-, and 4-color conditions for each observer. The red, blue, and green symbols represent the value of the parameter z' for observer CCW, CPY, and HYC respectively. The amount of the parameter z' for each observer decreases with the increment of the number of the colors in the images.

In sum, our results show that for an observer who has prior knowledge of the orientation of the symmetry axis in a chromatic image, the inhibition from the symmetric patterns is relatively small compared with that from the noise. However, when the images contain more colors, the less interference the noise produces to the symmetry channel. This may be due to that the effect of noise is to interfere with symmetry perception by introducing a percept other than symmetry. As the number of color in an image increases, the number of the dots in each color decreases. In this case, the number of the matching candidates for each noise dot decreases and in turn the interference with the symmetry channels decreases. *Figure 7.10* illustrates the possible pairs a red noise dot x' can form in the 1- and 4-color images. As the figure shown, the pairs a noise dot form are much less in the 4-color (panel b) than in the 1-color image (panel a). Such reduction of interference improves the detection performance at median to high noise densities.

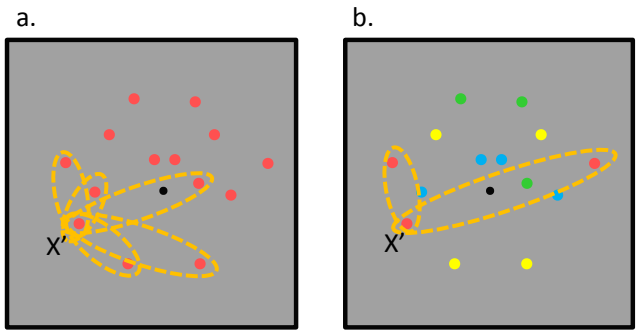

Figure 7.10. The number of the possible candidates each noise dot can pair with decreases when the number of the colors increases. The yellow dashed ovals in Panel a and b represent the possible pairs a red noise dot x' can form in the 1- and 4-color images respectively. The red noise dot x' can pair with all the dots in the image in the panel a while can only pair with two dots in the panel b.

Chapter 8 Color Facilitation in Symmetry Detection under Uncertainty of Axis Orientation

In Chapter 7, we demonstrated that the increment of the number of the colors in the images facilitated symmetry detection by decreasing inhibition from the noise. Notice that, this result was obtained when the observers had a prior knowledge of the axis orientation. In the daily life, however, symmetric objects may appear at any location in the visual field with any axis orientation. In this case, human visual system has to compare the responses of different color-orientation selective symmetry channels to detect symmetry. To our best knowledge, no research concerns this issue up to now. Whether and how color in this case helps us to detect symmetry is unclear.

In this chapter, we manipulated the orientation of the symmetry axis to be either left-diagonal or right-diagonal and the number of the colors in the images, to investigate the effect of the number of the colors on symmetry detection and its mechanism when there is uncertainty of axis orientation. Also, we compared this effect in both isoluminance and luminance images, to examine the difference between chromatic and luminance symmetry detection mechanism.

8.1. Method

Participant. Three observers attended this experiment: CCW, CPY, and RYT. RYT was naïve to the purpose of the experiment.

Stimuli. There were five conditions including three isoluminance and two luminance conditions. The three isoluminance conditions were R, RG, and RGBY while the two luminance conditions were W and WK, where R, G, B, Y, W, and K

refer to red, green, blue, yellow, white and black respectively (see Table 4.1 in Chapter 4 for the definition of the color). The R and W were 1-color condition. The stimuli contained only one color. In another three conditions, the stimuli contained two (2-color condition, i.e., RG and WK) or four colors (4-color condition, i.e., RGBY) with equal density. The stimuli consisted of a symmetric-dot target or a random-dot noise control superimposed on a random-dot noise mask in each trial. The axis orientation of symmetric target was either 45° or 135° from horizontal. The target, noise control and noise mask contained 1, 2, or 4 colors with equal density depended on the condition. All the target, the noise control and the noise mask were of the same color. The density of noise mask was from 0 to 10%. The center region of 1.4° * 1.4° visual angle and the grids on and near the two diagonal axes (0.7°) did not contain any dot to prevent observers from using only the information near the axis to make a judgment.

Procedure. The 2AFC procedure was the same as that in the previous chapters. The observers' task was to judge which stimulus interval contained a symmetric pattern. The observers were informed that the axis orientation of target was either 45° or 135° from horizontal. The order of the three isoluminance conditions and the two luminance conditions was randomized.

8.2. Results

Figure 8.1 shows the TvD functions for three isoluminance conditions. Each panel represents the TvD functions from one observer. The red, green and blue symbols in the figure denote the TvD functions for the 1- (R), 2- (RG), and 4-color (RGBY) isoluminance conditions respectively. The smooth curves are fits of the model discussed below.

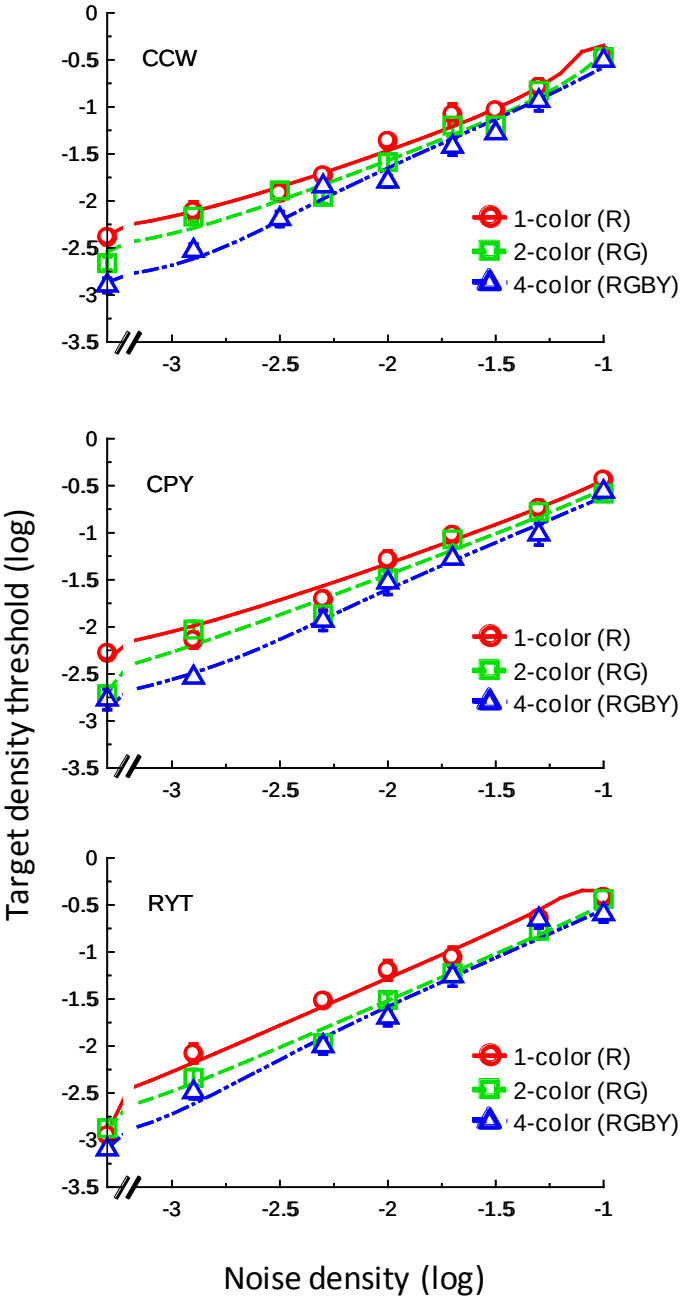

Figure 8.1. Target threshold vs. mask density (TvD) functions for three isoluminance conditions. Each panel represents the data from one observer. The red, green and blue symbols represent the data points of the 1- (R), 2- (RG), and 4-color (RGBY) conditions respectively. The smooth curves are fits of the model (see text for details).

For the three conditions, the target density threshold increased with the noise density. The slope of the TvD functions ranged from 0.78 to 1.09 in log-log coordinates across all conditions and observers. Averaged across observers, the slopes of the TvD functions for the 1-, 2-, and 4-color isoluminance conditions were 0.88, 0.91, and 1.03 respectively. The slope of the TvD function for the 4-color condition was greater than that for the 1- and 2-color conditions (all $t(2) > 4.43$, $p < .02$, no difference in the slope between the 1- and the 2-color conditions). This indicates that the magnitude of the threshold reduction in the 4-color condition was larger at low to median noise densities than at high noise densities.

Figure 8.2 shows the facilitation effect of the number of the colors in the three isoluminance conditions. The green and purple symbols in the figure denote the threshold difference between the 2-color (RG) and the 1-color (R) conditions and between the 4-color (RGBY) and the 1-color (R) conditions respectively, averaged across three observers. The magnitude of the threshold reduction was from 0.06 to 0.28 log unit (1.14 to 1.9 fold change) in the 2-color condition and was from 0.12 to 0.41 log unit (1.3 to 2.6 fold change) in the 4-color condition, greater from zero (all $t(6) > 4.28$, $p < .0026$). The magnitude of the threshold reduction was larger in the 4-color condition than in the 2-color condition ($t(6) = 3.2$, $p = .009$).

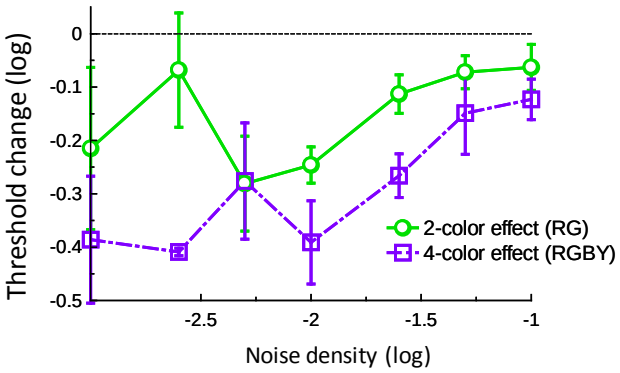

Figure 8.2. The average threshold change produced by the increment of the number of the colors at different noise densities in the isoluminance conditions. The green and purple symbols represent the threshold difference between the 2-color (RG) and the 1-color (R) conditions and between the 4-color (RGBY) and the 1-color (R) conditions respectively.

Figure 8.3 shows the TvD functions for the two luminance conditions. Each panel represents the TvD functions from one observer. The gray and brown symbols in *Figure 8.3* represent the TvD functions for the 1- and 2-color luminance conditions respectively. The smooth curves are fits of the model discussed below. The effect of the increment of the number of the colors in the luminance conditions was similar to that in the isoluminance conditions. The slope of the TvD functions for the 1- and 2-color luminance conditions were 1.01 and 1.03 respectively. No difference between the slopes of these two conditions ($t(2) = 0.4$, $p = .72$). Averaged across observers, the magnitude of the threshold difference between the 2-color (WK) condition and the 1-color (W) condition was from 0.09 to 0.3 log unit (1.2 to 2 fold change, see *Figure 8.4*), similar to that of the isoluminance conditions.

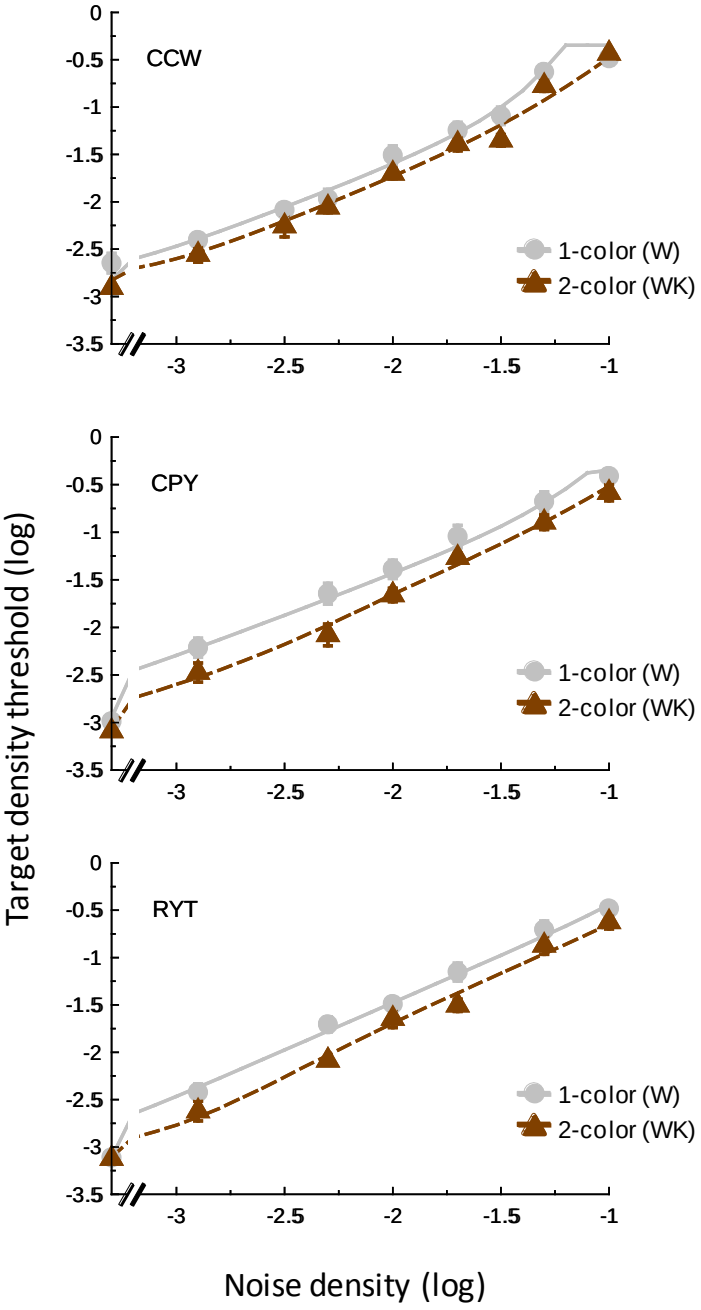

Figure 8.3. Target threshold vs. mask density (TvD) functions for luminance conditions. Each panel represents the data from one observer. The gray and brown symbols represent the data points of the 1- (W) and the 2-color (WK) condition respectively. The smooth curves are fits of the model (see text for details).

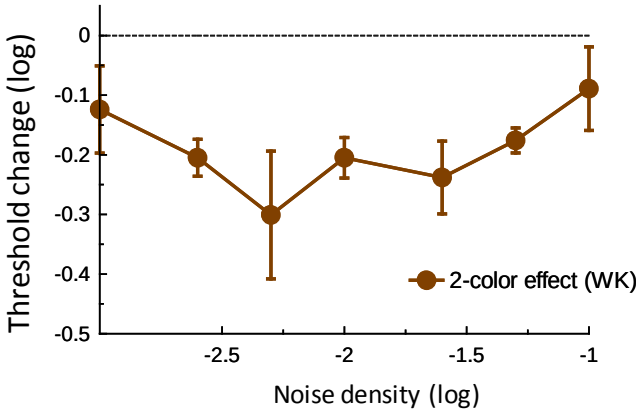

Figure 8.4. The average threshold change between the 2-color (WK) and the 1-color (W) luminance conditions. The error bar represents the standard error.

Our results also showed that the target density thresholds and the TvD function slope for the isoluminance and the luminance conditions were different. *Figure 8.5* represents the TvD functions for the 1-color condition in the isoluminance and luminance conditions respectively, while *Figure 8.6*, the 2-color conditions. These TvD functions are the same with those in Figure 8.1 and *Figure 8.3*. As *Figure 8.5* shown, the slope of the TvD function for the 1-color isoluminance condition (M = 0.88, SE = 0.06) was slightly lower than that for the 1-color luminance conditions (M = 1.01, SE = 0.03), $t(2) = -1.95$, $p = .09$. This difference is more pronounced in the 2-color conditions. As *Figure 8.6* shown, the slope of the TvD function for the 2-color isoluminance condition (M = 0.91, SE = 0.04) was lower than that for the 2-color luminance conditions (M = 1.03, SE = 0.02), $t(2) = -4.84$, $p = .02$. These two figures also showed lower target density threshold in the luminance conditions than in the isoluminance conditions.

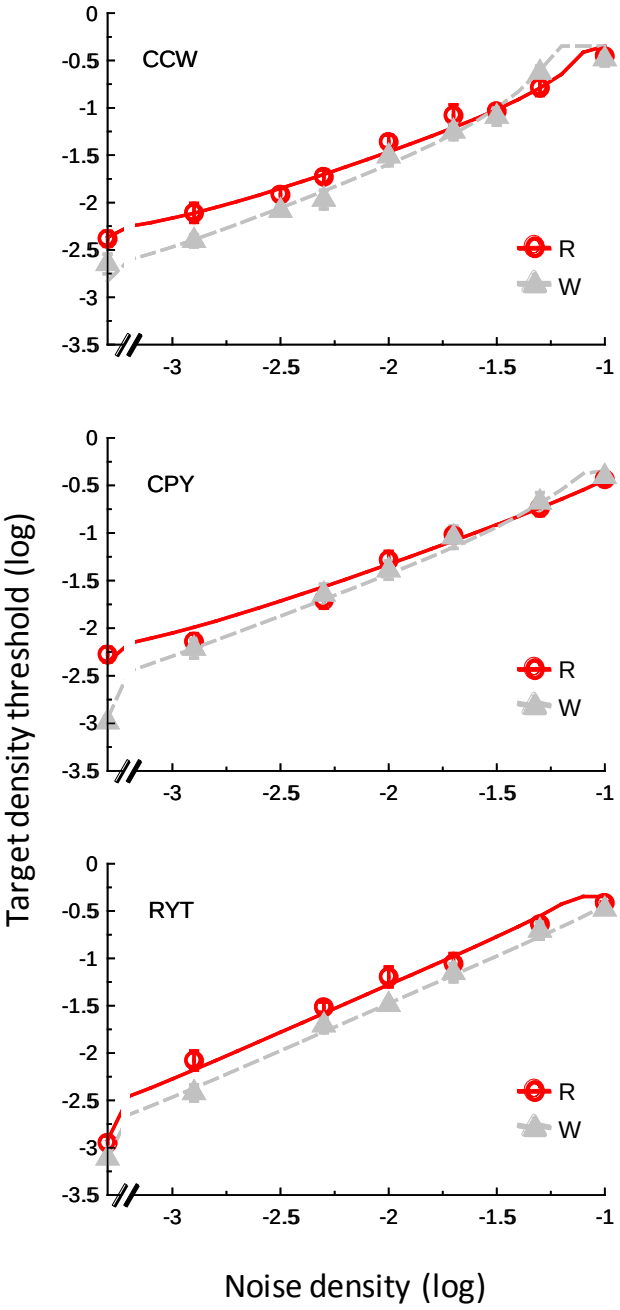

Figure 8.5. Target threshold vs. mask density (TvD) functions for the 1-color isoluminance (R) and luminance (W) conditions. Each panel represents the data from one observer. The red and gray symbols represent the data points of the R and W condition respectively. The smooth curves are fits of the model.

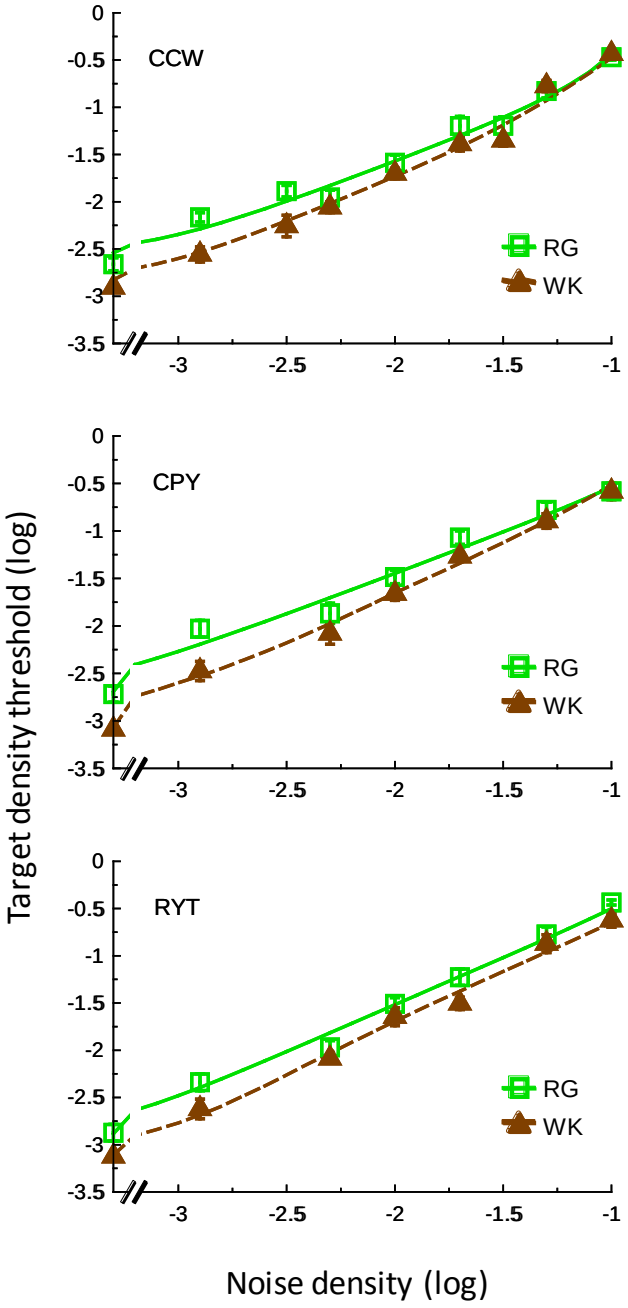

Figure 8.6. Target threshold vs. mask density (TvD) functions for the 2-color isoluminance (RG) and luminance (WK) conditions. Each panel represents the data from one observer. The green and brown symbols represent the data points of the RG and WK conditions respectively. The smooth curves are fits of the model.

Averaged across three observers, the target density thresholds in the luminance conditions were lower than those in the isoluminance conditions when the images contained the same number of the colors ($t(8) = -3.22$, $p = .006$ for the 1-color condition and $t(8) = -4.9$, $p < .001$ for the 2-color condition). The red and blue symbols in *Figure 8.7* represent the average threshold difference in symmetry detection between the 1-color isoluminance and luminance conditions and between the 2-color isoluminance and luminance conditions respectively. In both 1- and 2-color images, the threshold difference between the isoluminance and the luminance conditions was pronounced at low to median noise densities than at high noise densities.

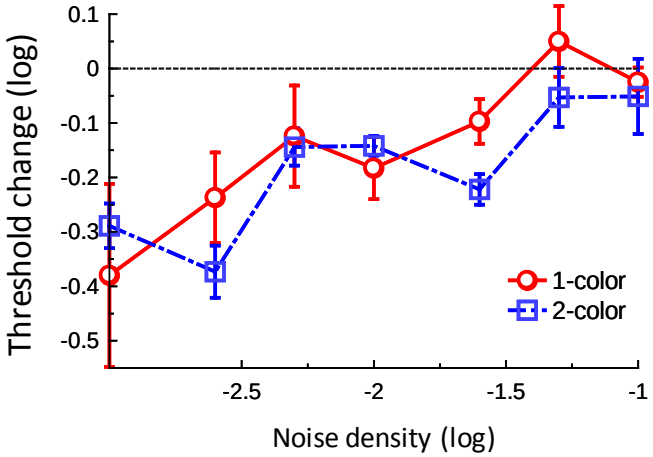

Figure 8.7. The average threshold difference in the target density threshold between isoluminance and luminance conditions. The red and blue symbols represent the threshold difference between the 1-color (R vs. W) isoluminance and luminance conditions and between the 2-color (RG vs. WK) isoluminance and luminance conditions respectively.

8.3. Discussion

Our results showed that the increment of the number of the colors in the images facilitated the symmetry detection. In Chapter 7, we reported that the increment of the number of the colors in the images facilitated symmetry detection at median to high noise densities when the observers had prior knowledge of the symmetry axis orientation. Here, we found that the facilitation effect from the increment of the number of the colors was more pronounced at low to median than high noise densities when there was an uncertainty of axis orientation. This suggests different mechanisms of the facilitation were involved in these two situations. Our results also showed better symmetry detection performance in the achromatic images than in chromatic images. This suggests the larger internal response or the smaller variability of the response distribution in the luminance symmetry channels than isoluminance ones. Here we apply the model proposed in Chapter 3 to account for the above results.

Model implementation. Recall that the target in each trial of the visual task presented in Chapter 7 was a vertical symmetric pattern and the observers had full knowledge about it axis orientation. There was no uncertainty of the axis orientation. Hence, all color-selective vertical symmetry channels matching the color of the target were relevant channels for the decision stage. However, in this experiment, the orientation of the symmetric target might be left-diagonal or right-diagonal. The decision stage needs to monitor both the color-selective left-diagonal and right-diagonal symmetry channels to detect symmetry. For these channels, only half of them whose orientation selectivity matches the chromatic symmetric target in the images are relevant channels while another half are irrelevant channels. Hence, the number of the channels the visual system has to monitor in this experiment is double that in Chapter 7.

As in Chapter 7, we set the density of the symmetry component in a random-dot noise pattern as the square of the whole density. Since the symmetric target is merely a random-dot pattern for the symmetry channels selective to non-target axis orientation, the density of the symmetric component is the square of the density of that symmetric target for those channels. Hence, in the interval containing target plus mask, Eq. (2) can be presented as

$$E'_{j.r,(b+t)} = Se_t \cdot \frac{1}{n} \cdot \left(D_t + D_b^2\right) \tag{17}$$

for the relevant color-selective channels while as

$$E'_{j.ir,(b+t)} = Se_t \cdot \frac{1}{n} \cdot \left(D_t + D_b\right)^2 \tag{18}$$

for the irrelevant channels, where the subscript *r* and *ir* indicate the relevant and irrelevant channel respectively, D_t and D_b are the target and noise densities respectively, Se_t is the sensitivity of the symmetry channel to the symmetric pattern, and *n* is the number of the colors in the image. In the interval containing noise control plus mask, Eq. (2) can be presented as

$$E'_{j,(b+c)} = Se_t \cdot \frac{1}{n} \cdot \left(D_t + D_b\right)^2 \tag{19}$$

Again, we used a typical value of 2 for the power for the divisive inhibition input q in Eq. (4) (Foley, 1994; Foley & Chen, 1999; Hegger, 1992). The response of the individual relevant channel in the interval containing target plus mask in Eq. (3) thus

can be expressed by

$$R_{j.r,(b+t)} = \frac{E'_{j.r,(b+t)}{}^{p}}{\left(Si_{t.tc}\cdot\frac{1}{n}\cdot D_t\right)^2+\left(Si_{t.nc}\cdot\frac{n-1}{n}\cdot D_t\right)^2+\left(Si_{b.tc}\cdot\frac{1}{n}\cdot D_b\right)^2+\left(Si_{b.nc}\cdot\frac{n-1}{n}\cdot D_b\right)^2+z'} \tag{20}$$

while that of the irrelevant channel can be expressed by

$$R_{j.ir,(b+t)} = \frac{E'_{j.ir,(b+t)}{}^{p}}{\left(Si_{t.tc}\cdot\frac{1}{n}\cdot D_t\right)^2+\left(Si_{t.nc}\cdot\frac{n-1}{n}\cdot D_t\right)^2+\left(Si_{b.tc}\cdot\frac{1}{n}\cdot D_b\right)^2+\left(Si_{b.nc}\cdot\frac{n-1}{n}\cdot D_b\right)^2+z'}; \tag{21}$$

the response of the individual channel in the intervals containing noise control plus mask in Eq. (3) can be expressed by

$$R_{j,(b+c)} = \frac{E'_{j,(b+c)}{}^{p}}{\left(Si_{b.tc}\cdot\frac{1}{n}\cdot D_b\right)^2+\left(Si_{b.nc}\cdot\frac{n-1}{n}\cdot D_b\right)^2+z'}, \tag{22}$$

where $Si_{t.tc}$, $Si_{t.nc}$, $Si_{b.tc}$, $Si_{b.tc}$, z’ and p are the parameters in the model. As mentioned above, only half of the channels in this task are relevant while another half are irrelevant in the interval that contains target and mask. Hence, $m = 2n$ in Eq. (6). In other words, the visual system needs to monitor 2*n* channels, of which only n channels are relevant in the n-color condition. The mean of the response R’ in Eq. (6) and (7) can be expressed by

$$R'_{b+t} = \left(\sum_{j=1}^{n} R_{j.r,(b+t)}^4 + \sum_{j=n+1}^{2n} R_{j.ir,(b+t)}^4\right)^{1/4} \quad (23)$$

and

$$R'_{b+c} = \left(\sum_{j=1}^{2n} R_{j,(b+c)}^4\right)^{1/4} \quad (24)$$

respectively. Also, we replaced the $v*D_b^2$ in Eq. (5) with $(v*D_b)^2$ in practice. Hence, Eq(5) can be expressed as

$$\sigma_r = \left((v \cdot D_b)^2 + \sigma_a^2\right)^{1/2}. \quad (25)$$

The decision variable can be calculated by Eq. (8), where γ = 0.83, 0.71, and 0.62 for the 1-, 2- and 4-color conditions respectively, since the standard deviation of the max distribution of two, four and eight independently and identically distributed samples is 0.83, 0.71 and 0.62 times the standard deviation of the original distribution (Chen & Tyler, 1999). Hence, Eq. (17) – (25) define the whole computation and all the parameters in the model.

Again, we fixed Se_t to be 1000 and the effect of the internal noise, σ_a^2, to be 1 in all conditions to reduce the mathematical redundancy in the model in practice. We empirically found that fixing all other parameters except $Si_{t.tc}$ and v provided a good fit to the data.

Model fits. The model fits are shown as smooth curves in *Figure 8.1* and *Figure 8.3*. The model explains 98-99% of the all variability in the thresholds across observers (36 free parameters). The root mean square error (RMSE) is between 0.07

to 0.09 log unit across observers, on par with the average standard error of measurement. Table 8.1 shows the fitted model parameters.

Table 8.1.

Fitted model parameters.

			CCW	CPY	RYT
Se_t*			1000	1000	1000
$Si_{t.tc}$					
Isoluminance conditions					
	1-color	R	1162	1204	967
	2-color	RG	1177	1177	884
	4-color	RGBY	0.86	1.61	1.16
Luminance conditions					
	1-color	W	960	992	756
	2-color	WK	578	22	8.4
$Si_{t.nc}$			3.42	7.38	0.2
$Si_{b.tc}$			2097	3637	2644
$Si_{b.nc}$			1185	1019	1100
z			0.72	0.3	0.38
v					
Isoluminance conditions			11.71	5.07	3.41
Luminance conditions			32.67	20.43	4.34
p			2.1	2.14	2.00
Other fixed parameters used in the model fits					
σ_a^2*			1	1	1
q*			2	2	2
n*	1-color		1	1	1
	2-color		2	2	2
	4-color		4	4	4
γ*	1-color		0.83	0.83	0.83
	2-color		0.71	0.71	0.71
	4-color		0.62	0.62	0.62

*fixed value, not a free parameter

As Table 8.1 shown, the increment of the number of the colors in the images reduces the inhibition from the symmetry components of the target color ($Si_{t.tc}$) in both isoluminance and luminance conditions. For the convenience of comparison, we plotted the amount of $Si_{t.tc}$ in *Figure 8.8*. The red and gray symbols in *Figure 8.8* show the amount of $Si_{t.tc}$ in the three isoluminance and the two luminance conditions respectively. This inhibition term in the 1-color isolminance condition is about 1.21 to 1.28 times larger than that in the 1-color luminance condition. The magnitude of $Si_{t.tc}$ in the 2- and 4-color isoluminance condition was about 91% and less than 1% of that in the 1-color isoluminance condition. The amount of this inhibition term decreases when the images contain more than two isluminance colors. At low noise levels, the inhibition term from the noise patterns is negligible when compared with that from the symmetric patterns and the additive constant z'. Hence, the denominator of the response function (Eq. (20)) is mainly dominated by the inhibition term from the symmetric patterns and the constant z'. Hence, the reduction of the inhibition term from symmetric patterns when the images contain more than one color produces the pronounced threshold reduction at low than high noise levels in the 2- and 4-color conditions, as *Figure 8.2* shown.

The magnitude of $Si_{t.tc}$ reduction in the luminance conditions is greater than that in the isoluminance conditions. The reduction in the 2-color luminance condition reaches as much as 79%, much greater than that in the 2-color isoluminance condition (3%). The greater reduction of this inhibition term in the luminance condition than the isolminance condition produces the greater threshold reduction at low than high noise levels in the luminance conditions, as shown in *Figure 8.7*.

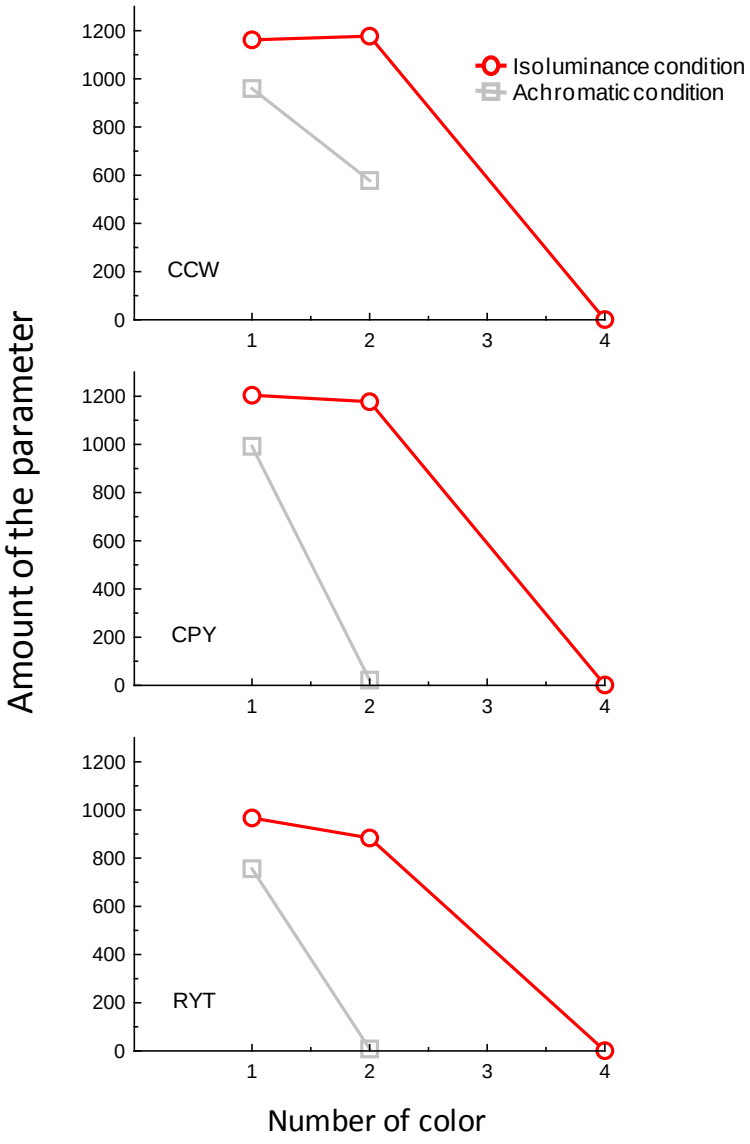

Figure 8.8. The amount of the parameter $Si_{t.tc}$ in the isoluminance and luminance conditions. The red symbols represent the amount of $Si_{t.tc}$ in the 1- (R), 2- (RG), and 4-color (RGBY) isoluminance conditions. The gray symbols represent the amount of $Si_{t.tc}$ in the 1- (W) and 2-color (WK) luminance conditions.

The model fitting results also showed that the parameter v is larger in the luminance conditions than in the isoluminance conditions. This indicates larger effect

of achromatic noise (v^2 in the luminance conditions) than the chromatic noise (v^2 in the isoluminance conditions). The increment of this noise density dependent parameter makes the larger variability of the achromatic external noise at high than low noise densities. Hence, the difficulty in achromatic symmetry detection increases with the increment of the noise density, compared to chromatic symmetry detection. The decrease of the inhibition term from the symmetric patterns and the increase of the parameter v jointly produce the greater threshold reduction at low to median noise densities in the multi-color conditions in the luminance conditions.

In Chapter 7, we showed that the increment of the number of the colors in an image reduced the inhibition from the noise patterns. However, when the observer had no prior knowledge of the symmetry axis orientation, the increase of the number of the colors in an image instead reduces the inhibition from the symmetric patterns. This difference may reflect the effect of prior knowledge on the matching of image features in symmetry processing. The prior knowledge of axis orientation helps the observers to exclude a number of matching candidates for each dot in a symmetric pattern. When the prior knowledge of the axis orientation is not available, the observer has to consider many matching candidates across multiple possible axes. Such increment of the number of the candidates in a symmetric pattern interferes with the function of the symmetry channels. Hence, the inhibition from the symmetric pattern is relatively large when the observers have no prior knowledge of axis orientation compared with that when they have prior knowledge of axis orientation. The increment of the number of the colors however decreases the number of the dots in each color. Hence, for each dot, the number of the matching candidates decreases. For example, the dot x' in *Figure 8.9* can pair with several dots in the 1-color symmetric image (panel a) while can only pair with only one dot in the 4-color image

(panel b). The interference from the symmetric pattern thus decreases with the increment of the number the colors. Such reduction of interference leads to better detection performance when the number of the colors increases.

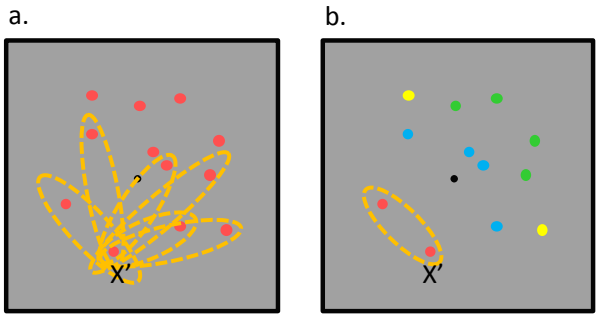

Figure 8.9. The number of the possible candidates each dot in the symmetric pattern can pair with decreases when the number of the colors increases. The yellow dashed ovals in Panel a and b represent the possible pairs a red dot x' can form in the 1- and 4-color symmetric images respectively. The dot x' can pair with all the dots in the image in the panel a while can pair with only one dot in the panel b.

Chapter 9 The Integration of Color-Selective Symmetry Detection Channels within the Same and between the Different Axes

In Chapter 7 and 8, we manipulated the number of the colors in the images to investigate the integration of information from color selective symmetry channels at different levels of uncertainty. In these two chapters, all the symmetric image components shared the same symmetry axis. Hence, under these situations, the visual system only needs to monitor color-selective channels tuned to the same axis orientation. However, symmetry perception in a nature scene can be more complicated than this. Sometimes we need to detect two symmetric images or objects in a scene. In this case, these two images or objects do not necessarily share the same symmetry axis. For example, the red apple and the green leaf in the apple tree usually have different symmetry axes. To detect multiple symmetric patterns, the visual system in this case instead monitors channels sensitive to different orientations.

The ecological significance behind these two cases is quite different. The roles of the color in these two cases may also differ. In the latter case, the color information helps object segmentation (Shevell & Kingdom, 2008). That is, the visual system uses color information to distinguish two objects. In the former, however, the visual system instead needs to incorporate different colors into the same pattern to form a coherent percept of a symmetric pattern. Due to such difference, there is a possibility that the mechanisms underlying theses two processes are different. Specifically, maybe the integration between chromatic symmetry channels selective to the same

orientation axis and to different axes is different. For example, it is possible that the detecting symmetry is more difficult when two symmetric patterns share the same axis than not for the segmentation of two images with different colors helps symmetry detection. In this chapter, we manipulated the orientation of two chromatic symmetric patterns that superimposed on each other, to investigate how these symmetry channels works to achieve these ecological purposes. We also compared the above symmetry detection performance in both chromatic and achromatic images.

9.1. Method

Participant. Three observers attended this experiment: CCW, CPY, and RYT. RYT was naïve to the purpose of the experiment.

Stimuli. There were four conditions in this experiment, two isoluminance and two luminance conditions. In each condition, the stimuli in each trial consisted of two symmetric-dot targets or two random-dot noise control superimposed on a random-dot noise mask. The target was a 45° or 135° diagonal symmetric-dot pattern containing only one color. The two isoluminance conditions were RG-S and RG-D, and the two luminance conditions were WK-S, and WK-D, where two capital letters before the hyphens denoted the colors of the two targets respectively (The latter R, G, W, and K were the abbreviation of red, green, white, and black respectively, see Table 4.1 in Chapter 4 for the definition of the color) and the letters after the hyphens denoted the same (S) or the different (D) axis orientations of the two targets. In the same (S) orientation condition, the axis orientations of the two symmetric targets were both 45° or both 135° from horizontal. In the different (D) orientation conditions, the axis orientation of one symmetric target was 45° and that of another one was 135° from horizontal. The color and the density of the two noise controls were the same as those

of the two targets. The noise mask was a random-dot noise pattern containing the same color as the two targets. The density of noise mask was from 0 to 5%. The center region of 1.4° * 1.4° visual angle and the grids on and near the two diagonal axes (0.7°) contained no dot to prevent observers from using only the information near the axis to make a judgment.

Procedure. The 2AFC procedure was the same as that in the previous chapters. The observers' task was to judge which stimulus interval contained any symmetric pattern. The observers were informed that the axis orientation of the two targets was either the same (both 45° or both 135° from horizontal) or different (45° and 135° from horizontal). The isoluminance and luminance conditions were run separately, in which the trials of the same and different axis orientation conditions were randomized in the same block to prevent observers from using the top-down strategy.

9.2. Results

Figure 9.1 shows TvD functions for the two isoluminance conditions (RG-S and RG-D). Each panel represents the TvD functions from one observer. The red and green symbols denote the TvD functions for the RG-S and the RG-D conditions respectively. The smooth curves are fits of the model discussed below.

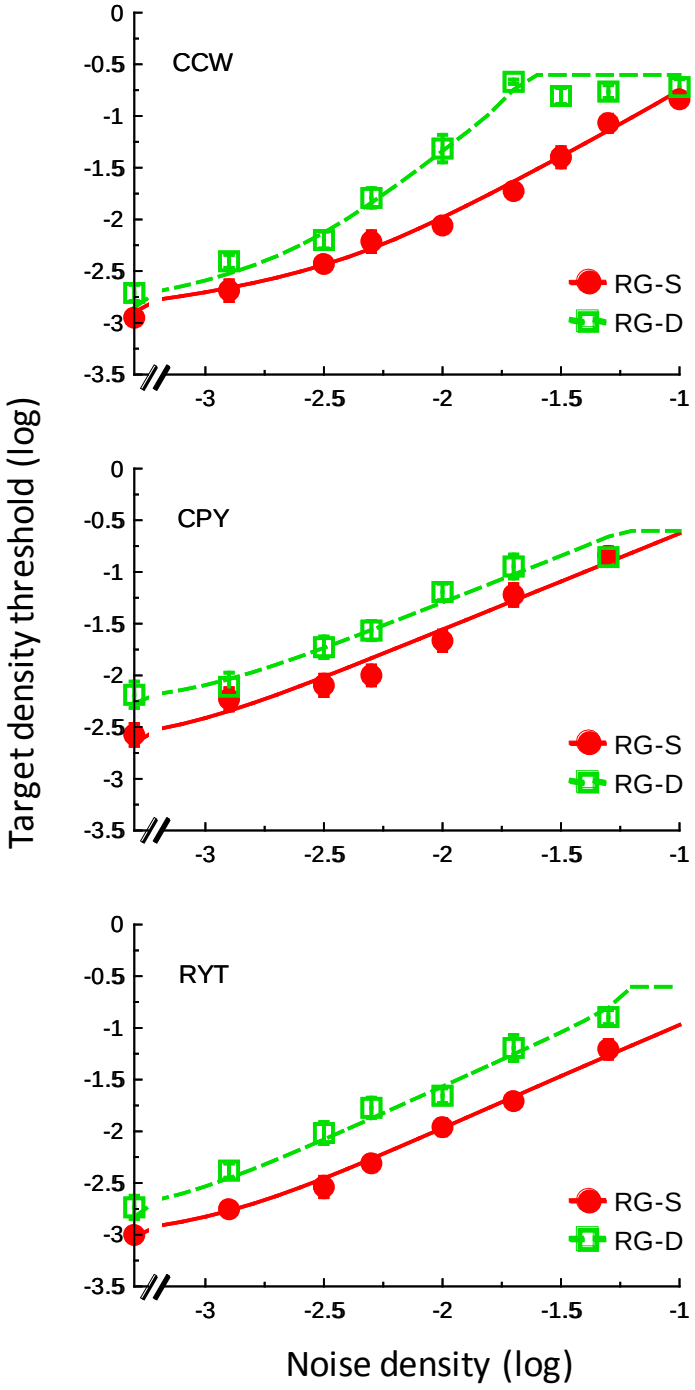

Figure 9.1. Target threshold vs. mask density (TvD) functions in the isoluminance condition. Each panel represents the data from one observer. The red and green symbols represent the data points of the RG-S and RG-D conditions respectively. The smooth curves are fits of the model (see text for details).

For these two isoluminance conditions, the target density threshold increased with noise density. The slope of the increment function was 0.96 in log-log coordinates, averaged across conditions and observers (*SE* = 0.08). The slope of the TvD functions had no difference between the same- (i.e., RG-S, *M* = 0.87, *SE* = 0.04) and the different-orientation conditions (i.e., RG-D, *M* = 1.05, *SE* = 0.16) when averaged across three observers (*Figure 9.2*), $t(2) = 0.98$, $p = .43$. The target density threshold was lower in the same-orientation condition than in the different-orientation condition. The red symbols in *Figure 9.3* show the threshold difference between the RG-S and the RG-D conditions, averaged across three observers. The orientation effect was from 0.2 to 0.62 log unit (or 1.6 to 4.2 fold change) in threshold measurement.

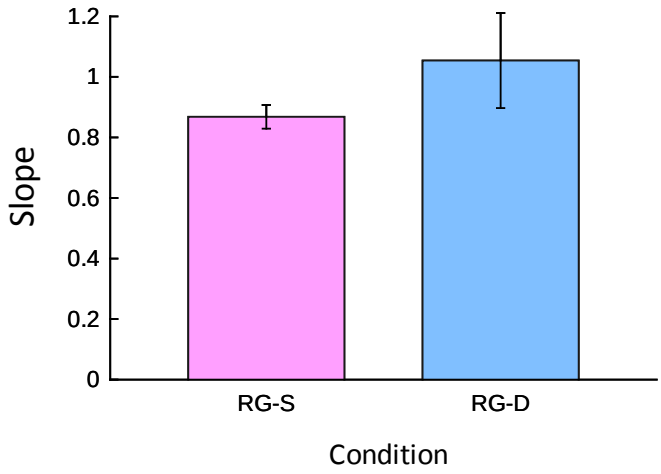

Figure 9.2. Slope of the target threshold vs. mask density (TvD) functions in isoluminance conditions. The red and blue bars represent the slopes of the RG-S and the RG-D conditions respectively. The error bar was standard error. There was no significant difference in the slopes of the TvD functions between two conditions.

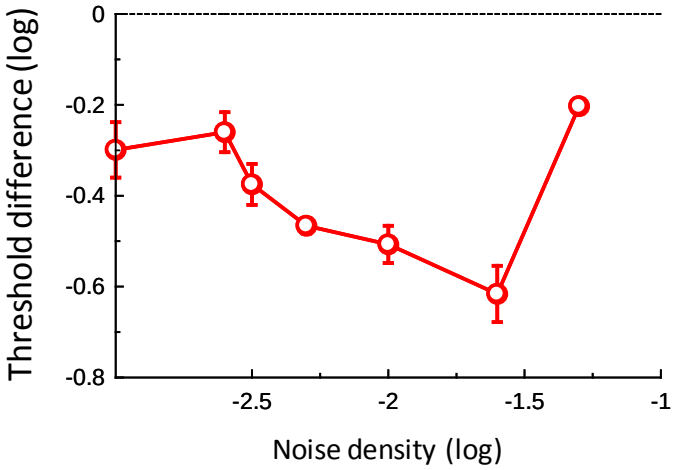

Figure 9.3. The threshold difference between the same- and the different-orientation conditions in the isoluminance conditions, averaged across three observers. The red symbols represent the threshold difference between the RG-S and the RG-D conditions.

The results of the luminance conditions, WK-S and WK-D, were similar to that of the isoluminance conditions. The gray and brown symbols in *Figure 9.4* denote the TvD functions for the WK-S and the WK-D conditions respectively. The slope of the TvD functions showed no difference between the same- (i.e., WK-S, M = 0.89, SE = 0.06) and the different- orientation conditions (i.e., WK-D, M = 1.04, SE = 0.13) when averaged across three observers (*Figure 9.5*), $t(2) = 0.83$, $p = .49$. Also, the target density threshold was lower in the same-orientation condition than in the different-orientation condition, as *Figure 9.6* shown. The gray symbols in *Figure 9.6* represent the threshold difference between the WK-S and the WK-D conditions, averaged across three observers. The threshold reduction in the WK-S condition was from 0.24 to 0.52 log unit, equivalent to 1.7 to 3.3 fold change.

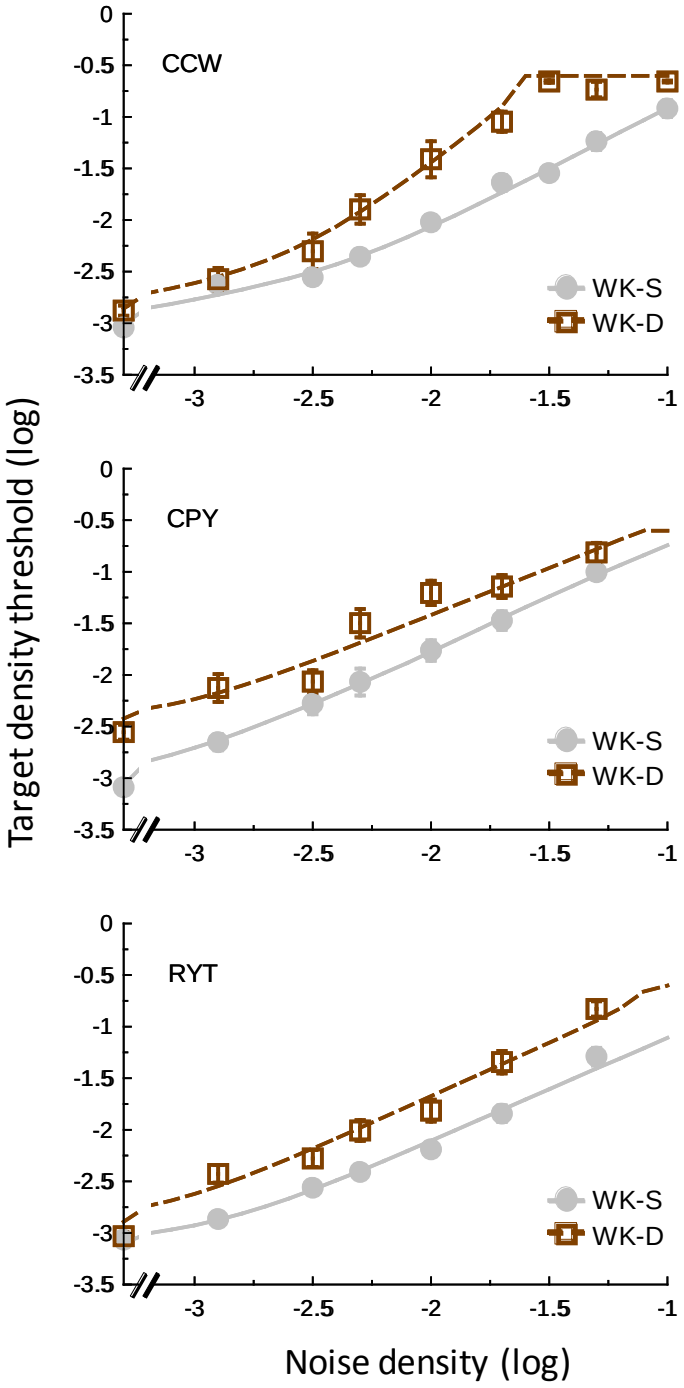

Figure 9.4. Target threshold vs. mask density (TvD) functions in the luminance conditions. Each panel represents the data from one observer. The gray and brown symbols represent the data points of the WK-S and the WK-D conditions respectively. The smooth curves are fits of the model (see text for details).

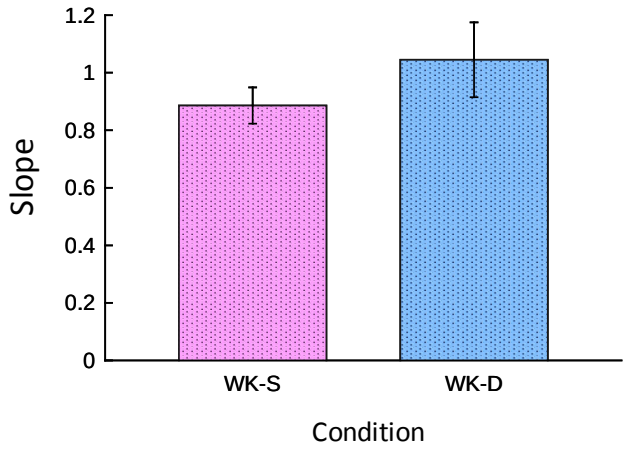

Figure 9.5. Slope of the target threshold vs. mask density (TvD) functions in luminance conditions. The red and blue bars represent the slopes of the WK-S and the WK-D conditions respectively. The error bar was standard error. There was no significant difference in the slope of the TvD functions between two conditions.

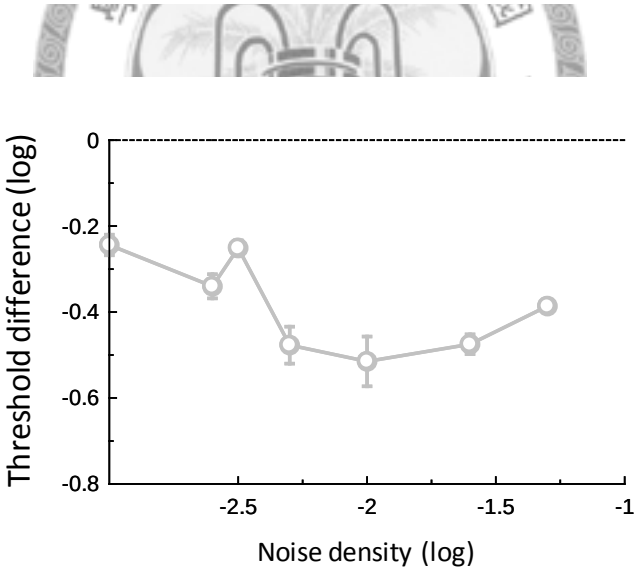

Figure 9.6. The threshold difference between the same- and the different-orientation conditions in the luminance conditions, averaged across three observers. The gray symbols represent the threshold differences between the WK-S and the WK-D conditions.

Our results also showed the difference in the target density thresholds between the isoluminance and the luminance conditions. *Figure 9.7* represents the threshold difference between the two same-orientation conditions (i.e., RG-S and WK-S, pink symbols) and between the two different-orientation conditions (i.e., RG-D and WK-D, green symbols), averaged across three observers. The amount of the threshold difference was from 0.1 to 0.3 log unit, equivalent to 1.2 to 2 fold change, except for the difference between the two different-orientation conditions at the highest noise density.

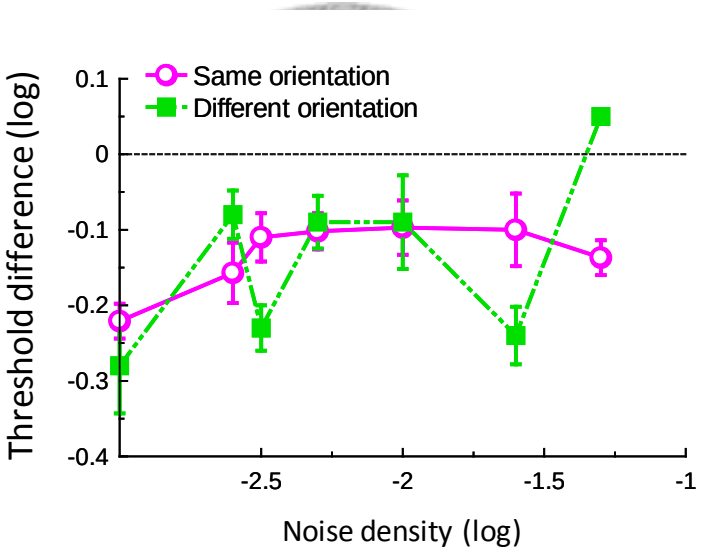

Figure 9.7. The threshold difference between two same-orientation and between two different-orientation conditions, averaged across three observers. The pink symbols represent the threshold difference between the RG-S and the WK-S conditions. The green symbols represent the threshold difference between the RG-D and the WK-D conditions.

9.3. Discussion

Our results showed better symmetry detection performance when two symmetric targets shared the same axis than those did not. This suggests different mechanisms mediating these two conditions. Here we applied the model proposed in Chapter 3 to account for our data.

Model implementation. As discussed in Chapter 8, there are occasions that the visual system needs to monitor more channels than those relevant to the visual task. In this task, the two symmetric targets of different colors either shared the same axis (i.e., both left- or right-diagonal) or had different axes (i.e., left- and right-diagonal). Hence, the system needs to monitor four channels to detect symmetry, two of which are relevant and another two are irrelevant. Take the RG-D condition for example. Since the observer had no prior knowledge of the axis orientation of the target, the visual system needs to monitor all the red left-diagonal, red right-diagonal, green left-diagonal and green right-diagonal symmetry channels to detect symmetry. The two targets were either one red left-diagonal and one green right-diagonal symmetric pattern or one green left-diagonal and one red right-diagonal symmetric pattern. Hence, only red left-diagonal and green right-diagonal symmetry channels or green left-diagonal and red right-diagonal symmetry channels among the four monitored channels are relevant. Hence, $m = 2n$ in Eq. (6), where $n = 2$ in this task. The only difference between the same-orientations and the different-orientations is that the two relevant channels are selective to the same orientation in the same-orientation conditions while are selective to the different orientation in the different-orientation conditions.

Again, we set the density of the symmetric component in a random-dot noise pattern as the square of the whole density of that pattern. Hence, the Eq. (2) in the

interval that contains two targets plus mask can be presented as

$$E'_{j.r,(b+t)} = Se_t \cdot \left(2D_t + \frac{1}{n} D_b^2 \right) \tag{26}$$

for the two relevant color-selective channels while as

$$E'_{j.ir,(b+t)} = Se_t \cdot \frac{1}{n} \cdot \left(2D_t + D_b \right)^2 \tag{27}$$

for the two irrelevant channels, where the subscript *r* and *ir* indicate the relevant and irrelevant channel respectively, D_t and D_b are the target and noise densities respectively, Se_t is the sensitivity of the symmetry channel to the symmetric pattern, and *n* is the number of the colors in the image. Here we set *n* to be 2 for the noise mask contains two colors that are the same as the two targets. Eq. (2) in the interval that contains two noise control plus mask can be presented as

$$E'_{j,(b+c)} = Se_t \cdot \frac{1}{n} \cdot \left(2D_t + D_b \right)^2 . \tag{28}$$

Again, we used a typical value of 2 for the power for the divisive inhibition input q in Eq. (4) in model implementation (Foley, 1994; Foley & Chen, 1999; Hegger, 1992). The response of the individual relevant channel in the intervals containing target plus mask in Eq. (3) thus can be expressed by

$$R_{j.r,(b+t)} = \frac{E'_{j.r,(b+t)}{}^{p}}{\left(Si_{t.tc} \cdot D_t\right)^2 + \left(Si_{t.nc} \cdot D_t\right)^2 + \left(Si_{b.tc} \cdot \frac{1}{n} \cdot D_b\right)^2 + \left(Si_{b.nc} \cdot \frac{n-1}{n} \cdot D_b\right)^2 + z'} \tag{29}$$

while that of irrelevant channel can be expressed by

$$R_{j.ir,(b+t)} = \frac{E'_{j.ir,(b+t)}{}^{p}}{\left(Si_{t.tc} \cdot D_t\right)^2 + \left(Si_{t.nc} \cdot D_t\right)^2 + \left(Si_{b.tc} \cdot \frac{1}{n} \cdot D_b\right)^2 + \left(Si_{b.nc} \cdot \frac{n-1}{n} \cdot D_b\right)^2 + z'}; \tag{30}$$

the response of the individual channel in the intervals containing noise control plus mask in Eq. (3) can be expressed by

$$R_{j,(b+c)} = \frac{E'_{j,(b+c)}{}^{p}}{\left(Si_{b.tc} \cdot \frac{1}{n} \cdot D_b\right)^2 + \left(Si_{b.nc} \cdot \frac{n-1}{n} \cdot D_b\right)^2 + z'}, \tag{31}$$

where $Si_{t.tc}$, $Si_{t.nc}$, $Si_{b.tc}$, $Si_{b.tc}$, z' and p are the parameters in the model. The mean of the response R' in the interval containing two targets plus mask and noise control plus mask can be expressed by Eq.(23) and (24) in Chapter 8 respectively, where n = 2 in this task as mentioned above. Also, we replaced the $v*D_b^2$ in Eq. (5) with $(v*D_b)^2$ in practice. Hence, Eq(5) can be expressed as Eq. (25) in this task. The γ in the decision variable in Eq. (25) is set to be 0.71 for all conditions for the standard deviation of the max distribution of four independently and identically distributed samples is 0.71 times the standard deviation of the original distribution (Chen & Tyler, 1999). Hence,

Eq. (23) – (31) define the whole computation and all the parameters in the model.

Again, we fixed Se_t to be 1000 and the effect of the internal noise, σ_a^2 to be 1 in all conditions to reduce the mathematical redundancy in the model in practice. We empirically found that fixing all other parameters except $Si_{t.tc}$ and $Si_{t.nc}$ provided a good fit to the data.

Model fits. The model fits are shown as smooth curves in *Figure 9.1* and *Figure 9.4*. Since five data points of CCW in the high noise densities reached the highest threshold (three data points in the RG-D condition and two data points in the WK-D condition respectively), we excluded these data points in model fitting. Other than that, the model explains 98-99% of the all variability in the thresholds across observers (27 free parameters). The root mean square error (RMSE) is between 0.06 to 0.1 log unit across observers, on par with the average standard error of measurement. Table 9.1 shows the fitted model parameters.

The model fitting results showed that the inhibition from the same-orientation symmetric components of the non-target color ($Si_{t.nc}$ in the same-orientation conditions) was less than 13% of that from the different-orientation ones ($Si_{t.nc}$ in the different-orientation conditions) across three observers. That is, the mutual inhibition between mechanisms responding to the two symmetric patterns sharing the same axis is smaller than that between mechanisms responding to two symmetric patterns about different orientation axes. This suggests that the human visual system integrates the same-axis information by reducing the inhibition between the same-axis channels. On the other hand, when the symmetric components have different axes, the greater inhibition they produced makes the visual system easier to tell them apart. However, the increase of the mutual inhibition also impairs the symmetry detect performance among them. Thus, the difference in the inhibition terms subserves the two ecological

implications of these two conditions.

Table 9.1.

Fitted model parameters.

	CCW	CPY	RYT
Se_t*	1000	1000	1000
$Si_{t.tc}$			
Isoluminance conditions	272	1920	693
Luminance conditions	55	62	144
$Si_{t.nc}$			
Same-orientation conditions	8.4	269	158
Different-orientation conditions	680	2708	1228
$Si_{b.tc}$	701	8227	1208
$Si_{b.nc}$	342	135	286
z	2.96	1.50	1.00
v	2642	1163	1942
p	2.56	3.12	2.96
Other fixed parameters used in the model fits			
σ_a^2*	1	1	1
q*	2	2	2
n*	1	1	1
γ*	0.71	0.71	0.71

*fixed value, not a free parameter

Our results also showed that the inhibition from the target in the luminance conditions was less than 21% of that in the isoluminance conditions across three observers. This corresponds to the better detection performance in the luminance conditions than in the isoluminance conditions. This result is partially consistent with that in Chapter 8. In Chapter 8, we found that both the inhibition term from the symmetric patterns ($Si_{t.tc}$) and the effect of the external noise (v^2) differ between the isoluminance and the luminance conditions. However, our results in this experiment only showed the difference of the inhibition term from the symmetric patterns ($Si_{t.tc}$)

between the isoluminance and the luminance conditions. There is no difference in the effect of the external noise between the two conditions. This might be due to the difference in the procedures between these two experiments. As Table 9.1 shown, the mixture of the trials of the same- and the different-orientation conditions in this experiment produced a great deal of increment of the effect of the external noise in both the isoluminance and the luminance conditions. The effect of the external noise (v^2) in this experiment reaches 3,000-200,000 times as much as that in the experiment in Chapter 8. The lack of the effect of the external noise between the two conditions might be due to the ceiling effect.


國立臺灣大學
人格教育・學生愛國

Chapter 10 General Discussion

In this thesis, we investigated how form and color are integrated in the high-level vision by studying symmetry detection in noise. We distinguished multiple stages of the symmetry processing and conducted five experiments to investigate the role of color in each stage. In Chapter 5, we demonstrated that it was easier to detect symmetric than anti-symmetric patterns. This suggests that the matching stage is color-selective. In Chapter 6 we demonstrated that the pooling stage had a specific color tuning. This suggests that there are multiple independent symmetry encoders, each of which has a distinct color property. These results supported our chromatic symmetry detection model proposed in Chapter 3, in which we assumed that there are a band of color selective symmetry channels in the visual system. In Chapter 7 to 9, we manipulated orientation and the number of the colors in the symmetric patterns to investigate how information carried by these channels was integrated in symmetry detection. Our results showed that (1) the increment of the number of the colors in an image facilitated symmetry detection regardless of the uncertainty level in axis orientation, (2) it was easier to detect two symmetric patterns about the same axis than those about different axes.

We provided our chromatic symmetry detection model to account for the above results. In this model, each symmetry channel has its own symmetry encoder. The symmetry encoder contains the initial matching stage and the later pooling stage. In the matching stage, the symmetry encoder pairs the image features of its target color. Then the pooling stage analyzes the midpoints of these pairs to determine the position of the axis. The pairs whose midpoints form the axis are the signal of the symmetry

channel while others are noise. The response of each symmetry channel is a nonlinear transducer function that raised the excitation by a power and then divides it by the sum of the divisive inhibition term and an additive constant. For each channel, the response is limited by the sum of external and intrinsic source of noise. The symmetry detection performance relies on the max response of all the channels monitored.

We distinguished several sources of the divisive inhibition term. A symmetry channel receives the inhibition from both the symmetric patterns and the noise of its target and non-target colors. The inhibition from different sources explains the symmetry detection performance in different conditions. For the observer who has prior knowledge of the orientation of the symmetry axis, the inhibition from the symmetric patterns is relatively small compared with that from the noise (Chapter 6). The difference in the symmetry detection performance among images that contain different number of the colors is mainly due to the change of inhibition from the noise patterns that has the same color as the target. This result may be due to that the effect of noise is to interfere with symmetry perception by introducing a percept other than symmetry and that the increment of the number of the colors in an image decreases the number of dots in each color and in turn decreases the interference from the noises. Such reduction of interference improves the detection performance.

When the observer has no prior knowledge of the symmetry axis orientation, the increment of the number of the colors in an image does not reduce the inhibition from the noise patterns. Instead, it reduces the inhibition from the symmetric patterns (Chapter 7). This difference reflects the effect of prior knowledge on the matching of image features in symmetry processing. The prior knowledge of axis orientation helps the observers to exclude a number of matching candidates for each dot in a symmetric pattern. When the prior knowledge of the axis orientation is unavailable, the observer

has to consider many matching candidates across multiple possible axes. Such increment of the number of the candidates in a symmetric pattern interferes with the function of the symmetry channels. Hence, the inhibition from the symmetric patterns is relatively large when the observers have no prior knowledge of axis orientation compared with that when they have prior knowledge of axis orientation. The increment of the number of the colors however decreases the number of the dots in each color. Hence, for each dot, the number of the matching candidates decreases. The interference from the symmetric patterns thus decreases with the increment of the number the colors. Such reduction of interference leads to better detection performance when the number of the colors increases.

The inhibition between symmetric patterns sharing the same axis is smaller than that between those having different axes (Chapter 8). Hence, detecting two symmetric patterns sharing the same axis is easier than detecting those having different axes. Since the two symmetric patterns sharing the same axis can be regarded as a single symmetric pattern containing two colors, this result implies that our visual system forms a coherent symmetry percept by reducing the mutual inhibition from these two components. Our results also showed that the symmetry detection performance in the achromatic images was better than that in the chromatic images in the above conditions. The response of the achromatic symmetry channels was greater than that of the chromatic ones, suggesting different response properties of these two kinds of symmetry channels.

10.1. Color Selective in the Higher-Order Form Mechanism

As mentioned in Chapter 1, there is no consensus in the literature on whether the global form detection mechanism is color selective or color invariant. From the

studies on the global form detection in Glass patterns, some suggested that the higher-order form mechanism is mediated by a non color-selective mechanism (Wilson & Swikes, 2005) while others showed a clear color tuning properties of the global form mechanism (Cardinal & Kiper, 2003).

In the current study, we used symmetry as a tool to further investigate this issue. In symmetry detection, even the initial matching stage requires a long-range interaction. This property makes the symmetry encoder definitely a high-order form mechanism. Our results showed that both the matching stage and the pooling stage of the symmetry processing are color-selective. This suggested that the higher-order form mechanism is color-selective.

10.2. Integrative Color-Form Processing

In this study, we proposed a band of color-orientation selective symmetry channels in the visual system. This indicates that only the symmetric patterns whose color and orientation match the color-orientation selectivity of the symmetry channel excite the response of that channel. Only the form or color matches could not excite the channel. In other words, the symmetry channels response to the combination of color and form information. These color-orientation selective symmetry channels imply an integrative processing of form and color information. The color and form processing is not completely distinct. This contradicts to a traditional view of separate color and form processing.

The evidence of separate pathways for the processing of form versus color comes from both functional dissociation of the patients with brain lesion and the recent neuroimaging studies. For example, the well-known patient with visual form agnosia, DF, is unable to use form information to recognize object, but can use surface

property information such as color and texture (Goodale & Milner, 2004; Humphrey et al., 1994; Milner et al., 1991), whereas the other, MS, showed the converse pattern (Newcombe & Ratcliff, 1975). The recent function magnetic resonance imaging (fMRI) studies also showed that lateral occipital area (LO) plays a critical role in the processing of the geometric structure of objects in object recognition (Cant & Goodale, 2007; Large, Aldcroft, & Vilis, 2005; Malach et al., 1995; Peuskens, et al., 2004) while the processing of the material properties of objects depends on the neural networks that are located more medially in the fusiform and parahippocampal regions (Cant & Goodale, 2007; Hadjikhani, Liu, Dale, Cavanagh, & Tootell, 1998; Mckeefry & Zeki, 1997; Peuskens et al., 2004; Tootell et al., 2003).

Our results, however, showed that the symmetry channels respond to the combination of color and form information. This is inconsistent with the notion of separate color and form processing. However, our result is consistent with the single cell recording (Ito, Fujita, Tamura, & Tanaka, 1994; Tanaka, Saito, Fukada, & Moriya, 1991) and fMRI evidence (Cavina-Pratesi, Kentridge, Heywood, & Milner, 2010). With the single cell recording of the IT neurons in Macaque monkeys, Tanaka and colleges found that the critical feature for the activation varied from cell to cell: Some show orientation selectivity; some are color-selective; and still some others require the combination of a shape and a color for the activation (Ito et al., 1994; Tanaka et al., 1991). These “combination cells” act somewhat like our color-orientation selective symmetry mechanisms. Both require the combination of color and form for activation. More recently, Cavina-Pratesi et al. (2010) showed with fMRI study of health human observers not only the double dissociation between medial and lateral occipitotemporal cortices in processing surface (texture and color, also activate separate foci respectively) versus shape properties but also the areas responding to the

shape, texture and color together (bilateral anterior and posterior fusiform gyrus). The common activations for shape, texture, and color processing support the concurrent processing of form and color, as our results suggested. Taken together, our visual system might process color and form information separately at some aspects. However, there are also some mechanisms selective to the compound features as our results suggested. The human visual system needs to integrate these mechanisms to form a global chromatic form perception.

10.3. Independent Luminance and Chromatic Processing

The distinction of the luminance and chromatic pathways is a long-time controversy. The idea that luminance and chromatic signals travel along at least partially different pathways received support from anatomical and physiological findings, but there is still much controversy about the extent to which these pathways are non-overlapping and independent. Some research showed that the luminance and chromaticity pathways in the simple feature detection are independent (Gegenfurtner & Kiper, 1992; Krauskopf, Williams, & Heeley, 1982). For example, Krauskopf et al. (1982) showed that thresholds for detecting chromatic changes are raised following viewing a field modulated sinusoidally in chromaticity but not in luminance. Thresholds for changes in luminance are raised following viewing a field varying in luminance but not altered by exposure to purely chromatic variation.

Our results further suggest that the luminance and chromatic processing are independent even in the higher-order form processing. As the results in Chapter 6 shown, the pooling stage of symmetry processing is color-selective. The achromatic noise did not produce masking effect on chromatic symmetry detection, and vice versa. The results in Chapter 7 to 9 further suggested that the different response

properties of chromatic and achromatic symmetry channels. Overall, the inhibition of luminance symmetry channels is smaller than that of chromatic symmetry channels. This produces a greater response of luminance symmetry channels than chromatic ones. Hence, detecting achromatic symmetry is easier than detecting chromatic symmetry.

The difference between the luminance and chromatic symmetry channels might trace back to the different properties of P and M layers in the LGN, in which the P pathway is often considered to be the color pathway, while the M pathway is described as luminance pathway (Derrington, et al., 1984; Shapley, 1990). The cells in these two types of layers in the LGN differ in several of their physiological properties. Cells in the P layers have higher spatial and lower temporal resolutions for luminance variations than those in the M layers. M cells have considerably higher contrast sensitivity and gain than the P cells. It is possible that the different performance between chromatic and achromatic symmetry detection is due to the spatial and temporal properties of the stimuli we used. If so, we should expect that increasing the size of the dots and duration of stimulus presentation can reduce the above difference.

10.4. Contributions and Limitations

Even though many researchers agree that color is highly useful in image segmentation during the early visual processing (Callaghan, 1984; Gegenfurtner & Rieger, 2000; Li & Lennie, 1997), the role of color in high-level vision is still a controversy in the literature. Some claimed the facilitation of the color in object representations while some others argued no role of the color in object representations (for a review, see Tanaka, Weiskopf, & Williams, 2001). To investigate the effect of

the color in objects representation, previous researches manipulated the color of the objects as the appropriate, inappropriate and monochromatic colors to measure their effect on recognition times. However, three reasons prohibit us to draw a definite conclusion from those studies. First, the chromaticity and luminance components of their stimuli were not well separated. The so called "color stimuli" is usually composed of both chromatic and luminance components. The chromaticity and luminance are mediated by different post-receptoral mechanisms and their effects do not necessary sum linearly. A stimuli contained both components may produce quite different effects in different channels. Hence, a comparison between the color and monochromatic effect makes little sense. Second, the number of the color-selective channels that involve in the so called color conditions was ill defined. The number of the channels involved may influence the performance. Hence, it is a possibility that the inconsistency among previous research is due to the stimuli they selected. For the stimuli that contain more colors, the color showed facilitation effect on object representations while for the stimuli that contains less color, the color did not show facilitation effect. Third, the stimuli in these studies were the objects familiar to the observers, such as a banana or vegetables. The observers have a prior knowledge of their form and color. Color might provide useful information for the recognition of some, but not all, objects (Tanaka, et al., 2001). For example, although ‘red’ might be an informative cue for identifying fire engines, but is certainly not a very useful cue for identifying automobiles or bicycles. Similarly, the form of some objects might be easier to recognize so that the effect of the color is hard to observe. Hence, the effect of the color depends on the selected objects. The results make sense only when the researchers control the observers’ form and color knowledge to each object. Recently, the research has noticed the color knowledge issue while still ignore the form

knowledge issue.

In this thesis, we use symmetry as a tool to investigate the role of color in high-order form perception. The advantage of using symmetry as the stimuli is preventing the influence of the prior knowledge of both form and color. In addition, we selected the colors on the three cardinal axes of the color space to separate the chromaticity and luminance. This also controls the number of the color-opponent channels involved. Our results should more appropriately demonstrate the role of color in high-order form perception. As summarized above, our results showed that given the same number of the colors in the images, the chromatic colors do not facilitate higher-order form detection comparing to the achromatic colors. However, the more colors in the images, the easier to detect symmetry of them regardless of chromatic or achromatic colors. Our model can fully account for the above results. This helps us further understanding the possible mechanisms behind.

Even though our manipulation avoids several pitfalls in the previous studies concerning the higher-order color vision, some might still argue that our results cannot generalize to the real-life objects or the nature scenes for our stimuli were rather abstract and looked unlike a real life object. After all, our stimuli were composed of sparse random dots while the objects or images in the nature scenes contain denser texture. In addition, the colors in our stimuli distributed randomly while those in the real-life objects or scenes tend to be well organized. We however consider that our results should have no problem to generalize to the real-life objects or scenes. First, the increment of the number of the colors facilitates symmetry detection by reducing the inhibition term of symmetry channels. That is, the more colors in an image, the less inhibition term the symmetry channels have. The inhibition term is proportional to the density of the image components (either

symmetric pattern or noise). Hence, as long as the increment of the overall density does not change the density relationship among the images contain different number of the colors and in turn their inhibition strength to the symmetry channels, our results would have no problem applying to the dense texture. Second, while the colors in our stimuli distributed randomly and thus were not well-organized, we can still observe an increase of facilitation effect to the symmetry channels as the number of the colors increases. Hence, we can expect that this effect is even more obvious in the real-life well-organized objects or scenes.

However, our results did show the influence of the prior knowledge on high-order form detection. For example, the mechanisms of the facilitation of the number of the colors on symmetry detection differ when the observer has and has no prior knowledge of the axis orientation of the symmetric patterns (Chapter 7 and 8). Hence, it is likely that the prior knowledge of the color in the images or objects influence the detection performance. In this study, we did not manipulate the prior knowledge of the color. The mechanism of the prior knowledge of the color in symmetry detection is unclear. However, based on the current understanding of color-form integration in this study, we can further investigate the influence of learning, experience, and knowledge on chromatic form detection in the future, to get a full picture of higher-order color and form vision.

10.5. Future Directions

In sum, we investigated the color and form integration in higher-order visual processing by symmetry detection in this thesis. We demonstrated the color selectivity properties of matching and pooling stage of the symmetry channels. We also provided a model to account for how visual system integrates the response of these channels to

detect symmetry under different situations. These results can serve as the basis of the future studies.

First, it is worth to further investigate the influence of learning, experience, and knowledge on global form detection based on the current model. Previous research has shown that practice (or learning) would facilitate the simple spatial feature detection, such as contrast detection (Dorais & Sagi, 1997; Dosher & Lu, 1999). Dosher and Lu (1999) suggested that the mechanism of this perceptual learning is improvement of the exclusion of external noise and suppression of additive internal noise. Whether and how the practice or learning facilitates the higher-order form detection is unclear. Based on the model proposed in this thesis, we can further investigate the effect of practice on symmetry detection and its mechanism to see whether the perceptual learning in early and high-order vision is driven by the same mechanism.

Second, it may be beneficial to examine whether our results can apply to well-organized dense images. In this model, we assume that the outputs of all chromatic pairs in the sparse image are linearly summed to form the signal of the symmetry operator. However, it is possible that the outputs of these signal pairs are not linearly summed when the density of the images exceeds a value. This is critical for the generalization of our results to dense images. We can examine whether this assumption holds in the dense images in the future.

Third, it may be informative to investigate the chromatic symmetry detection along the intermediate directions between two cardinal directions. The colors of the real-life objects or scenes seldom locate in the cardinal axis of the color space. Instead, they are usually the combinations of three color opponent directions. In this thesis, we distinguished six independent symmetry channels selective to the six cardinal

directions (or three opponent cardinal directions) on the color space. Whether these channels can predict the symmetry detection along intermediate directions or more than these channels are needed is a question. Actually, whether there are additional multiple mechanisms beyond the cardinal ones or whether there are higher-order color mechanisms at some higher level of the visual system is still a debate (Eskew, 2009). Investigating the symmetry detection along intermediate directions can provide us an opportunity to get an extensive understanding of the higher-order color mechanism.

Reference

Barlow, H. B., & Reeves, B. C. (1979). The versatility and absolute efficiency of detecting mirror symmetry in random dot displays. *Vision Research, 19*, 783-793.

Blum, H. (1973). Biological shape and visual science. *Journal of Theoretical Biology, 38*, 205-287.

Bowmaker, J. K., & Dartnall, H. J. A. (1980). Visual pigments of rods and cones in a human retina, *Journal of Physiology* (*London*), *298*, 501-511.

Brainard, D. H. (1996). Cone contrast and opponent modulation color spaces. In P. K. Kaiser, & R. M. Boynton, *Hunam color vision*. Washington DC: Optical Society of America.

Brooks, A., & van der Zwan, R. (2002). The role of ON- and OFF-channel processing in the detection of bilateral symmetry. *Perception, 31*, 1061-1072.

Burbeck, C. A., & Pizer, S. M. (1995). Object representation by cores: Identifying and representing primitive spatial regions. *Vision Research, 35*, 1917-1930.

Callaghan, T. (1984) Dimensional interaction of hue and brightness in preattentive field segregation. *Perception & Psychophysics, 36*, 25-34.

Cant, J. S., & Goodale, M. A. (2007). Attention to form or surface properties modulates different regions of human occipitotemporal cortex. *Cerebral Cortex, 17*, 713-731.

Cardinal, K. S., & Kiper, D. C. (2003). The detection of colored Glass patterns. *Journal of Vision*, *3*(3):2,199-208.

Carmody, D. P., Nodine, C. F., & Locher, P. J. (1977). Global detection of symmetry.

Perceptual & Motor Skills, 45, 1267-1273.

Cavina-Pratesi, C., Kentridge, R. W., Heywood, C. A., & Milner, A. D. (2010). Separate channels for processing form, texture and color: evidence from fMRI adaptation and visual object agnosia. *Cerebral Cortex, 20*, 2319-2332.

Chen, C. C. (2009). A masking analysis of Glass pattern perception**.** *Journal of Vision, 9*(12):22, 1-11.

Chen, C. C., & Tyler, C. W. (1999). Accurate approximation to the extreme order statistics of Gaussian samples. *Communications in Statistics: Simulation and Computation, 28*, 177-188.

Chen, C. C., & Tyler, C. W. (2010). *Symmetry: modeling the effect of masking noise, axial cueing and salience. Public Library of Science One, 5*, 1-10.

Chen, C. C., Foley, J. M., & Brainard, D. H. (2000). Detection of chromoluminance patterns on chromoluminance pedestals I: threshold measurements, *Vision Research, 40*, 773-788.

Csathó, A., van der Vloed, G., & van der Helm, P. A. (2004). The force of symmetry revisited: symmetry-to-noise ratios regulate (a)symmetry effects. *Acta Psychologica, 117*, 233-250.

CIE (2007). Fundamental chromaticity diagram with physiological axes - Parts 1 and 2. Technical Report 170-1. Vienna: Central Bureau of the Commission Internationale de l' Éclairage.

Dakin, S. C., & Herbert, A. M. (1998). The spatial region of integration for visual symmetry detection. *Proceedings of the Royal Society of London, Series B: Biological Sciences, 265*, 659-664

Dakin, S. C., & Hess, R. F. (1997). The spatial mechanisms mediating symmetry perception. *Vision Research, 37*, 2915-2930.

Dakin, S. C., & Watt, R. J. (1994). Detection of bilateral symmetry using spatial filters. *Spatial Vision, 8,* 393-413.

De Valois, R. L., & De Valois, K. K. (1993). A multi-stage color model. *Vision Research, 22,* 549-559.

Derrington, A. M., Krauskopf, J., & Lennie, P. (1984). Chromatic mechanisms in lateral geniculate nucleus of macaque. *Journal of Physiology* (*London*), *357,* 241-265.

Dosher, B. A., & Lu, Z. L. (1999). Mechanisms of perceptual learning. *Vision Research, 39,* 3197-3221.

Dorais, A., & Sagi, D. (1997). Contrast asking effects change with practice. *Vision Research, 37*(13), 1725-1733.

Dow, B. M., & Gouras, P. (1973). Color and spatial specificity of single units in rhesus monkey foveal striate cortex. *Journal of Neurophysiology, 36,* 79-100.

Driver, J., Baylis, G. C., & Rafal, R. D. (1992). Preserved figure-ground segregation and symmetry in visual neglect. *Nature, 360,* 73-75.

Eskew, R. T. Jr. (2009). Higher order color mechanisms: A critical review. *Vision Research, 49,* 2686-2704.

Foley, J. M. (1994). Human luminance pattern-vision mechanisms: Masking experiments require a new model. *Journal of the Optical Society of America A, Optics, Image Science, and Vision, 11,* 1710-1719.

Foley, J. M., & Chen, C. C. (1997). Analysis of the effect of pattern adaptation on pattern pedestal effects: A two-process model. *Vision Research, 37,* 2779-2788.

Foley, J. M., & Chen, C. C. (1999). Pattern detection in the presence of maskers that differ in spatial phase and temporal offset: threshold measurements and a

model. *Vision Research, 39,* 3855-3872.

Gegenfurtner, K. R., & Kiper, D. C. (1992). Contrast detection in luminance and chromatic noise. *Journal of the Optical Society of America A, 9,* 1880-1888.

Gegenfurtner, K. R., & Kiper, D. C. (2004). The processing of color in extrastriate cortex. In L. M. Chalupa & J. S. Werner (Eds.), *The visual neurosciences* (pp. 1017-1028). Boston, MA: MIT Press.

Gegenfurtner, K. R., Kiper, D. C., & Fenstemaker, S. B. (1996). Processing of color, form, and motion in macaque area V2. *Visual Neuroscience, 13,* 161-172.

Gegenfurtner, K. R., Kiper, D. C., & Levitt, J. B. (1997). Functional properties of neurons in macaque area V3. *Journal* of *Neurophysiology, 77,* 1906-1923.

Gegenfurtner, K. R., & Rieger, J. (2000) Sensory and cognitive contributions of color to the recognition of natural scenes. *Current Biology, 10,* 805-808.

Giulianini, F., & Eskew, R. T. Jr., (1998). Chromatic masking in the (DL/L, DM/M) plane of cone-contrast space reveals only two detection mechanisms. *Vision Research, 38,* 3913-3926.

Glass, L. (1969). Moire effect from random dots. *Nature, 223,* 578.

Glass, L., & Perez, R. (1973). Perception of random dot interference patterns. *Nature, 246,* 360-362.

Goodale, M. A., & Milner, A. D. (2004). *Sight unseen: An exploration of conscious and unconscious vision*. Oxford: Oxford University Press.

Gouras, P. (1974). Opponent-colour cells in different layers of foveal striate cortex. *Journal* of *Physiology, 199,* 533-547.

Graham, N., Robson, J. G., & Nachmias, J. (1978). Grating summation in fovea and periphery. *Vision Research, 21*(3), 409-418.

Green, D. M. and Swets, J. A. (1966). *Signal detection theory and psychophysics.*

New York: Wiley.

Gurnsey, R., Herbert, A. M., & Kenemy, J. (1998). Bilateral symmetry embedded in noise is detected accurately only at fixation. *Vision Research, 38,* 3795-3803.

Hadjikhani, N., Liu, A. K., Dale, A. M, Cavanagh, P., & Tootell, R. B. (1998). Retinotopy and color sensitivity in human visual cortical area V8. *Nature Neuroscience, 1,* 235-241.

Hansen, T., & Gegenfurtner, K. R. (2006). Higher level chromatic mechanisms for image segmentation. *Journal of Vision, 6,* 239-259.

Harris, J. M., & Parker, A. J. (1995). Independent neural mechanisms for bright and dark information in binocular stereopsis. *Nature, 374,* 808-811.

Hegger, D. J. (1992). Half-squaring in responses of cat striate cells. *Visual Neuroscience, 9,* 427-443.

Hogben, J. H., Julesz, B., & Ross, J. (1976). Short-term memory for symmetry. *Vision Research, 16,* 861-866.

Huang, L., & Pashler, H. (2002). Symmetry detection and visual attention: A "binary-map" hypothesis. *Vision Research, 42,* 1421-1430.

Humphrey, G. K., Goodale, M, A,, Jakobson, L. S., & Servos, P. (1994). The role of surface information in object recognition: studies of a visual form agnosic and normal subjects'. Perception, *23,* 1457-1481.

Ito, M., Fujita, I., Tamura, H. and Tanaka, K. (1994) Processing of contrast polarity of visual images in the inferotemporal cortex. *Cerebral Cortex, 5,* 499-508.

Jacobs, G. H., & Neitz, J. (1993). Electrophysiological estimates of individual variation in the L/M cone ratio. In B. Drum (Ed.), *Documenta Ophthalmologica Proceedings Series 56, Colour Vision Deficiencies XI* (pp. 107-112). Dordrecht, The Netherlands: Kluwer Academic Publishers.

Johnson, E. N., Hawken, M. J., & Shapley, R. (2001). The spatial transformation of color in the primary visual cortex of the macaque monkey. *Nature Neuroscience*, *4*, 409-416.

Julesz, B. (1971). *Foundations of cyclopean perception*. Chicago: University of Chicago Press.

Knoblauch, K., & Shevell, S. K. (2004). Color appearance. In L. M. Chalupa & J. S. Werner (Eds.), *The visual neurosciences* (pp. 892-907). Boston, MA: MIT Press.

Koffka, K. (1935). *Principles of Gestalt psychology*. London: Routledge and Kegan Paul.

Köhler, W. (1929). *Gestalt psychology*. New York: Liveright.

Komatsu, H., & Ideura, Y. (1993). Relationships between color, shape and pattern selectivities of neurons in the inferior temporal cortex of the monkey. *Journal of Neurophysiology, 70*(2), 677-694.

Komatsu, H., Ideura, Y., Kaji, S., & Yamane, S. (1992). Color selectivity of neurons in the inferotemporal cortex of the awake macaque monkey, *Journal* of *Neuroscience*, *12*(2), 408-424.

Kontsevich, L. L., & Tyler, C. W. (1999). Bayesian adaptive estimation of psychometric slope and threshold. *Vision Research, 39*, 2729-2737.

Kovacs, I., Feher, A., & Julesz, B. (1998). Medial-point description of shape: A representation for action coding and its psychophysical correlates. *Vision Research, 38*, 2323–2333.

Krauskopf, J., Williams, D. R., & Heeley, D. W. (1982). Cardinal directions of color space. *Vision Research, 22*, 1123-1131.

Large, M. E., Aldcroft, A., & Vilis, T. (2005). Perceptual continuity and the

emergence of perceptual persistence in the ventral visual pathway. *Journal of Neurophysiology, 93,* 3453-3462.

Leeuwenberg, E. L. J., & Buffart, H. F. J. M. (1984). The perception of foreground and background as derived from structural information theory. *Acta Psychologica, 55,* 249-272.

Lennie, P. (1999). Color coding in the cortex. In K. R. Gegenfurther & L. T. Sharpe (Eds.), *Color vision* (pp. 235-247). Cambridge: Cambridge University Press.

Leventhal, A. G., Thompson, K. G., Liu, D., Zhou, Y., & Ault, S. J. (1995). Concomitant sensitivity to orientation, direction, and color of cells in layers 2, 3, and 4 of monkey striate cortex, *Journal of Neuroscience, 15,* 1808-1818.

Levitt, J. B., Kiper, D. C., Movshon, J. A. (1994). Receptive fields and functional architecture of macaque V2. *Journal of Neurophysiology, 71,* 2517-2542.

Li, A., & Lennie, P. (1997). Mechanisms underlying segmentation of colored textures. *Vision Research, 37,* 83-97.

Livingstone, M. S., & Hubel, D. H. (1984). Anatomy and physiology of a color system in the primate visual cortex, *Journal of Neuroscience, 4,* 309-356.

Locher, P. J., & Nodine, C. F. (1989). The perceptual value of symmetry. *Computers & Mathematics with Applications, 17,* 475-484.

Lu, Z. L., & Dosher, B. A. (2008). Characterizing observers using external noise and observer models: assessing internal representations with external noise. *Psychological Review, 115,* 44-82.

MacLeod, D. I. A., & Boynton, R. M. (1979). A chromaticity diagram showing cone excitation by stimuli of equal luminance. *Journal of the Optical Society of America, 69,* 1183-1186.

Malach, R., Reppas, J. B., Benson, R. R., Kwong, K. K., Jiang, H., Kennedy, W. A.,

Ledden, P. J., Brady, T. J., Rosen, B. R., Tootell, R. B. H. (1995). Object-related activity revealed by functional magnetic resonance imaging in human occipital cortex. *Proceedings of the National Academy of Sciences of the United States of America*, *92*, 8135-8139.

Mancini, S., Sally, S. L., & Gurnsey, R. (2005). Detection of symmetry and anti-symmetry. *Vision Research*, *45*(16), 2145-2160.

Mandelli, M. J., & Kiper, D. C. (2005). The local and global processing of chromatic Glass patterns. *Journal of Vision*, *5*(5):2, 405-416.

Marr, D. (1982). *Vision*. San Francisco: W.H. Freeman and Company.

McKeefry, D. J., & Zeki, S. (1997). The position and topography of the human colour centre as revealed by functional magnetic resonance imaging. *Brain*, *120*, 2229-2242.

Michael, C. R. (1978a). Color vision mechanisms in monkey striate cortex: dual-opponent cells with concentric receptive fields. *Journal of Neurophysiology*, *41*, 572-588.

Michael, C. R. (1978b). Color vision mechanisms in monkey striate cortex: simple cells with dual opponent-color concentric receptive fields. *Journal of Neurophysiology*, *41*, 1233-1249.

Michael, C. R. (1978c). Color-sensitive complex cells in monkey striate cortex. *Journal* of *Neurophysiology*, *41*, 1250-1266.

Michael, C. R. (1979). Color-sensitive hypercomplex cells in monkey striate cortex. *Journal* of *Neurophysiology*, *42*, 726-744.

Milner, A. D., Perrett, D. I., Johnston, R. S., Benson, P. J., Jordan, T. R., Heeley, D. W., Bettucci, D., Mortara, F., Mutani, R., & Terazzi, E. (1991). Perception and action in 'visual form agnosia'. *Brain*, *114*, 405-428.

Morales, D., & Pashler, H. (1999). No role for colour in symmetry perception. *Nature, 399,* 115-116.

Newcombe, F., & Ratcliff, G. (1975). Agnosia: a disorder of object recognition. In F. Michel & B. Schott (Eds.), Les Syndromes de disconnexion calleuse chez l'homme (pp.317-340). Lyon: Colloque International.

Osorio, D. (1996). Symmetry detection by categorization of spatial phase, a model. *The Proceedings of the Royal Society: Biological Sciences, 263*, 105-110.

Pelli, D. C. (1985). Uncertainty explains many aspects of visual contrast detection and discrimination. *Journal of the Optical Society of America A, 2*, 1508-1532.

Peuskens, H., Claeys, K. G., Todd, J. T., Norman, J. F., Van Hecke, P., Orban, G. A. (2004). Attention to 3-D shape, 3-D motion, and texture in 3-D structure from motion displays. *Journal of Cognitive Neuroscience, 16*, 665-682.

Quick, R. F. (1974). A vector magnitude model of contrast detection. *Kybernetic, 16*, 65-67.

Rainville, S. J., & Kingdom, F. A. (1999). Spatial-scale contribution to the detection of mirror symmetry in fractal noise. *Journal of the Optical Society of America A, 16*, 2112-2123.

Rainville, S. J., & Kingdom, F. A. (2000). The functional role of oriented spatial filters in the perception of mirror symmetry--psychophysics and modeling. *Vision Research, 40,* 2621-2644.

Rainville, S. J., & Kingdom, F. A. (2002). Scale invariance is driven by stimulus density. *Vision Research, 42*, 351-367.

Rentzeperis, I., & Kiper, D. C. (2010). Evidence for color and luminance invariance of global form mechanisms. *Journal of Vision*, *10*(12):6, 1-14.

Shapley, R. (1990). Visual sensitivity and parallel retinocortical channels. *Annual*

Review of Psychology, *41*, 635-658.

Shevell S. K. and Kingdom F. A. A. (2008) Color in complex scenes. *Annual Review of Psychology*, *59*, 143-166.

Saarinen, J., & Levi, D. M. (2000). Perception of mirror symmetry reveals long-range interactions between orientation-selective cortical filters. *Neuroreport, 11*, 2133-2138.

Sasaki Y, Wanduffel W, Knutsen T, Tyler C, Tootell R. (2005). Symmetry activates extrastriate visual cortex in human and non-human primates. *Proceedings of the National Academy of Sciences of the United States of America*, *102*, 359-363.

Schein, S. J., & Desimone, R. (1990). Spectral properties of V4 neurons in the macaque. *Journal of Neuroscience*, *10*, 3369-3389.

Schiller, P. H. (1992). The ON and OFF channels of the visual system. *Trends in Neurosciences*, *15*(3), 86-92

Schnapf, J. L., Kraft, T. W., & Baylor, D. A. (1987). Spectral sensitivity of human cone photoreceptors, *Nature*, *325*, 439-441.

Scognamillo, R., Rhodes, G., Morrone, C., & Burr, D. (2003). A feature-based model of symmetry detection. *Proceedings of the Royal Society of London Series B-Biological Sciences, 270*, 1727-1733.

Smith, M. A., Bair, W., & Movshon, J. A. (2002). Signals in macaque striate cortical neurons that support the perception of Glass patterns. *Journal of Neuroscience, 22*, 8334-8345.

Smith, V. C., & Pokorny, J. (1975). Spectral sensitivity of the foveal cone photopigments between 400 and 500nm. *Vision Research*, *15*, 161–171.

Stockman, A., & Sharpe, L. T. (2000). Spectral sensitivities of the middle- and long-

wavelength sensitive cones derived from measurements in observers of known genotype. *Vision Research, 40,* 1711-1737.

Switkes, E., Bradley, A., & De Valois, K. K. (1988). Contrast dependence and mechanisms of masking interactions among chromatic and luminance gratings. *Journal of the Optical Society of America A, 5,* 1149-1162.

Tanaka, K., Saito, H., Fukada, Y., & Moriya, M. (1991). Coding visual images of objects in the inferotemporal cortex of the macaque monkey. *Journal of Neurophysiology, 66,* 170–189.

Tanaka, J., Weiskopf, D., & Williams, P. (2001). The role of color in high-level vision. *Trends in Cognitive Science, 5*(5), 211-215.

Thorell, L. G., De Valois, R. L., & Albrecht, D. G. (1984). Spatial mapping of monkey V1 cells with pure color and luminance stimuli, *Vision Research, 24,* 751-769.

Tjan, B. S., & Liu, Z. (2005). Symmetry impedes symmetry discrimination. *Journal of Vision, 5,* 888-900.

Tootell, R. B. H., Mendola, J. D., Hadjikhani, N. K., Ledden, P. J., Lui, A. K., Reppas, J. B., Sereno, M. I., & Dale, A. M. (1997). Functional analysis of V3A and related areas in human visual cortex. *Journal of Neuroscience, 17,* 7060-7078.

Troscianko, T. (1987). Perception of random-dot symmetry and apparent movement at and near isoluminance. *Vision Rearch, 27,* 547-554.

Ts'o, D.Y., & Gilbert, C.D. (1988). The organization of chromatic and spatial interactions in the primate striate cortex. *The Journal of Neuroscience, 8*(5), 1712-1727.

Tyler, C. W., Baseler, H. A., Kontsevich, L. L., Likova, L. T., Wade, A. R., Wandell, B. A. (2005). Predominantly extra-retinotopic cortical response to pattern

symmetry. *Neuroimage, 15*, 306-314.

Tyler, C. W., & Chen, C. C. (2000). Signal detection theory in the 2AFC paradigm: attention, channel uncertainty and probability summation. *Vision Research*, *40*, 3121-3144.

Tyler, C. W., & Hardage, L. (1996). Mirror symmetry detection: predominance of second order pattern processing throughout the visual field. In C. W. Tyler (Ed.), *Human Symmetry Perception and its Computational Analysis* (pp. 157-171). Utrecht: VSP.

van der Helm, P. A., & Leeuwenberg, E. L. (1996). Goodness of visual regularities: a nontransformational approach. *Psychological Review*, *103*, 429-456.

van der Helm, P. A., & Leeuwenberg, E. L. J. (1999). A better approach to goodness: Reply to Wagemans (1999). *Psychological Review*, *106*, 622-630.

Van der Zwan, R., Badcock, D. R., & Parkin, B. (1999). Global form perception: Interactions between luminance and texture information. Australian and New Zealand Journal of Ophthalmology, *27*(3-4), 268-270.

von Kries, J. (1905). Die Gesichtsempfindungen, In W. Nagel (Ed.), *Handbuch der Physiologie des Menschen* (pp. 109-282). Braunschweig: Vieweg.

Vos, J. J., & Walraven, P. L. (1971). On the derivation of the foveal receptor primaries. *Vision Research*, *11*, 799-818.

Wagemans, J., Van Gool, L., & d'Ydewalle, G. (1991). Detection of symmetry in tachistoscopically presented dot patterns: effects of multiple axes and skewing. *Perception & Psychophysics*, *50*, 413-427.

Wagemans, J., Van Gool, L., Swinnen, V., & Van Horebeek, J. (1993). Higher-order structure in regularity detection. *Vision Research*, *33*, 1067-1088.

Webster, M. A., De Valois, K. K., & Switkes, E. (1990). Orientation and spatial-

frequency discrimination for luminance and chromatic gratings. *Journal of the Optical Society of America A, Optics and image science, 7,* 1034–1049.

Wenderoth, P. (1996). The effects of the contrast polarity of dot-pair partners on the detection of bilateral symmetry. *Perception*, *25*, 757-771.

Wertheimer, M. (1938). Laws of organization in perceptual forms. In W. Ellis (Ed.), *A source book of Gestalt psychology*. New York: Harcourt.

Wilson, J. A., & Switkes, E. (2005). Integration of differing chromaticities in early and midlevel spatial vision. *Journal of the Optical Society of America A*, *22*, 2169-2181.

Wilson, J. A., Switkes, E., & De Valois, R. L. (2004). Glass pattern studies of local and global processing of contrast variations. *Vision Research*, *44*, 2629-2641.

Wilson, H., & Wilkinson, F. (1998). Detection of global structure in Glass patterns: Implications for form vision. *Vision Research*, *38*, 2933-2947.

Yates, J. T. (1974). Chromatic information processing in the foveal projection (area striata) of unanesthetized primate. *Vision Research*, *14*, 163-173.

Zhang, L., & Gerbino, W. (1992). Symmetry in opposite-contrast dot patterns. *Perception*, *21*, Supplement 2, 95.

Zeki, S. (1973). Color coding in rhesus monkey prestriate cortex. *Brain Research*, *53*, 422-427.


國立臺灣大學
人格教育・學生愛國

Appendix Contrast Detection Threshold Measurement of the Selected Color

Since the visual sensitivity to each color are different (Chen et al., 2000), we set the contrast of each color at its equal sensitivity level for each observer to control the salience of the colors. We used a temporal 2AFC paradigm to measure the symmetry contrast threshold of the symmetric patterns of colors selected in the experiment for each observer. On each trial, a vertical symmetric-dots image was randomly presented in one of the two intervals while the random-dot image was presented in another interval. The densities of both images were 1%. The duration was 233 ms and the inter-stimulus interval (ISI) was 600 ms. An audio tone was placed to indicate the beginning of each interval. The observers' task was to judge which interval contains a vertical symmetric pattern. An audio feedback for the response was provided. The PSI threshold-seeking algorithm (Kontsevich & Tyler, 1999) was used to measure the threshold at 75% correct level. There were 40 trials for each threshold measurement. The order of the tested colors was randomized.

By this measurement, we got the contrast threshold of each color. In all of the experiments, we set the contrast of each color at its three fold threshold for each observer based on this measurement.


國立臺灣大學
人格教育．學品勵愛

Curriculum Vitae

吳佳瑾

Chia-Ching Wu

Education

2011 Ph. D. in Psychology, National Taiwan University.

2001 B.S. in Psychology, with a minor in Sociology, Social Work Division, National Taiwan University.

Research Interests

Color vision, Spatial vision, Mathematical modeling, Thinking and reasoning, Causal reasoning.

Publications

1. Chen, C. C.*, Wu, J. H. & **Wu, C. C.** (2011). Reduction of image complexity explains aesthetic preference to symmetry. *Symmetry*, *3*(3), 443-456. *(SCI)*
2. **Wu, C. C.** & Chen, C. C.* (2010). Distinguishing lateral interaction from uncertainty reduction in collinear flanker effect on contrast discrimination, *Journal of Vision*, *10*(3), 1-14. *(SCI)*
3. Chen, C. C.*, Cho, S. L., Horszowska, K., Chen, M. Y., **Wu, C. C.**, Chen, H. C., Yeh, Y. Y. & Cheng, C. M. (2009). A facial expression image database and norm for Asian population: A preliminary report. *SPIE Proceedings*, *7242*, 72421D-1-72421D-9. *(EI)*

Conference Presentations

1. Wu, C. C. & Chen, C. C. (2011). The role of luminance and chromaticity in symmetry detection. The Asia-Pacific Conference on Vision 2011, Hong Kong.
2. Wu, J. H., Chen, C. C., & Wu, C. C. (2011). Complexity reduction explains preference to symmetric patterns. The Asia-Pacific Conference on Vision 2011, Hong Kong.
3. Wu, C. C. & Chen, C. C. (2011). The integration of color information in symmetry detection. Vision Science Society 11th Annual Meeting, Naples, Florida, USA.
4. Wu, C. C. & Chen, C. C. (2010). The effect of the chromaticity of image elements on symmetry detection. The Asia-Pacific Conference on Vision 2010, Taipei, Taiwan.
5. Wu. C. C. & Chen, C. C. (2009). Distinguishing lateral interaction from uncertainty reduction in collinear flanker facilitation of contrast discrimination. The 32nd European Conference on Visual Perception, Regensburg, Germany.
6. 吳佳瑾、連韻文(2005)。因果脈絡對假設檢驗測試策略的影響。第 44 屆台灣心理學年會。中原大學，桃園。
7. Wu, C. C. & Lien, Y. W. (2004). The influence of goal on the performance of concept attainment. The 28nd international congress of psychology, Beijing, China.
8. 黃永廣、連韻文、吳昭容、蘇順隆、李俊岳、陳亦媛、吳佳瑾、及許勝程(2002)。研究孩童歸納能力的電腦輔助學習環境。第七屆人工智慧與應用研討會，朝陽科技大學，台中，606-611。